Review Vol. 17, No. 2 / June 2025 / Advances in Optics and Photonics 375

High-precision optical time and frequency transfer

EMILY D. CALDWELL,[1] THEODORA M. TRIANO,[2] AND LAURA C. SINCLAIR[1,*]

[1]National Institute of Standards and Technology, 325 Broadway, Boulder, Colorado 80305, USA
[2]Department of Electrical, Computer and Energy Engineering, University of Colorado Boulder, Boulder, Colorado 80309, USA
*laura.sinclair@nist.gov

Received October 16, 2024; revised February 25, 2025; accepted February 25, 2025; published 2 May 2025

High-precision optical time and frequency transfer is accomplished by a collection of laser-based techniques that achieve time dissemination with subpicosecond instabilities and frequency dissemination with instabilities below one part in 10^{16}. The ability to distribute and compare time and frequency at these precisions enables current optical timing networks such as interconnected optical atomic clocks for the redefinition of the second, relativistic geodesy, and fundamental physics tests as well as time and frequency dissemination systems for large-scale scientific instruments. Future optical timing networks promise to expand these applications and enable new advances in distributed coherent sensing, precise navigation, and more. The field of high-precision optical time and frequency transfer has made significant advances over the last 20 years and has begun to transition from technique development to deployment in applications. Here, we present a review of approaches to high-precision optical time and frequency transfer. We first present a brief overview of the metrics used to assess time and frequency transfer. We then provide a discussion of the difference between time transfer and frequency transfer and review the various technical noise sources. We also provide a background on the optical frequency comb and its role in optical time and frequency transfer for additional context. The next sections of the paper cover specific time–frequency transfer techniques and demonstrations beginning with time and frequency transfer over fiberoptic links including continuous-wave (CW) laser-based frequency transfer, CW-laser-based time transfer, and frequency-comb-based time transfer. We then discuss approaches for time and frequency transfer over free-space including pulsed-source time transfer, CW-laser-based frequency transfer, and frequency-comb-based time transfer. Since no known existing review article covers frequency-comb time transfer over free-space, we provide additional details on the technique. Finally, we provide an outlook that outlines outstanding challenges in the field as well as possible future applications.

https://doi.org/10.1364/AOP.545290

High-precision optical time and frequency transfer

EMILY D. CALDWELL, THEODORA M. TRIANO, AND LAURA C. SINCLAIR

1. INTRODUCTION

High-precision optical timing networks, here defined as networks that reach uncertainties below 1 ps in time and below one part in 10^{16} in frequency, hold tremendous potential for a wide range of applications. These applications include the redefinition of the second and the requisite time and frequency dissemination that will follow [1–4], a variety of fundamental physics tests [5–20], chronometric geodesy [21], high-precision navigation [22], distributed coherent sensing such as very-long-baseline interferometry (VLBI) [23–30], and earthquake detection [31], as sketched in Fig. 1.

An optical timing network can take many forms but has two main components: a stable reference oscillator (or oscillators), and the optical time or frequency transfer links that allow dissemination and comparison of these references. In an ideal case, the limitations of optical timing networks will be set by the reference oscillator performance or measurement needs rather than the links between them. As such, the link requirements will vary with application.

When targeting extremely low uncertainties, these networks can support state-of-the-art optical atomic clocks as the optical references at all nodes. Connecting and comparing state-of-the-art optical atomic clocks, for instance, is crucial for the redefinition of the second [1]. In chronometric geodesy, these clocks are used to measure the geopotential between two sites [21]. Clock-based fundamental physics tests include clock comparisons to probe general relativity and standard model physics through measurements of the gravitational redshift [5–12,19], tests of local Lorentz invariance, position invariance, and Lorentz symmetry [6,16,17,19,32], and searches for variations in fundamental constants [6,12,18] and dark matter [12–15,20]. Cases such as these will require the links to preserve the exceptional frequency uncertainties of the optical clocks (possibly exceeding 10^{-18}) but may not require phase transfer or real-time synchronization of sites.

In an intermediate uncertainty case, one could use a full state-of-the-art optical atomic clock and a timing network to steer an array of lower performance clocks such as intermediate-performance optical clocks (10^{-15}-level instability) [33–36], cavity-stabilized lasers, or even microwave oscillators. Examples of this kind of network include the eventual time and frequency dissemination that will follow the redefinition of the second [1–4], high-precision navigation [22], and state-of-the-art optical clock comparisons where the clocks are linked through intermediate nodes as proposed in Ref. [37]. Applications such as these may not require exquisite 10^{-18}-level uncertainties but may require active feedback across links to ensure the phase coherence of the follower sites with the guide site.

Lastly, one could envision networks without optical clocks that rely on optical time transfer and very tight feedback loops to enforce femtosecond-level synchronization across multiple low-stability references. Such networks could, for example, be used to enable distributed coherent sensing and Earth sensing in the millimeter-wave.

Figure 1

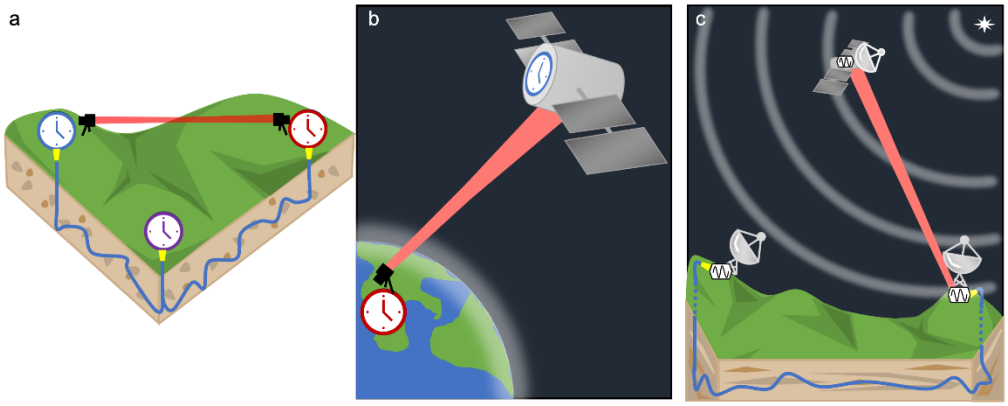

Concepts for future time/frequency networks. (a) Frequency ratio measurement of optical atomic clocks over fiberoptic and free-space links. (b) Fundamental physics test between an optical atomic clock on the ground and in space through measurement of accumulated time difference. (c) Distributed coherent sensing with phase coherence established over fiberoptic and free-space links between optical oscillators.

At the heart of all high-precision optical time and frequency transfer is the removal of the link-induced accumulated phase noise that is inherent in the initial one-way propagation of the light from an optical oscillator or optical atomic clock to a remote location. For either a fiberoptic or a free-space link, the link-induced phase noise (time-of-flight fluctuations) can easily exceed the relative phase noise of the references. As sketched in Fig. 2, all methods of high-precision optical time and frequency transfer will take advantage of the reciprocity associated with the bidirectional propagation of the optical signal either through sending a partial reflection back to the source or performing a two-way measurement. Partial reflection allows for a measurement of double the link-induced phase noise that can be used in active phase noise cancellation. Bidirectional propagation, meanwhile, generates two one-way signals that can be combined to remove common phase noise.

Our review is structured as follows. Following the introduction, in Section 2, we present a brief discussion of the metrics by which we assess frequency and time transfer. Section 3 contains a discussion of the distinction between time transfer and frequency transfer. In Section 4, we present considerations affecting time or frequency transfer approaches such as noise sources, signal distortions, and loss. In Section 5, we provide a brief introduction to the optical frequency comb and the comb's role in enabling high-precision optical time and frequency transfer. In Section 6, we discuss fiber-based time and frequency transfer techniques including continuous-wave (CW) laser-based frequency transfer, frequency-comb-based time transfer, and the subset of CW-laser-based time transfer that reaches below 1 ps in timing performance. In Section 7, we cover free-space time and frequency transfer techniques including CW-laser-based frequency transfer, pulsed-source (laser ranging) based time transfer, and frequency-comb-based time transfer. Following this review of the techniques, in Section 8 we present an outlook that includes both a discussion of outstanding challenges in the field and a forward-looking discussion focused on applications and future timing networks. Finally, we present a brief conclusion summarizing the information presented.

This review focuses on high-precision time–frequency transfer at uncertainties below 1 ps in time and below one part in 10^{16} in frequency. This definition of high-precision has resulted in a focus only on *optical* time and frequency transfer in this

Figure 2

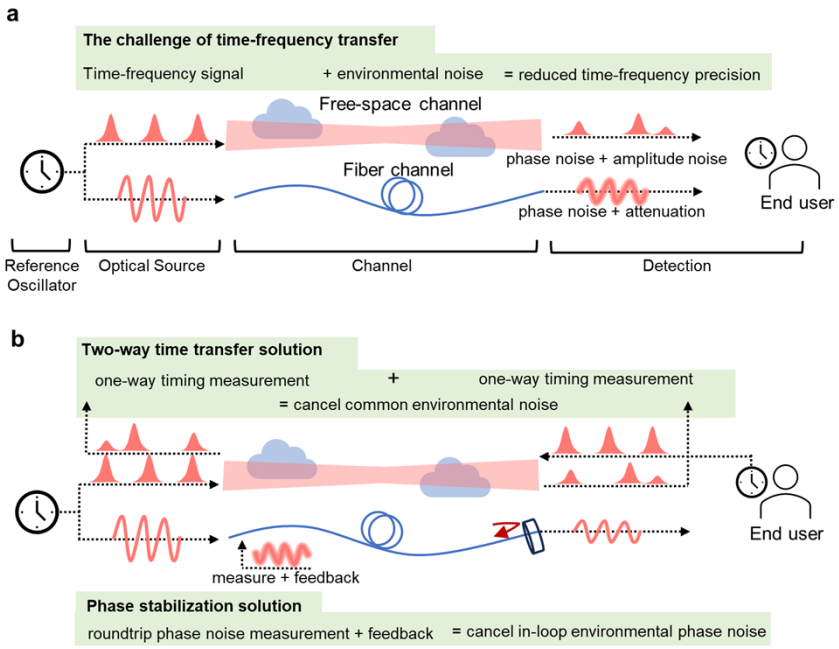

Basic concept of optical time and frequency transfer. (a) The frequency and phase of a reference oscillator are encoded onto the output of an optical source. The optical signal is then transmitted through a channel to be detected by the end user. (See also Fig. 5 for a discussion of the rough breakdown of any optical time or frequency transfer into the four main components of reference oscillator, optical source, channel, and detection.) Whether the optical source is a CW or a stable pulsed laser, transmission through the channel causes the signal to be distorted by a variety of noise sources resulting in accumulated phase noise at the end of the link. This occurs both for propagation over a free-space or fiberoptic link. Here, we illustrate the transmission of a stable CW laser frequency over a fiberoptic link and the transmission of a coherent pulse train (transferring both frequency and time) over a free-space link. For the fiberoptic link, acoustic noise will also have a significant impact, while for the free space link, atmospheric turbulence will result in increased phase noise and link interruptions. (b) Two different solutions to mitigate the distortion of the optical signal. In both cases the solution is to create reciprocal links such that the phase noise fluctuations accumulated during the transmission of the signal are measured and accounted for or removed.

review. Radio-frequency (RF)-based time and frequency transfer techniques including Global Navigation Satellite Systems (GNSS) methods [38–40] and two-way satellite time-frequency transfer (TWSTFT) [41] have allowed for intercontinental clock comparisons down to one part in 10^{16} in frequency. Extending beyond this, however, is extremely challenging due to the limitations imposed by a microwave carrier frequency and noise in the RF detection chain. Proposed microwave links for the Atomic Clock Ensemble in Space (ACES) [42,43] and Space-Time Explorer and Quantum Equivalence Principle Space Test (STE-QUEST) [44] missions anticipate performance averaging down below one part in 10^{16} at long averaging times but are not discussed here. Similarly, some RF-over-optical methods, where an optical carrier is modulated with an RF signal, approach these levels of precision. As these methods are CW-laser-based, they are discussed briefly in Section 6. We also note for generating optical time scales and the redefinition of the SI second, connecting relative optical time measurements to local time scales, UTC(k), involves additional complexity not covered here [45].

In this review, we discuss work written at many different points in time and from different communities each with their own traditions in terms of language. Here, we have chosen a consistent set of terminology for ease of comparison across different approaches. For timing-frequency networks where there is asymmetry between nodes such as a single stable reference laser distributed to a distant location or a timing node that receives feedback for synchronization, we describe the sites as "local" and "remote." For cases where the two sides of the link are symmetric, we simply use "site A" and "site B." We also differentiate between "transfer" and "comparison" with "transfer" denoting frequency or time dissemination that can occur in both real-time and postprocessing whereas "comparison" is used strictly for comparing frequencies at two nodes (e.g., two optical atomic clocks).

2. METRICS FOR ASSESSING TIME AND FREQUENCY TRANSFER

Since the invention of the first mechanical clock, counting the revolutions (phase advance) of a given oscillator has been used to mark the passage of time. The accumulated (unwrapped) phase of an oscillator at a given reference plane and time t is $\theta(t)$ and the accumulated time measured by that oscillator, $x(t)$, is just the phase scaled by the nominal frequency of the oscillator, ν_0, i.e., $x(t) = \theta(t)/2\pi\nu_0$. Accumulated phase noise can then be introduced as $\theta(t) = 2\pi\nu_0 t + \delta\theta(t)$, where the first term is the expected phase advance during t and $\delta\theta(t)$ is phase noise. The corresponding accumulated time is then given by $x(t) = t + \delta\theta(t)/2\pi\nu_0$ with the second term capturing the timing noise. As we are concerned, for the most part, with relative time and/or phase, we have dropped the calibration terms necessary to connect this time to coordinated universal time (UTC) or some other time scale outside the timing network being assessed.

We can characterize the phase and timing noise by their power spectral densities (PSDs), $S_\theta(f)$ in units of rad^2/Hz or dBc/Hz and $S_x(f)$ in units of s^2/Hz, respectively [46–48]. The time instability as a function of averaging time is given by the time deviation (TDEV) through application of a filter function to the time PSD [46–48].

The instantaneous frequency $\nu(t)$ is simply the derivative of the phase advance, $\nu(t) = (1/2\pi)d\theta(t)/dt = \nu_0 + (1/2\pi)d\delta\theta(t)/dt$, where the first term is the nominal frequency, ν_0 and the second term is the frequency noise. The frequency noise is characterized by its PSD, $S_\nu = f^2 S_\theta(f)$, and its corresponding fractional frequency noise PSD, $S_y = S_\nu/\nu_0^2$. The two sample variance is then given by application of a filter function $H(f)$ to the PSD, $\sigma_y^2 = \int_0^\infty S_y(f)|H(f)|^2 df$, where differing choices of $H(f)$ return the Allan variance (AVAR) or modified Allan variance (MVAR) [46–48]. The filter function for the AVAR is given by $|H(f)|^2 = \frac{2\sin^4(\pi f\tau)}{(\pi f\tau)^2}$ while for the MVAR, $|H(f)|^2 = \frac{2\sin^6(\pi f\tau)}{(\pi f\tau)^4}$ where τ is the averaging time. When computed from a time series of data, use of overlapped samples and the corresponding overlapping algorithm to compute the AVAR produces a smaller uncertainty and mitigates the erroneous response to cyclic noise sources [46–48]. As a nonoverlapped AVAR is seldom used, we follow Ref. [47] and refer to the overlapped AVAR as simply the AVAR here. Throughout, this paper, we use the square-root of the Allan and Allan-like variances, the Allan deviation (ADEV), and modified Allan deviation (MDEV).

For the varying approaches to high-precision time and frequency transfer discussed in this review, the dominant character of the noise varies with Fourier frequency or averaging time. Random additive noise processes lead to the appearance of white noise in either phase or frequency. Colored noises, e.g., flicker phase noise, flicker frequency noise, or frequency random walk noise, typically arise from parametric noise processes such as thermal noise within an RF detection chain. Reference [47]

presents a detailed discussion of the expected scaling associated with the phase noise and fractional frequency PSDs as well as those associated with the AVAR and MVAR.

For intercomparison of different frequency transfer results, we will focus on the fractional frequency instability through the MDEV as this allows for differentiation of white and flicker phase noise. Some data in Fig. 8 –12 were originally presented as the ADEV and for these papers we have converted to the MDEV according to MDEV $\approx$ ADEV/$\sqrt{2}$, recognizing this is only strictly true for white frequency noise and only approximate for other noise types. For intercomparison of time transfer results, we focus on the TDEV that is related to the MDEV by TDEV = $\tau \times$ MDEV/$\sqrt{3}$, where τ is the averaging time as above. Since it is straightforward to go from a time transfer measurement to a frequency transfer measurement, we will also present the fractional frequency instabilities for intercomparison of frequency transfer results. When possible, we also present in the text assessment of systematic biases and total uncertainties.

For frequency measurements, frequency counters are a common tool with each frequency computed from a weighted average of phase measurements over a given gate time. Counters with dead time between samples will result in an increase in the instability (MDEV or ADEV) [49]. Frequency counters also make use of different weighting functions with common variants including: a uniform-weight average (pi-type counter), a triangular-weight average (lambda-type counter), and a parabolic-weight average (omega-type counter) [47,49–51]. The choice of weight function will affect the estimation of the frequency noise [47,49,51]. For instance, a lambda-type counter will reject the white phase noise associated with the triggering of the counter leading to a better noise estimate than that from a pi-type counter for systems dominated by white frequency noise [47]. Likewise, if the system under measurement is dominated by white phase noise over the averaging times of interest, an omega-counter will provide an optimal estimate of the noise [50]. With modern digital signal processing tools that allow for the rapid digitization and recording of phase measurements, similar considerations of weighting functions arise in the analysis of the data.

In all cases, phase noise must be measured relative to some reference and there are multiple strategies to isolate the contribution of the residual link phase noise from the reference phase noise. In some cases, the reference oscillators may have known instabilities that are well below the residual phase noise from the time or frequency transfer approach being tested. In such cases, the phase noise determined from measuring a frequency or phase offset between references reflects the phase noise of the transfer itself.

For higher-performing links the residual phase noise from the transfer is anticipated to be well below that of even state-of-the-art optical clocks. In this case, several choices exist to probe the phase noise of the transfer through changes in network topology. First, two spatially separated links can be run in parallel with the same reference oscillators and the results are compared in postprocessing. Second, a link may be folded to allow either for a common reference oscillator at both ends or to allow for a short out-of-loop verification link between two reference oscillators. Third, two separate approaches to time or frequency transfer may be used simultaneously over the same link between reference oscillators.

3. TIME TRANSFER VERSUS FREQUENCY TRANSFER

Many of the applications of precision optical time–frequency networks can be supported by both frequency transfer and time transfer, as shown in Fig. 3, due to the derivative-integral relationship between the two. Take, for example, the measurement

Figure 3

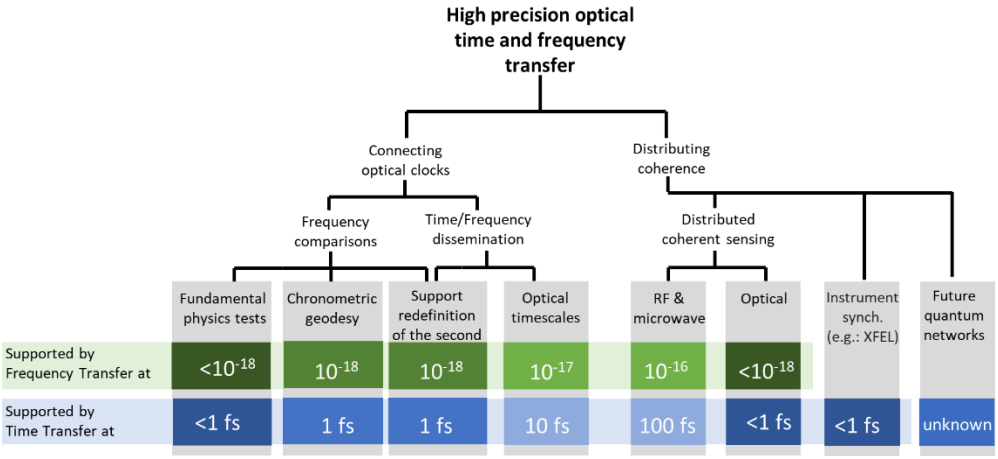

Taxonomy of applications for precision time and frequency transfer. Many of the applications above are built around frequency measurements such as determining frequency ratios between clocks of different atomic species (fundamental physics tests [6,13–15,17,18,52], metrics to support the redefinition of the second [45]) or frequency differences between clocks (chronometric geodesy [21] and tests of general relativity [5–12,19,20]). These frequency measurements can be supported by both frequency transfer and time transfer. Optical time scale generation also relies primarily on frequency measurements as the frequency of the flywheel local oscillator is compared and steered to the optical frequency standard [54–57]. In contrast, distributed coherent sensing requires both frequency reference distribution and instrument timing synchronization [23–30]. Optical distributed sensing such as astronomical optical interferometry will have more stringent time/frequency requirements than microwave-based sensing [58]. For large-scale infrastructure such as electrical grids and datacenters, GPS offers sufficient synchronization, but for high precision instruments such as X-Ray Free Electron Laser (XFEL) optical time synchronization is used to meet the more stringent timing requirements of attosecond physics [59]. The level of relative timing synchronization needed for future quantum networks is here marked as unknown as these requirements are an on-going research effort and are dependent on the selected network architecture: recent work suggests requirements might range from the tens of picoseconds [60,61] to less than 1 fs [62].

of the frequency ratio between separated optical clocks with different atomic species. The frequency ratio can be measured by transferring an optical frequency reference locked to one clock to the other site and measuring this optical frequency relative to the second clock. The frequency ratio can also be measured through time transfer where the derivative of the accumulated time offset (unwrapped phase) between the two sites gives the frequency ratio. References [52,53] show these two methods agree to within 6×10^{-19}. Similarly, time can be obtained from frequency measurements through integration over continuous measurement segments. (We note that in some sense a "frequency measurement" is often a series of derivatives of phase measurements each made over an interval set by the averaging time, e.g., a 1-second gate time on a lambda-type frequency counter.)

In the presence of link interruptions, frequency measurements can no longer be used to determine time since the loss of signal introduces an unknown phase offset that cannot be determined from the frequency measurement itself (Fig. 4). In contrast, a time-based measurement can continue across a link interruption as long as the time offset accumulated during the link downtime does not exceed the nonambiguity range

Figure 4

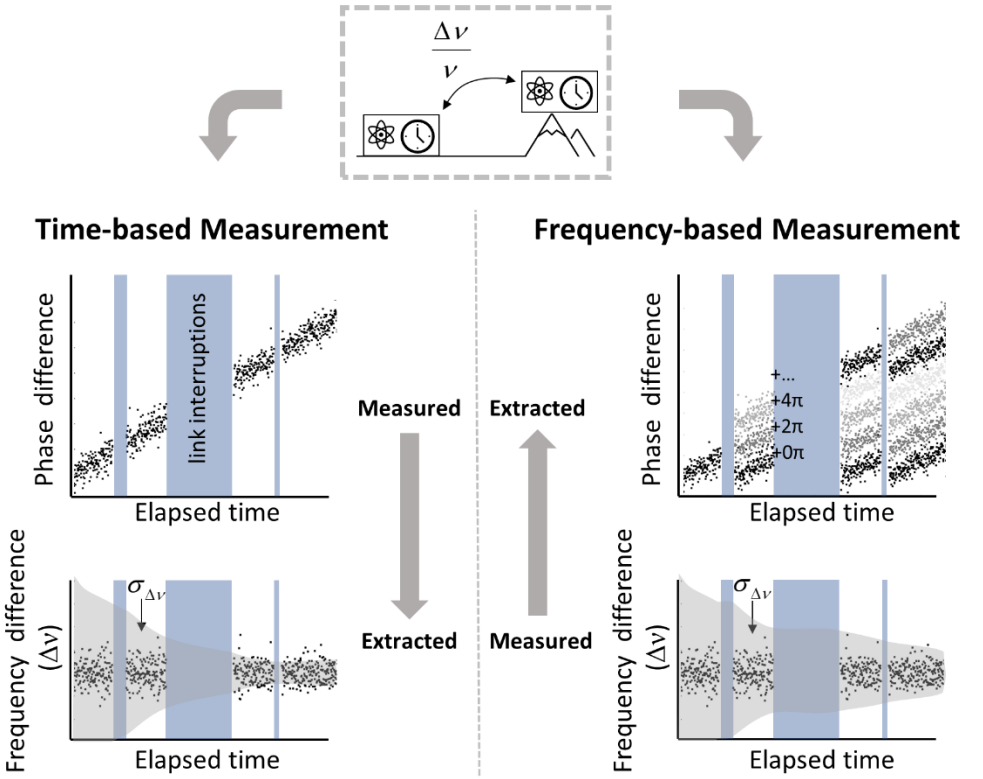

Difference between time- (phase-)based measurements and frequency-based measurements illustrated through a hypothetical gravitational redshift measurement made by observing the frequency difference between two clocks, $\Delta\nu$, across link interruptions (blue shaded regions). Time-based measurements measure the phase difference between the clocks, and this phase can be differentiated to determine the frequency difference. As shown here, a constant frequency difference would result in a ramped phase offset. Time-based measurements can maintain phase continuity across link interruptions and the uncertainty in the frequency difference, $\sigma_{\Delta\nu}$, indicated by the gray shaded region, is reduced immediately upon reacquisition of the signal, i.e., it effectively decreases across the interruption. This is analogous to Ramsey spectroscopy where precision increases with a longer noninteraction zone [65]. In contrast, frequency-based measurements directly measure the frequency difference, and the phase is extracted through integration. Across link interruptions, however, an unknown phase offset is introduced: only uninterrupted measurement periods are considered phase-continuous. For determining the frequency difference, the uncertainty, $\sigma_{\Delta\nu}$, is not reduced immediately upon signal reacquisition assuming the measurement is SNR-limited, i.e., it remains constant across the interruption.

of the timing signals. Depending on the technique, this nonambiguity range is typically nanoseconds to milliseconds. For example, comb-based optical time transfer with 200 MHz repetition rate combs will have a nonambiguity range of 5 ns whereas use of a pseudorandom binary sequence on an optical carrier can offer a nonambiguity range of 1 ms or more [63,64]. For applications that only seek to transfer frequencies but in the presence of link intermittencies, starting from time transfer can result in more robust operation.

While time transfer offers a continuity advantage for links with persistent intermittencies, frequency transfer techniques offer the advantage of higher precision due to using the optical carrier directly and oftentimes less complexity, though complexity clearly

grows for large-scale fiber networks. In addition, as fiber-based frequency transfer has matured, link reliability and uptimes have increased. Reference [66] used 680 km of active telecommunication fiber carrying data to transfer frequency at the 1.7×10^{-20} level with uptimes of >99.9% over 5 days. On longer time scales, Ref. [67] showed uptimes on the order of 60–75% for 2 years and ~85% for 6 months for various links of length 22–1410 km in the REFIMEVE+ (Réseau Fibré Métrologique à Vocation Européenne) network in Europe. The authors of Ref. [67] anticipate uptimes >90% over long time scales will be possible in coming years with further automation and engineering (see Section 8.1c). With nearly 100% uptime, fiberoptic links would offer the possibility of performing time transfer over reasonable durations. It is less clear if free-space links with spans greater than a few tens of kilometers will reach the same level of uptimes and lack of cycle slips.

For cases where time transfer is not strictly necessary (e.g., frequency comparison between two atomic clocks), link intermittencies still impact the uncertainty associated with a frequency transfer link. Reference [68], however, showed that careful replacement of missing data with simulated noise allows for calculating long-term stabilities with uncertainties that can support clocks at the level of $<10^{-18}$. The authors found this to be true for missing data caused by both the link itself and clock downtime.

4. CONSIDERATIONS AFFECTING TIME OR FREQUENCY TRANSFER TECHNIQUES

Here, we review several key considerations that affect time or frequency transfer links (see also Fig. 5). First, we discuss the effect of environmental noise on time–frequency transfer and how this leads to the requirement of at least partial reciprocity. Second, we discuss sources of potential signal distortion due to dispersion and nonlinear effects. Third, we discuss the effects of loss, signal fades, and link disruptions and the implications for increasing the span of an optical timing network. Finally, we briefly touch on the considerations of platform motion.

4.1. Environmental Noise Sources and the Requirement for Partial Reciprocity

Precision optical time–frequency transfer, regardless of specific technique, requires links that are at least partially reciprocal: light must travel bidirectionally through the link to measure or cancel the link-induced phase noise. Without leveraging the reciprocity, achieving a 10^{-16} relative frequency instability would require knowledge or control of all link-induced Doppler shifts to 30 nm s^{-1}. To achieve 1 ps relative timing would require knowledge or control of the optical path length to better than 300 μm in air. To support state-of-the-art optical clocks with 10^{-18} level instability and subfemtosecond timing, these requirements drop to control below 0.3 nm s^{-1} and 300 nm, respectively. For almost all timing networks, this level of stability is not achievable with one-way links due to the presence of environmental noise sources.

For optical transfer over both fiberoptic and atmospheric free-space connections, temperature and relative humidity fluctuations result in index changes that lead to optical path length fluctuations. For standard telecommunications fiber designed for 1550-nm light, a 1°C temperature change leads to one part in 10^5 optical path length change [69] and a 1% change in relative humidity leads to one part in 10^6 path length change [70]. Even nominally "free-space" links will contain short stretches of optical fiber that will be subject to these same temperature- and humidity-dependent length changes. In addition, for a free-space link with light at a 200-THz carrier frequency, a weather-driven 1°C temperature change will lead to 2 parts in 10^7 fractional optical path length change and a 1% change in relative humidity will lead to a 2 parts in 10^9 path length change [71]. Fortunately, most temperature and relative humidity fluctuations occur on relatively slow time scales associated with heating, ventilation,

Figure 5

a

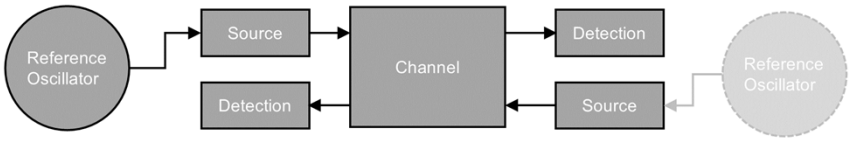

b

Sub-system	Options				
Reference oscillator	**Microwave oscillator**	**Microwave clock**	**Optical oscillator** e.g. cavity-stabilized laser	**Intermediate-performance optical clock**	**State-of-the-art optical clock**
Source	**CW laser** *Considerations*: Time transfer versus frequency transfer, phase continuity	**Pulsed laser** *Considerations*: Stability, non-ambiguity range	**Optical frequency comb** *Considerations*: locking technique, non-ambiguity range		
Channel	**Fiber** *Considerations*: Loss and amplification, stimulated Brillouin and Raman scattering, self-phase modulation, cross-phase modulation, group velocity dispersion, vibration, thermo-optic effects, polarization scrambling, fiber or channel availability (sections 4.1-4.3)	**Free-space** *Considerations*: Loss, link disruptions and scintillation, atmospheric optical turbulence, platform motion, group velocity dispersion (sections 4.1-4.4)			
Detection	**Direct** *Considerations*: precision	**Linear optical heterodyne** *Considerations*: local oscillator source, differential dispersion,	**Nonlinear** (balanced optical cross-correlation) *Considerations*: nonlinear medium, received power requirements		
Techniques	**Fiber-based frequency transfer (6.1):** CW laser + fiber channel + linear optical heterodyne detection **Fiber-based time transfer (6.2):** CW laser + fiber channel + direct detection **Fiber-based frequency comb time transfer (6.3):** Optical frequency comb + fiber channel + nonlinear detection **Free-space pulsed time transfer (7.1):** Pulsed source + free-space channel + direct detection **Free-space frequency transfer (7.2):** CW laser + free-space channel + linear optical heterodyne detection **Free-space frequency comb time transfer (7.3):** Optical frequency comb + free-space channel + linear optical heterodyne detection				

Considerations in time–frequency transfer. (a) The fundamental building blocks of an optical time–frequency transfer system are the reference oscillator, the optical source, the channel, and the detection scheme. The transfer system can be used for time–frequency dissemination, requiring only one reference oscillator, or for time–frequency comparisons that require two oscillators. (b) Table breaking down the available options for the building blocks shown in (a), implementation considerations associated with each building block, and how these building blocks are put together into the techniques described in this paper. Relevant sections are noted in parentheses.

and air conditioning (HVAC) cycle times, diurnal weather patterns or longer-term weather shifts. As a consequence, use of a link that is reciprocal on these time scales allows for cancellation of the optical path length changes even for long distance links where feedback bandwidths are limited to a few hertz at most due to propagation delays, as described in Section 6.1a.

In the case of a free-space link, in addition to the slowly varying fluctuations due to changing weather patterns, the faster index fluctuations of clear air turbulence also lead to optical path length fluctuations as well as scintillation, beam wander, and wavefront aberrations [72–74]. These turbulence-driven optical path length fluctuations, also referred to as piston noise, place a limit on the order of 1×10^{-15} in fractional frequency stability for optical signals with carrier frequencies of the order of 200–300 THz transmitted across one-way free-space links of a few kilometers [75,76]. For future ground-to-space links, the piston noise contribution is expected to be similar. While a ground-to-space laser link will be longer than a terrestrial link, the total integrated turbulence will be similar as turbulence is strongest close to the ground and then rapidly weakens due to the exponential decay of atmospheric pressure through the troposphere [77–79].

In the case of fiberoptic links, acoustic noise also plays a significant role in inducing path length fluctuations through the strain-induced variation in the fiber index. Indeed, multiple researchers have now used the dominance of the acoustic noise over the laser noise at key Fourier frequencies to build exquisite sensors for geophysics networks [31,80,81]. The acoustic noise will be the dominant source of noise up to a cutoff frequency ranging from a few kilohertz to a few tens of kilohertz. Up to that cutoff frequency, the resulting phase noise PSD of a laser propagating through an optical fiber will follow a white frequency noise power law: $S_{env} \simeq h_{env} L f^{-2}$ where f is the Fourier frequency in hertz, L is the length of the fiber in meters, and h_{env} is the magnitude of the environmental noise in rad^2·Hz/m [82,83]. Acoustic environments can vary dramatically with values of h_{env} ranging from 5×10^{-4} rad^2 · Hz/m to 0.2 rad^2 · Hz/m [82,84,85]. While acoustic noise at Fourier frequencies below the measurement rate and the feedback bandwidth can be canceled through bidirectional propagation of the optical signal, bandwidth limitations coupled with harsh environments may set the limit on the achievable fractional frequency instability as discussed in Section 6.

4.2. Potential Signal Distortions from Nonlinearities and Dispersion

Some of the time and frequency transfer approaches discussed in the following rely on accurate detection of the arrival time of an optical pulse. For shot-noise-limited detection, the precision with which the arrival time of a pulse can be measured scales as τ_p/SNR where τ_p is the pulse width and SNR is the signal-to-noise ratio. In addition, detection of the pulse arrival times may rest on the assumption of a symmetric pulse shape that follows a Gaussian or hyperbolic secant profile.

The propagation of an optical pulse through an optical fiber can be described, in a reference frame traveling at the group velocity, by the nonlinear Schrödinger equation in which the group-velocity dispersion (GVD), pulse power, pulse width, and the nonlinearities of the fiber all combine to determine the evolution of the pulse as it propagates [86,87]. The fiber nonlinearity can give rise to self-phase modulation (SPM) or in the case of overlapping pulses, cross-phase modulation (XPM). SPM can lead to unwanted distortion of the pulse shape through the self-steepening of the pulse leading to a bias in the measured pulse arrival times. Spectral broadening arising from the nonlinear index of refraction of the fiber at high peak powers can also reduce heterodyne efficiency between pulses and thus precision in systems that rely on optical heterodyne detection against a local oscillator. Even for nominally free-space approaches, the presence of small fiberoptic sections to connect to free-space optical terminals contain enough fiber for nonlinearity to be problematic especially in the case of high peak powers. For pulses in long fiber links, the nonlinear index provides a mechanism for pulse power fluctuations to manifest as optical path delay changes and it can also disrupt link reciprocity if pulse powers are not balanced for each direction.

The GVD and higher-order dispersion terms can result in signal distortions that limit the achievable frequency or time transfer precision. Standard single-mode fibers that transmit light around 1.5 μm, such as Corning SMF-28, have anomalous dispersion with a dispersion parameter of $D_{fiber} \sim 16$ps/km/nm [87]. For a pulse with a 10-nm spectral bandwidth centered at 1.5 μm and an initial time-bandwidth limited pulse width of 350 fs, propagation through 10 m of a standard telecom fiber will lead to a significantly broadened, or chirped, pulse duration of 1.6 ps.

Use of specialized dispersion compensating fibers (DCF) [88,89] to balance out the dispersion of standard telecommunications fibers can allow for the transmission of optical pulses without distortion as in the time transfer demonstrations of Ref. [90,91]. One limitation in the use of DCF is that it may not suppress third-order dispersion

that can then lead to a lingering asymmetric pulse broadening. Another early approach developed for optical fiber communications is the use of a programmable pulse shaper in addition to DCF for the transmission of subpicosecond pulses over kilometers of fiber to handle the third-order and higher dispersion effects [92].

Often in the case of optical heterodyne detection, it is the total differential dispersion between the signal and local oscillator pulses that matters, and thus careful balancing of fiber lengths can lead to an unchirped transform-limited heterodyne signal even if the underlying pulses are chirped. This balancing can be particularly useful for approaches where most of the pulse propagation takes place in air as $D_{air} \simeq -5\text{fs/km/nm}$ for a pulse centered at 1.5 μm. The differing sign coupled with the 3200-fold smaller magnitude of the dispersion parameter for air over fiber allows for the addition of meters of fiber leading up to free-space optical telescopes to balance the GVD from many kilometers of air, e.g., 3 m of optical fiber compensates for the dispersion of 10 km of air. Note, this only compensates for the second-order dispersion (GVD). When combining these precompensated over-the-air pulses with fiber-bound local oscillator pulses, third-order dispersion must be either negligible or equal for both pulse paths to generate an unchirped transform-limited optical heterodyne signal.

When light propagates through fiber, stimulated Raman scattering and stimulated Brillouin scattering (SBS) can arise [86,87]. Here, Raman scattering results from the interaction between the light and optical phonons associated with vibrational transitions of the glass and its dopants. This leads to loss for narrowband systems, and spectral distortions and cross talk for broadband systems. SBS arises from the interaction of light with stimulated acoustic waves in the fiber. This leads to frequency shifts on the order of 10 GHz and, thus, even relatively narrowband systems can see spectral distortions and cross talk from these shifts. Interestingly, SBS can also be the foundation of high-gain bidirectional amplifiers for CW optical frequency transfer [93]. As with Raman scattering and SBS, four-wave mixing in optical fibers can led to cross talk when fiber lengths exceed tens of kilometers and input powers exceed 1 mW [87]. However, for approaches which rely on an extremely narrowband detection of a heterodyne signal, four-wave mixing results only in slightly increased loss as any cross talk will be outside the detection filter bandwidth.

Unlike environmental noise, the nonlinear effects and linear dispersion cannot be removed through use of a partially or fully reciprocal link. As a consequence, the choice of time–frequency transfer approach must factor in the transmission medium(s) and span in order to achieve the desired levels of precision and accuracy.

4.3. Effects of Loss, Signal Fades, and Link Disruptions

Whether over fiber or free-space, loss is a significant concern especially for long-distance links. For fiber links, loss arises both from the inherent fiber loss, e.g., 0.2 dB/km for 1.5 μm light, and the losses associated with interconnections at various patch panels. This latter source of loss can completely dominate the loss budget for fiber links that span hundreds of meters to kilometers. The former source of loss is primarily due to Rayleigh scattering in the fiber, the magnitude of which can range from 0.12 to 0.18 dB/km for a wavelength of 1.5 μm [87]. For wavelengths closer to 1.4 μm, the loss per kilometer is elevated and approaches 1 dB/km due to the OH ion absorption peak at 1.37 μm [87]. While the fiber links reviewed here make use of silica fibers designed for optical communications at 1.5 μm, future links could make use of fibers constructed from fluoride glasses such as ZrF_4–BaF_2–LaF_3–AlF_3–NaF (ZBLAN) which could exhibit losses of as low as 0.01 dB/km at a 2.5 μm wavelength [94]. To overcome both the interconnection and intrinsic losses of fiber links, amplification through bidirectional amplifiers that maintain link reciprocity is possible.

Many CW-laser-based approaches rely on heterodyne detection of the CW laser light transmitted across a fiber link with a local CW laser. In this case, polarization wander can directly lead to loss of signal amplitude and thus a link disruption. Fortunately, the polarization state wander is slow enough that corrections can be applied. While one early demonstration involved manual hourly polarization adjustments [82], later work such as Ref. [95] used microcontrollers to automatically measure and optimize the heterodyne signal. Recently, automated polarization control was a key element in achieving an uptime of 75% over one link and 66% over a second link for 2 years of continuous operation [67].

For free-space links, additional loss arises from any mismatch between the received beam size and receiver aperture size that can be induced by diffraction or atmospheric turbulence [74]. Atmospheric turbulence also causes phase-front distortions limiting the coherence length across the beam and, thus, the aperture over which the light can be coupled into a single-mode fiber, as required for heterodyne detection against a local oscillator and to ensure link reciprocity. Unlike in the fiber case, amplification along the path is not possible for free-space links and thus the total link loss will place a limit on the range of free-space systems.

All links will, at least occasionally, suffer from disruptions or signal fades. For fiberoptic links, interruptions may be caused by hardware failures such as an amplifier or regeneration station failing or a fiber breaking. As discussed, increased loss from changes in fiber strain or insufficient signal-to-noise ratio for detection due to polarization wander may also cause link interruptions. For free-space links, short duration interruptions will occur frequently due to turbulence-driven scintillation while precipitation, fog, or dust can increase absorptive and scattering losses leading to signal fading. The frequency and duration of these signal fades will impact the choice of approach.

4.4. Platform Motion

Using free-space techniques to transfer time to an aircraft or satellite means having to contend with significant platform motion. For ground-to-aircraft links, relative motion is expected to be on order of $10–10^2$ m s^{-1}. While a constant velocity of 100 m s^{-1} has straightforward solutions such as a compensatory carrier frequency shift or dynamically shifting the RF filter frequencies to maintain heterodyne detection in the presence of Doppler shifts, the acceleration and jerk associated with any aircraft's trajectory will require more sophisticated broad bandwidth filters, measurement of instantaneous path lengths and velocities, tracking filters, and real-time adjustment of carrier frequencies. In addition, with path lengths of at most a few hundred kilometers, ground-to-aircraft links require a nearly negligible point-ahead angle, which is the angle between the uplink and downlink beams needed due to movement of the target and the finite speed of light.

For ground-to-space links targeting a low Earth orbit (LEO) the relative closing velocities could swing from 6000 to −6000 m s^{-1} in approximately 5 minutes and the associated accelerations and jerks will require significant relativistic corrections [96,97]. The potential breakdown in reciprocity is also a concern due to the combination of high relative velocity and long distance. This breakdown in reciprocity, termed anisoplanatism, is due to the uplink beam passing through different turbulence than the downlink beam. Theoretical [77,98] and ground-based experimental investigations [99] have explored the effect of turbulence anisoplanatism on optical time transfer. These studies find the achievable timing precision will be limited at short averaging times due to differential phase noise on the uplink versus downlink, but that the effect is bounded to a few femtoseconds at long time scales.

For ground-to-geosynchronous orbit (GEO) links, the relative motion is quite modest and on the order of tens of meters per second. Encouragingly, terrestrial demonstrations have shown compatibility with this level of motion using both a CW-laser-based frequency transfer approach [100,101] and a comb-based time transfer approach [102,103].

Intrasatellite-cluster links should also see low relative velocities of 1 m s^{-1} or less since these satellite clusters are often deployed together in nearly identical orbits. For example, the tetrahedron formation of the Magnetospheric Multiscale Mission cluster [104] requires tight station-keeping to maintain its shape. Likewise, the station-keeping of the TerraSAR-X add-on for Digital Elevation Measurement (TanDEM-X) mission results in less than 1 m s^{-1} along-track relative speeds of two satellites in a helical configuration [105]. In this case, terrestrial solutions that work over 10-km-scale ranges should be directly applicable with the added benefit of no atmospheric turbulence. For these clusters, the major constraint may be the multiplexing needed to perform timing and ranging between multiple satellites with different trades in loss, system complexity, and size, weight, and power (SWaP) for temporal versus spatial multiplexing.

In contrast, intrasatellite-constellation links could again see the same complications of high relative motion of thousands of meters per second since these satellites follow distinct orbits and are often deployed independently (e.g., the GPS satellite constellation). As for intracluster links, intraconstellation links conveniently experience no atmospheric turbulence. This leads to the possibility of interesting architectures that rely on ground-to-GEO links in combination with GEO-to-MEO (medium Earth orbit), GEO-to-LEO, and LEO-to-LEO crosslinks to separate the effect of atmospheric turbulence and high loss from the effect of significant motion. One example of an intrasatellite-constellation architecture with optical crosslinks is the proposed Kepler mission [106].

5. OPTICAL FREQUENCY COMBS AND THEIR ROLE IN TIME AND FREQUENCY TRANSFER

The optical frequency comb [107,108] has become integral to the success of optical time and frequency transfer. While the comb has become nearly ubiquitous in frequency metrology, we can roughly divide its use into three roles. First, a comb can be used to coherently connect optical frequencies spanning hundreds of terhertz. Second, detection of the comb pulses on low-phase-noise detectors generates microwave frequency signals that are phase coherent with the comb's optical frequencies. Third, the pulsed nature of the comb can be used to generate labeled time markers. We detail these three roles of the frequency comb below before presenting a brief overview of the frequency comb technology and a few frequency comb equations to make the discussions of Sections 6–8 more comprehensible. Two recent reviews of optical frequency combs [107,108] provide much more extensive background. In addition, Refs. [109,110] present detailed discussions of the varied noise processes associated with frequency combs.

Optical clock transitions, chosen for their narrow linewidths and low systematic shifts, are not always at convenient wavelengths for transmission directly over long distance fiberoptic or free-space links; see Table 1. Frequency combs are the intermediate between the clock wavelengths and transmission wavelengths since a frequency comb can be phase-locked to the clock laser, often at visible wavelengths, and can generate phase coherent near-infrared light that can be used for time and frequency transfer.

Table 1. List of Optical Secondary Representations of the Second[a]

Transition	Frequency (THz)	Approximate Wavelength (nm)
^{87}Sr neutral atom $5s^2\ ^1S_0$–$5s5p\ ^3P_0$	429.2280042298730	698.4
$^{88}Sr^+$ ion $5s\ ^2S_{1/2}$–$4d\ ^2D_{5/2}$	444.7790440954865	674.0
^{171}Yb neutral atom $6s^2\ ^1S_0$–$6s6p\ ^3P_0$	518.2958365908636	578.4
$^{171}Yb^+$ ion $^2S_{1/2}$–$^2F_{7/2}$	642.1214967726450	466.9
$^{171}Yb^+$ ion $6s\ ^2S_{1/2}$–$5d\ ^2D_{3/2}$	688.3589793093083	435.5
$^{199}Hg^+$ ion $5d^{10}6s\ ^2S_{1/2}$–$5d^96s^2\ ^2D_{5/2}$	1064.7216098991453	281.6
$^{27}Al^+$ ion $3s^2\ ^1S_0$–$3s3p\ ^3P_0$	1121.0153932078573	267.4
^{199}Hg neutral atom $6s^2\ ^1S_0$–$6s6p\ ^3P_0$	1128.5752908081544	265.6

[a]As of 2017 from Ref. [111]. Many atomic transitions that are appealing for optical timing networks are ill-suited for direct use in optical frequency transfer or optical time transfer necessitating the use of optical frequency combs.

Prior to the first demonstrations of optical combs in 2000 [112–114], extensive time and effort was required to create multiple stage frequency chains linking different optical frequencies or linking optical and microwave frequencies. For instance, the calcium intercombination line was measured against the primary cesium standard using an extensive frequency chain composed of ten lasers and multiple microwave oscillators [115]. Almost immediately after the demonstration of the optical frequency comb, a single comb replaced the entire frequency chain and was used to measure the same calcium intercombination line against the cesium standard [116].

In addition to phase-coherently connecting a broad range of optical frequencies, e.g., a clock laser frequency to a telecommunications frequency, optical frequency combs' phase coherent connection of optical and microwave frequencies can turn them into low-phase-noise microwave generators in an approach known as optical frequency division. Fully stabilizing a comb to an optical reference transfers the exquisite fractional frequency stability of the optical reference to the comb pulse train. By directly detecting this pulse train with high fidelity, it is possible to generate ultraquiet microwave signals [117–119]. For example, at Fourier frequencies above 1 kHz, Ref. [119] achieved a phase noise of −173 dBc/Hz on a 12-GHz carrier. These ultralow-noise microwave signals ranging from megahertz to hundreds of gigahertz can then serve as local oscillators for millimeter-wave sensing [24,30] or support improved Doppler radar sensitivity among other applications.

The optical frequency comb also plays a critical role in optical time transfer through the generation of labeled time markers, e.g. the ticks of the clock. For optical atomic clocks, directly labeling and counting of the passage of fringes at petahertz rates to generate a local time scale is challenging and complicated by a nonambiguity range of only a few femtoseconds or less. However, directly labeling and counting the output pulses of a frequency comb phase-locked to the clock laser can be straightforward for repetition rates spanning 100 MHz to 10 GHz. This is analogous to the generation of the 1 pulse-per-second output common in microwave-based timekeeping, such as is produced via GNSS albeit at rates of 100 pulses-per-microsecond to 10 pulses-per-nanosecond, made possible by using short optical pulses and modern electronics. These labeled time markers can be utilized both to generate a local time scale [120] as well as transmitted directly over optical fiber (Section 6.3) or free-space (Section 7.3) for time transfer. Another advantage of using the frequency comb output to generate a local time scale is that the rate of this can be fine-tuned through the choice of comb locking parameters rather tuning the reference oscillator output directly.

Figure 6 provides a high-level sketch of the outputs of a frequency comb in both the time domain and frequency domain. The output of a frequency comb can be written as a function of time, t, as the sum of pulses with electric field E, labeled by integer k,

Figure 6

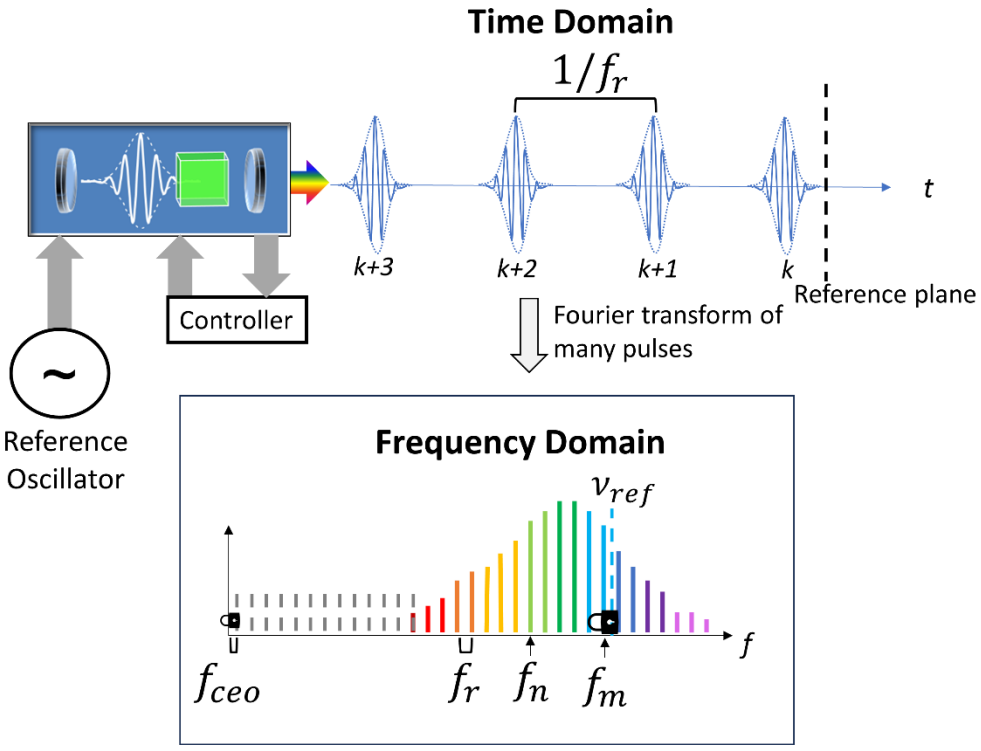

Frequency comb constructed from a laser that is stabilized (controlled) such that it outputs a train of pulses with a well-defined repetition period $1/f_r$ and a well-defined phase relationship between each pulse. When tightly phase-locked, the output pulse train preserves the phase stability of the reference oscillator. A local time scale can be defined by the passage of each labeled pulse across a chosen reference plane: a fixed point in space such as a beam combiner or detector face. In the frequency domain, this coherent pulse train results in a broad spectral envelope with underlying narrow linewidth comb modes (teeth) spaced by the repetition rate, f_r. Here f_n is the frequency of the nth comb tooth, whereas f_m is the comb tooth locked to the optical reference frequency, ν_{ref}, in one type of locking scheme.

with repetition frequency, f_r,

$$E(t) = e^{-i\theta} \sum_k E_k(t - x),$$
$$E_k(t) = e^{-ik\theta_{ceo}} A(t - k f_r^{-1}), \tag{1}$$

where θ is an arbitrary phase offset, x is an arbitrary time offset, θ_{ceo} is the carrier-envelope offset phase, and A defines the pulse amplitude. (Both θ and x can be chosen and controlled through the comb stabilization process as discussed in the following.) Note that the arbitrary phase offset, θ is distinct from the carrier-envelope offset phase, θ_{ceo}, as the latter is the relative carrier-to-envelope phase advance per pulse thus its appearance in Eq. (1) as $k\theta_{ceo}$. Through the Poisson sum formula, the output of the comb can also be written as

$$E(t) = f_r e^{-i\theta} \sum_n \tilde{A}_n e^{-i2\pi f_n (t-x)}, \tag{2}$$

where n is the index of the comb tooth with complex amplitude $\tilde{A}_n$ at frequency $f_n = nf_r + f_{ceo}$ where the carrier-envelope offset frequency $f_{ceo} \equiv (2\pi)^{-1}\theta_{ceo} f_r$. These equations hold independent of the method of stabilizing the frequency comb.

To fully stabilize the output time, x, and phase offset, θ, of the comb pulses, there are three distinct approaches: (i) phase-locking the repetition frequency, f_r, and the carrier-envelope offset frequency, f_{ceo}, to a microwave reference; (ii) phase-locking the frequency of the mth comb tooth at frequency, f_m, to an optical reference and the carrier-envelope offset frequency, f_{ceo}, to a microwave reference; or (iii) phase-locking the mth and pth comb teeth at frequencies, f_m and f_p, to two optical references. For (i) and (ii), generation of the f_{ceo} signal with sufficient SNR is one of the major challenges. As the carrier-envelope offset frequency, f_{ceo}, is the frequency of the comb mode closest to DC, it is outside the spectral envelope of the comb's output and requires nonlinear optics, e.g., $1f$–$2f$ frequency generation, to detect this RF frequency. In the literature, the term self-referenced is often applied to a frequency comb for which f_{ceo} is both detected and stabilized to a reference. (For more details see Refs. [107,108].)

Even in the context of *optical* time and frequency transfer, there will be occasions for which the comb will need to be stabilized to a microwave reference frequency, e.g., connection to a Cesium primary standard [121,122] or using a hydrogen maser as a flywheel in an optical clock network [52]. In this case, the repetition frequency of the comb is directly stabilized to the microwave reference frequency: $f_r = r_{ref} f_{ref}$, where f_{ref} is the microwave reference frequency, we use the symbol r to denote a rational fraction, and r_{ref} in particular is the rational fraction associated with the stabilization of the repetition rate with typical values ranging from 0.01 to 100. The carrier-envelope-offset frequency is also directly stabilized to the microwave reference frequency, i.e., $f_{ceo} = r_{ceo} f_{ref}$ with the typical values of r_{ceo} ranging from 0.01 to 100. This stabilization occurs through phase-locked loops that set the overall phase, θ, and the time offset, x, to arbitrary but fixed values. A paired set of equations for the repetition frequency, f_r, and the frequency of an arbitrary nth comb tooth, f_n, can then be written in terms of these rational fractions and the reference frequency, f_{ref},

$$\begin{aligned} f_r &= r_{ref} f_{ref} \\ f_n &= n f_r + f_{ceo} = (n r_{ref} + r_{ceo}) f_{ref}. \end{aligned} \tag{3}$$

In this configuration, it is apparent that any noise on the microwave reference will be multiplied up by the comb mode number n for the optical output at f_n used for optical time or frequency transfer. However, for a frequency ratio measurement between two optical clocks performed by comparing the beat frequencies generated by heterodyning two CW lasers referenced to the clocks against a common optical frequency comb, the contribution from the reference can still be negligible. For example, in the work of Ref. [52], the tens of terahertz optical span between CW lasers, led to an assessment of less than 1×10^{-20} contribution to the uncertainty budget from the hydrogen maser reference of the optical frequency comb.

As stated previously, the frequency comb can also be referenced directly to an optical reference, i.e., a CW laser. In many cases, this CW laser is itself either stabilized against an optical artifact, i.e., it is a cavity-stabilizer laser, or against an atomic transition. In this case, the carrier-envelope-offset frequency along with the comb tooth frequency, f_m, are stabilized where m is the tooth nearest the optical reference frequency at ν_{ref} (see Fig. 6). Depending on the reference frequency, additional nonlinear optical elements beyond those required for f_{ceo} generation may be required to expand the comb's spectral envelope such that the mth comb tooth has a nonnegligible amplitude as well. Both of these frequencies can be stabilized with respect to the repetition frequency: $f_{ceo} = r_{ceo} f_r$ and $f_m = \nu_{ref} - r_{ref} f_r$ where again we use the symbol r to denote a rational fraction with values typically ranging from −0.5 to 0.5. In this case, the repetition frequency itself is determined by these two frequencies, $f_r = (f_m - f_{ceo})/m$. In other words, the repetition frequency is set by the optical reference frequency.

As in the microwave reference case, the stabilization occurs through phase-locked loops. Note that use of a time-programmable frequency comb (TPFC) allows for the user-defined, variable choice of θ and x as opposed to the conventional arbitrary but fixed values [123]. Once phase-locked, we can again write a set of equations for the repetition frequency, f_r as well as the frequency of an arbitrary nth comb tooth, f_n in terms of only the optical reference frequency, ν_{ref} and two user-defined rational fractions, r_{ceo} and r_{ref},

$$\begin{aligned} f_r &= \frac{1}{m+r_{ref}+r_{ceo}}\nu_{ref} \\ f_n &= nf_r + f_{ceo} = \frac{(n+r_{ceo})}{m+r_{ref}+r_{ceo}}\nu_{ref}. \end{aligned} \tag{4}$$

The extremely large lever arm provided between the optical reference and repetition frequency, i.e., the value of m, underlies optical frequency division: the generation of quiet microwave signals such as in Ref. [117].

The strictest definition of self-referencing requires phase-locking f_m and f_{ceo} to frequencies generated from the repetition frequency, f_r, which is in turn defined through the phase-locking of the comb to the optical reference frequency, ν_{ref}. However, other choices can be made for the phase-locking frequencies if careful attention is paid to the book-keeping necessary for the specific application. If high mutual coherence between two combs in the optical domain is required, those two combs can have locking frequencies necessary to achieve a phase-lock to a free-running CW laser derived from a microwave reference. Measuring the repetition rates of both combs against that microwave reference can inform slow steering of the free-running CW laser to retain a connection to the microwave reference frequency. Another possible tool is to choose opposite signs but identical magnitudes for the locking frequencies, i.e., choice of r_{ceo} and r_{ref}. This causes the repetition frequency of the comb pulses to be independent of the locking frequencies; however, the optical carrier will still depend on the choice of carrier-envelope-offset frequency and, thus, the reference used to generate the locking frequencies.

The approach of phase-locking each of two comb teeth to a CW laser frequency to fully stabilize an optical frequency comb requires a single optical artifact, e.g., optical cavity, that in turn ties the two CW laser frequencies to one singular reference. This approach was used in an early demonstration of frequency-comb-based optical time transfer over the air [124] to demonstrate the limits of the comb-based measurement. Later work, such as Ref. [63], relied on self-referenced frequency combs phase-locked to an optical reference (see Section 7.3). Looking to the future, the use of microcombs [125] for time transfer (see the discussion in Section 7.3d) might be well-matched to this approach.

6. TIME AND FREQUENCY TRANSFER OVER OPTICAL FIBERS

6.1. CW-Laser-Based Frequency Transfer

Frequency transfer via the carrier frequency of a CW laser transmitted over a bidirectional fiberoptic link has seen many different demonstrations over the last 30 years reaching instabilities well below 10^{-18} [66,82,84,95,126–143]. Long distance (>1000 km) links connecting laboratories in Europe have been demonstrated using both amplified, single-span links where the entire link is stabilized together [137,138,141,142] and links with cascaded repeater stations with separate link stabilization [95,134,136]. In addition, laboratory-based demonstrations have shown the ability to simultaneously transfer frequency to multiple users in branched networks over links up to 50 km [139,140]. Recently, the focus of this mature technology has shifted from demonstrations of the fundamental principles to application support. This has resulted in links

with high-uptime operation over long distances, 10^2–10^3 km in length, for example in the work of Ref. [66].

The ability to transfer optical frequencies at 10^{-18} fractional frequency instability over fiber has led to a wide range of demonstrations. This includes a series of frequency ratio measurements between state-of-the-art optical atomic clocks [52,144–146] that are important steps toward the redefinition of the second [1,45]. These networks have also enabled exciting new tests of fundamental physics leveraging the extraordinarily low uncertainties possible with optical atomic clocks. For instance the frequency comparison of four optical clocks over fiber between the National Physical Laboratory (NPL) in the United Kingdom, Physikalisch-Technische Bundesanstalt (PTB) in Germany, and Systèmes de Référence Temps-Espace (SYRTE) in France leveraged the different velocities of the clocks in the inertial geocentric frame to test time dilation predicted by special relativity [32]. The ever-growing European fiber frequency transfer network was recently used to connect optical clocks to search for transient variations of the fine structure constant through variations in clock frequency ratios. In the absence of transients, researchers were able to add new constraints in the search for fine structure constant variations and topological dark matter [18].

When comparing the frequencies of optical atomic clocks that are separated in height, i.e., gravitational potential, chronometric geodesy becomes possible [10,147–149]. In a demonstration of the power of precise optical frequency comparisons between optical clocks, Ref. [10] was able to place a constraint on the α parameter that denotes the violation of general relativity ($\alpha = 0$ for no violation) to $(1.4 \pm 9.1) \times 10^{-5}$. This constraint is within a factor of four of the current lowest uncertainty of 2.48×10^{-5} that was made possible by the accidentally eccentric orbits of Galileo satellites 5 and 6 with a height difference of 8500 km [8]. The uncertainty of 9.1×10^{-5} on α also represents an improvement over the 14×10^{-5} uncertainty achieved by Gravity Probe A despite the fact that Gravity Probe A reached a maximum height of 10,000 km [150,151]. The strength of using optical clocks here can be seen from the fact that the measurement was possible with just a 450-meter vertical separation between clocks (the height of the Tokyo Skytree tower in Japan).

Precise frequency transfer over fiber has been used not only to compare two or more optical clocks but also in the dissemination of a stable frequency from one transmitting node to multiple receiving nodes, eliminating the need for multiple, expensive optical references. Distribution of precise RF signals over optical links, i.e., "RF-over-optical" transfer, can support radioastronomy telescope arrays such as the Atacama Large Millimeter Array (ALMA), the Square Kilometre Array (SKA), and the next-generation Very Large Array (ngVLA) amongst others [152–156]. Distribution of a single, stable frequency can also allow for a common VLBI reference to be distributed to remote antenna sites as in Ref. [30]. With sufficient infrastructure investment, stable frequency distribution of ~200 THz light can become a service of a national metrology laboratory such as in the REFIMEVE + project [66].

There are several techniques to transfer optical frequencies over fiber using CW lasers and these techniques can roughly be broken down into active, real-time fiber-noise-cancellation and noise removal in postprocessing using two-way measurements. Both techniques are described in detail in the following.

In general, time and frequency transfer over a fiber is an attractive solution any time an existing fiber network is available. It has the significant advantage of relatively high SNR and low likelihood of link interruption. The downside of this approach only arises if a fiber network is not available or available networks cannot support the requisite

two-way propagation of light. Typically, data networks operate in a unidirectional manner and can also be fragile. As such, it can be expensive to retrofit a network channel for bidirectional propagation and can at times be difficult to convince network owners to allow access. This approach can also suffer from the "last mile problem" common to fiber networks in which the optical fiber does not quite reach the end user's location. Importantly, it has been shown that data channels and frequency transfer can coexist on the same fiber [134].

6.1a. All-Optical CW-Laser-Based Active Fiber-Noise Cancellation

One of the most well-developed areas of time–frequency transfer is frequency transfer over optical fibers using the optical carrier with active fiber-noise cancellation. These active fiber-noise cancellation techniques require measuring and correcting for phase fluctuations across the link. To do this, a CW laser is sent from the local site, across the link, to the remote site as shown in Fig. 7(a). Upon arrival at the remote site, the light will have additional phase noise due to vibrations and temperature changes in the fiber link. We can write the phase accumulated on this one-way trip as $\phi_{forward}$. Part of this incident light is reflected back to the local site, accumulating phase $\phi_{backward}$, and is mixed with a local oscillator arm of the original transmission laser. In addition to accumulating phase across the link, the round-trip path also includes a double-pass through two acousto-optic modulators (AOMs), as shown in Fig. 7(a). The AOM at the local site is used for the active phase-noise cancellation. The AOM at the remote site provides an additional frequency shift that allows the remote site reflection to be easily separated from any other spurious reflections that may occur along the link. With double-passing, the final AOM induced shift on the return light is $2(f_{AOM1} + f_{AOM2})$. This frequency shift manifests as a phase ramp on the round-trip phase that is ignored in the following phase equations for simplicity.

The phase of round-trip light after the round-trip propagation time, T_{RT}, then is

$$\phi_{RT}(T_{RT}) = \phi_{ref}(0) + \phi_{forward} + \phi_{backward} + \phi_{AOM}(0) + \phi_{AOM}(T_{RT}). \tag{5}$$

The bandwidth of the actuator used in the cancellation, an AOM in this case, must be limited to at most $1/(2\pi T_{RT})$ allowing for the assumption that the last two terms are equal [158]. The measured phase difference between the round-trip and reference light is

$$\phi_{RT}(T_{RT}) - \phi_{ref}(T_{RT}) = \phi_{ref}(0) - \phi_{ref}(T_{RT}) + \phi_{forward} + \phi_{backward} + 2\phi_{AOM}. \tag{6}$$

The time-delayed phase difference of the underlying reference laser given by the first two terms on the right will cancel to a constant given a coherence time greater than T_{RT}. Finally, if we assume the noise on the forward and backward paths of the light are the same, $\phi_{forward} = \phi_{backward} = \phi_{one-way}$. The measured phase can then be simplified as

$$\phi_{RT} - \phi_{ref} = 2(\phi_{AOM} + \phi_{oneway}). \tag{7}$$

This phase error is used by a servo loop to adjust the AOM drive frequency to cancel the one-way phase noise. The performance of the noise cancellation is limited by the combination of the environmental noise present and the bandwidth of the servo control that is, in turn, limited by the length of the fiber span [82,159].

As mentioned in Section 4.1, environmental noise sources tend to result in a phase noise PSD of $S_{env} \simeq h_{env} L f^{-2}$ where f is the Fourier frequency in hertz, L is the length of the fiber in meters, and h_{env} is the magnitude of the environmental noise in rad^2·Hz/m. Assuming a high-SNR optical heterodyne signal, when the servo loop is activated, the

Figure 7

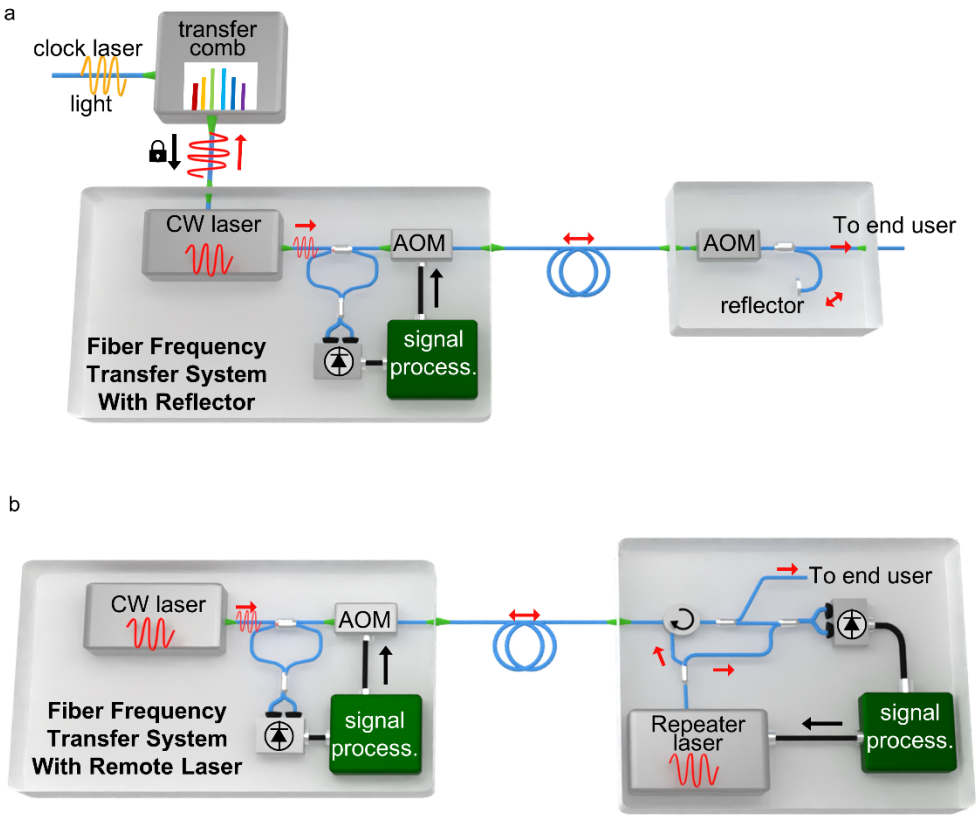

(a) Schematic of conventional fiber-noise-canceled link, also referred to as a "Doppler-canceled" link. Here a CW transfer laser is phase-locked to the clock laser light via a transfer frequency comb. This CW laser is then split into a local oscillator branch and a branch transmitted over the fiber. Detection of the phase noise accumulated due to propagation through the fiber is performed through detection of the heterodyne beat formed by mixing light reflected back across the fiber and the local oscillator with the nominal beat frequency set by the two double-passed AOMs. Phase-locking of this beat frequency through feedback to the local AOM allows for cancellation of the fiber link noise to achieve fractional frequency instabilities for the light delivered to the end user of less than 10^{-18}. This technique is implemented in Refs. [82,126–128,130,132,135,137–139,141,142]. (b) Variation on the fiber-noise canceled link that uses a repeater laser, phase-locked to the incoming transfer laser light, to return light to the local site. This method can be seen in Refs. [84,129,133,141,157].

one-way phase noise on the light to the end user has a resulting PSD of $a(2\pi f T_{prop})^2 S_{env}$ where $a \simeq 1/3$ and T_{prop} is the one-way propagation time of the light through the fiber [82]. As most environmental noise sources are relatively low frequency, this PSD will drop off far more rapidly above a cutoff frequency on order of a few kilohertz. As derived in Ref. [82], the resulting fractional frequency instability on the light that would reach the end user is given by $\sigma_{f_{cw}} = f_{CW}^{-1}\sqrt{8ah_{env}LT_{prop}t_{gate}^{-3/2}}$, where f_{CW} is the carrier frequency of the CW transfer laser and t_{gate} is the gate time of a high-resolution "Λ-type" frequency counter (see Fig. 7(a)). Note, as T_{prop} is proportional to the fiber length, the fractional frequency instability scales as $L^{3/2}$. For example, a 250-km link ($T_{prop} = 1.2$ ms) with fiber experiencing $h_{env} = 4 \times 10^{-3}$ rad$^2 \cdot$ Hz/m, as in Ref. [82], $f_{CW} = 200$THz, and $t_{gate} = 1$s, would result in a fractional uncertainty $\sigma_{f_{CW}} \simeq 3 \times 10^{-16}$ at 1-second averaging time, consistent with the data of Fig. 8(a).

Figure 8

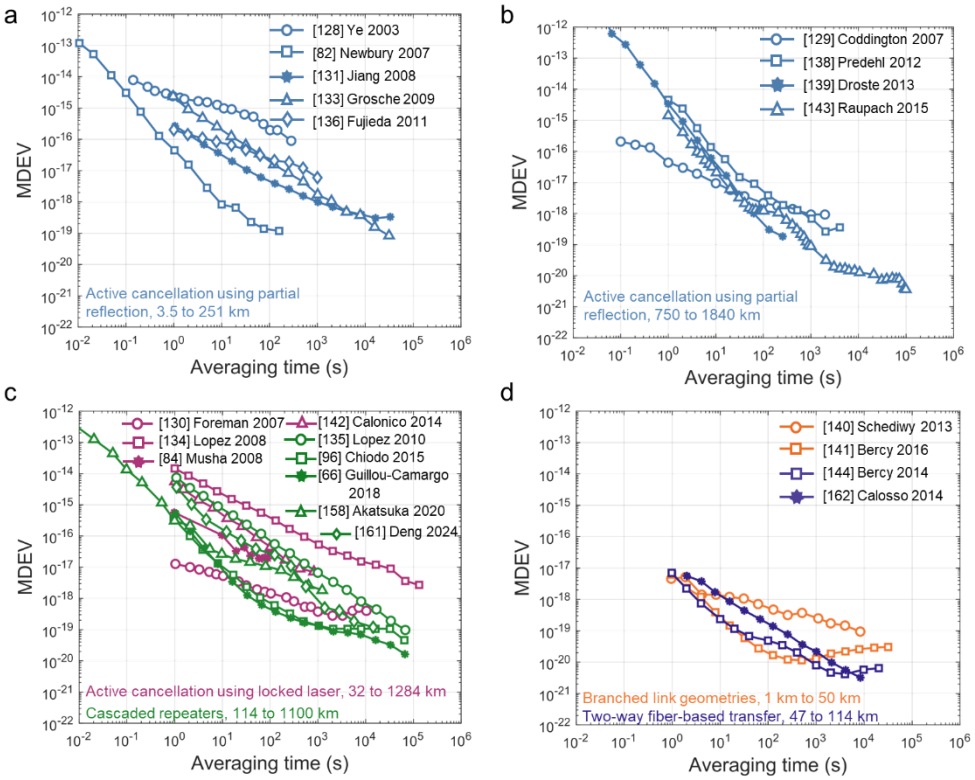

Comparison of fractional frequency instability of frequency transfer over fiber using CW lasers. (a) Frequency transfer results from the active noise cancellation method using a partial reflection from the remote site to correct the fiber phase noise at the local site. Links shown are <500 km. Data from Refs. [82,127,130,132,135]. (b) Same method as (a) but for links >500 km [128,137,138,142]. (c) Active noise cancellation by locking a laser at the remote site to incoming light and sending that laser back to the local site (purple) [84,129,133,141], and cascaded repeater method (green) [66,95,134,157,160]. (d) Results from branched link geometries (orange) [139,140] and two-way fiber-based frequency transfer (purple) [143,161].

Variations on this active noise-cancellation method exist. As described previously, an AOM actuator is used to adjust the phase of the optical carrier itself. Another variation involves phase-locking a laser at the remote site to the incoming light and then sending the phase-locked laser back across the link instead of using a partial reflection as shown in Fig. 7(b) [84,129,133,141,157].

For long-haul links, single-span schemes involving both bidirectional erbium-doped fiber amplifiers (EDFAs) and fiber Brillouin amplifiers achieved sub-10^{-18} fractional frequency instability [137,138,142]. Alternatively, cascaded repeater stations can be used to stabilize sections of a larger link separately [66,95,134]. These long-haul solutions preserve the SNR of the signals and thus lead to systems still limited by servo bandwidths rather than systems operating at a reduced precision due to loss of SNR. As was demonstrated in Ref. [157], cascaded repeater stations can also enable a low-fractional-frequency instability in the presence of elevated environmental noise, e.g., $h_{env} \simeq 0.2\ \mathrm{rad}^2 \cdot \mathrm{Hz/m}$, as the servo bandwidth is set by the propagation time for each individual segment. Similarly, Ref. [160] uses a repeater station topology across 972 km of fiber with an additional demonstration of a servo-free method of

phase correction using AOMs. Performance of these various techniques are shown in Fig. 8(a)–(d).

6.1b. All-Optical CW-Laser-Based Two-Way Fiber Frequency Transfer

Two-way frequency transfer techniques offer an alternative to the active noise cancellation described in Section 6.1a. Since the optical carrier is still used for the frequency transfer, two-way demonstrations have achieved instabilities well below 10^{-18} at long averaging times by canceling fiber noise in postprocessing [83,143,161]. This method works by sending stable lasers bidirectionally through a fiber link and measuring the phase between the incoming and local lasers at each site. These data streams are digitized, synchronized, and combined in difference to cancel the common fiber phase noise on the two data streams. Results from two-way frequency transfer are shown in Fig. 8(d).

6.1c. RF-Modulated CW-Laser-Based Frequency Transfer

Transmission of a CW laser or multiple CW lasers over an optical fiber can be employed not only for the transfer of the optical carrier phase or frequency but also a microwave phase or frequency. While the transfer of microwave frequencies in general is outside the scope of this review, in this section, we briefly touch upon two RF-over-optical techniques. These both involve the cancellation of fiber noise at levels similar to that of the all-optical frequency transfer discussed in Sections 6.1a and 6.1b. This distribution of microwave signals without degradation due to fiber noise over spans ranging from kilometers to hundreds of kilometers is of particular interest for the development of phased-array radio telescopes [131,152–156].

Modulation of the optical carrier with an RF tone is accomplished either through direct control of the laser [131,133] or through an external modulator [127,156]. Similar to the techniques of fiber noise cancellation discussed in Section 6.1a, either a portion of the modulated light is reflected back to the initial site or a second modulated laser signal is transmitted back to the initial site so that the round-trip fiber-noise-induced fluctuations can be measured and removed. In an early demonstration, a 1-GHz signal was distributed across a 6.9-km urban fiber link with an instability reaching 1×10^{-14} at 10,000 seconds of averaging [127]. Reference [133] demonstrated distribution of a 1-GHz signal across an 86 km urban fiber link with an instability of 2×10^{-18} at one day of averaging. Similarly, Ref. [131] demonstrated distribution of a 1-GHz signal across 114-km urban fiber link with instabilities reaching 6×10^{-18} at one day of averaging. The work of Ref. [156], in support of the future ngVLA, demonstrated stabilities of 2×10^{-14} over a 90-km urban network and also showed that if operation was restricted to the hours around midnight, the instability averages down to 1×10^{-16} illustrating the challenges of mitigating environmental noise in urban environments as discussed in Sections 4.1 and 6.1a.

In contrast to the direct modulation approach, a photomixing approach uses a second CW laser with a carrier frequency offset to generate the RF tone in optical heterodyne [152–155]. At the guide site, a guide and follower laser have carrier frequencies offset by the nominal desired RF frequency. Partial reflection of both the guide and follower lasers back from the remote site allows for detection of the heterodyne signal between the local copy of the guide laser and the reflected guide and follower lasers. This allows for feedback to correct for the detected fiber-induced phase noise. With this correction turned on, at the remote site, detection of the heterodyne signal on a photodetector produces the desired stable RF frequency. (Note, the follower laser can be replaced through use of a dual-parallel Mach–Zehnder modulator as in Ref. [153].) This photomixing approach is particularly appealing for starlike geometries for which there are many remote sites connected to one guide site.

Figure 9

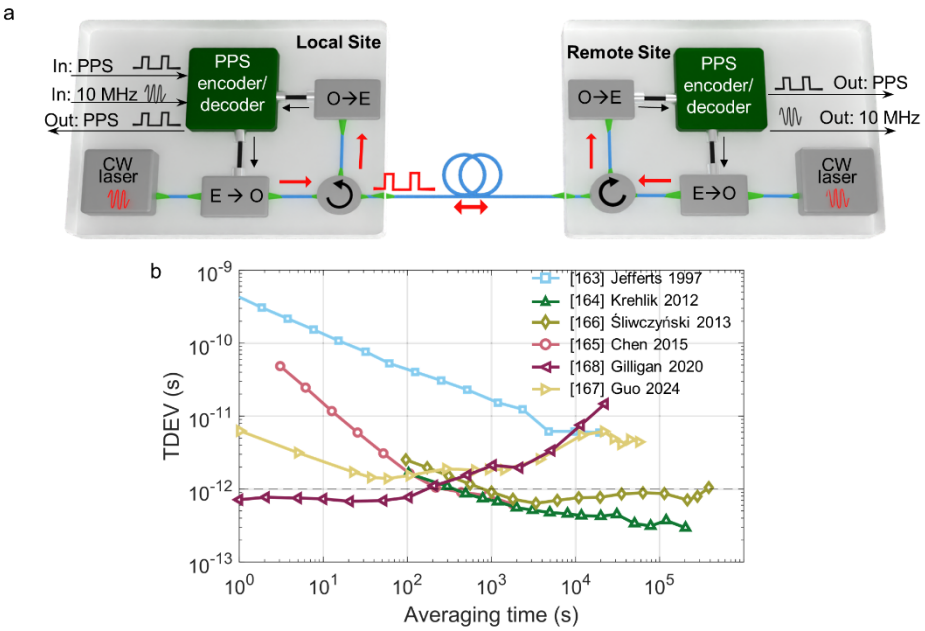

(a) Schematic of a modulated CW laser approach. (b) Representative TDEV curves demonstrating performance possible with two-way time transfer via a modulated CW laser. Data from Refs. [162–167].

Using the photomixing approach, Ref. [152] demonstrated that this could support the requirements of ALMA by demonstrating an instability of 2×10^{-12} at 1 second of averaging. At a day of averaging, Ref. [154] demonstrated an relative instability of 2×10^{-17} for the distribution of a 100-MHz signal over 50 km of fiber to two separate receivers. Reference [155] demonstrated that an instability of 1×10^{-16} could be attained in 20,000 seconds of averaging for the distribution of an 80-MHz signal over 310 km. Reference [153] demonstrated the distribution of an 8-GHz signal with an instability of 1×10^{-17} at 40,000 seconds of averaging over a 166-km urban fiber link.

6.2. RF-Modulated CW-Laser-Based Time Transfer

Use of a CW optical carrier to directly transfer time is limited due to the few femtosecond nonambiguity range that imposes a rigorous requirement on continuous tracking of the optical phase. In the limit of 100% link uptime, the all-optical methods for CW-laser frequency transfer could be used to continuously track phase and therefore perform time transfer. Reference [66] shows >99.9% uptime for a 680-km link over 5 days which nearly reaches this limit. For two optical frequency references with instabilities at the 10^{-17} level, however, even a 300-second interruption can lead to an accumulated time offset greater than 1 fs. Thus, to transfer time, an RF modulation of the optical carrier is currently required to track timing changes over intermittencies. Use of an RF modulation pattern instead of the optical carrier in turn results in worse timing precision. Most time transfer techniques using RF modulation do not reach our high precision metric of 1 ps while others reach 1 ps for a small subset of averaging times. A few demonstrations reach down to a few hundred femtoseconds at long averaging times. One such scheme of modulating the optical carrier is sketched in Fig. 9(a) with the instabilities achievable for this, as well as other similar approaches, illustrated by the data reproduced in Fig. 9(b).

An early demonstration implementing two-way time transfer using a telecommunications protocol (synchronous optical networking [SONET]) was able to achieve a instability on the order of 10 ps at long averaging times [162]. The work of Ref. [162] required very little bandwidth, just a single overhead byte per SONET frame, but only spanned 30 m of fiber. More recently, work has been done using two-way time transfer over urban fiber networks spanning 60 km [163] and 120 km [164], respectively. In this approach, an optical pulse-per-second (PPS) is generated through electro-optic modulation of a CW laser, and similar demodulation at the end of the link allows for the detection of the arrival times of the pulses. The difference of the timestamps recorded on both sites provides the time offset with the reciprocal time-of-flight fluctuations subtracted out due to the reciprocity of the fiber. The careful engineering of Refs. [163,164] has enabled subpicosecond TDEVs at averaging beyond 100 seconds, as shown in Fig. 9(b). A variation of this technique actively stabilizes the link through optical delay lines to reach PPS stability below 1 ps across 480 km [165,168]. To reach longer distances, Ref. [166] used repeater stations to show time transfer at the <2 ps level over 1829 km of fielded fiber. Relatedly, work making use of the White Rabbit protocol has reached instabilities below 10 ps over a wide range of averaging times [167,169] with a minimum TDEV of 800 fs over averaging times from 1 to 100 seconds [167].

6.3. Frequency-Comb-Based Time Transfer

As noted earlier, the pulse train of a fully stabilized optical frequency comb faithfully maintains the stability of a reference oscillator, and direct transmission of these pulses in a fiber offers an intriguing approach to time and frequency transfer. Early work showed that optical frequency combs could be used to transfer microwave frequencies at the 10^{-16}–10^{-17} level across fiber spans ranging from 6.9 km [170] to 86 km [171,172]. In these demonstrations, the optical frequency comb is locked to a microwave oscillator, such as a hydrogen maser, and detection of the pulses on a photodetector generates the microwave signals of interest in the form of the repetition rate or a harmonic of the repetition rate. In order to send the comb pulses across long spans of optical fiber, DCF is needed to manage pulse stretching and distortion while active phase compensation with fiber stretchers is used to reduce environmentally induced fiber noise. Reference [173] showed that optical detection of the fiber phase noise, as opposed to microwave detection, could further improve the transfer stability to better than 4×10^{-17} for the 80th harmonic of the repetition rate (8 GHz) and 4×10^{-18} for the optical modes. In this demonstration, the optical detection is performed through a heterodyne measurement between the round-trip reflection of the frequency comb across the link and a local copy of the comb that has been frequency shifted by an AOM. In a variation, Ref. [174] used an fiber-loop optical-microwave phase detector to measure phase noise across a 2.3-km link and canceled the noise with a PZT and delay stage reaching 10^{-18} level frequency transfer at 10^5 seconds.

An alternative optical detection technique, sketched in Fig. 10(a), first proposed in Ref. [175] and outlined in Refs. [90,91,176] is to combine the reflected comb pulses with a local copy of the comb in a nonlinear crystal to generate a balanced optical cross correlation: the nonlinear response is greatest at the peak powers when the comb pulses overlap providing a very precise measure of the pulse arrival times. Feedback to control the length of the optical fiber ensures the pulses arrive at the far end of the link without excess jitter on their arrival times. A second balanced optical cross correlation measurement at the far end of the link with a remote frequency comb enables feedback to the remote comb to steer its output to match that of the local site. Using this approach of careful optical engineering and optical detection using balanced optical cross correlation, the team of Ref. [90] achieved an integrated timing jitter of

1.1 fs integrated down to 100 μHz, and following a number of system improvements achieved an integrated timing jitter of 680 as integrated down to 1 μHz [91]. This performance does come at a cost, however, in terms of required received power that limits the span of the link and imposes requirements for amplification: received powers need to be greater than 1 mW with the local portion of the comb greater than 10 mW [90,91].

The subfemtosecond precision achieved (Fig. 10(c)) is particularly impressive given the challenges that dispersion and nonlinearity, discussed in Section 4.2, pose for directly sending optical frequency comb pulses over optical fiber. In Refs. [59,90,91,176] sufficient dispersion management for the 1–10 km links was provided by DCF. In addition, the pulsed source also limits the amplification that can be provided by polarization-maintaining (PM) EDFAs, since high peak powers will result in fiber nonlinearities. The 1–10 km link lengths, however, are well matched to the available amplification. In Ref. [90], 13 dB gain was sufficient to overcome the loss associated with 3.5 km of a dispersion-balanced link without distorting the pulses. The excellent timing performance makes optical cross correlation appealing for large-scale scientific instruments that require exquisite time synchronization across <10-km links such as x ray free-electron lasers, as outlined in the review of Ref. [59]. An alternative approach of sending frequency comb pulses through hollow-core optical fiber has also shown promising results [177].

7. TIME AND FREQUENCY TRANSFER OVER FREE SPACE

As optical clocks become increasingly mobile, we are confronted with the fact that two-way fiber networks will be inaccessible from most of the Earth's surface. In addition, if one or more of the optical references is on an aircraft or satellite, fiber networks will not be an option. These facts have driven extensive research into free-space time and frequency transfer. Much like fiber networks, free-space networks exploit two-way transfer to remove link noise but must also manage the additional challenges of link intermittency and potentially platform motion (particularly in the case of aircrafts and satellites).

Free-space time and frequency transfer techniques can be divided into roughly three categories: time and frequency transfer using pulsed-source satellite laser ranging (SLR) technology [178,179], frequency transfer using a CW laser [75,100,180–185], and time and frequency transfer using frequency combs [52,53,59,63,79,102,103,124,186–192]. The pulsed source method of time transfer, exemplified by the Time Transfer by Laser Link (T2L2) project, represents the highest technology readiness of the three but only supports a TDEV of about 1 ps at 100-second averaging time. The CW-laser-based approach applies the principles and equipment of fiber-based CW-laser frequency transfer, described in Section 6.1, to a free-space channel. Like its fiber-based counterpart, this technique realizes fractional frequency instabilities (MDEVs) ranging between 2×10^{-17} and 2×10^{-18} at averaging times of only 1 second, but of the three free-space methods, it is the most sensitive to link interruptions. Finally, the frequency comb-based methods combine the precision of the optical carrier reaching subfemtosecond time instability and sub-10^{-18} fractional frequency instabilities with the relative immunity to link interruptions characteristic of pulsed transfer methods at the cost of increased system complexity. In this section, we review these three categories of free-space time–frequency transfer.

7.1. Pulsed-Source Time Transfer

Pulsed-source time transfer is built upon the tools of SLR. Figure 11 provides a schematic of this approach with details from the T2L2 project [178,193–198]. Pulses of laser light, with a repetition period set by the reference, are launched from a ground

Figure 10

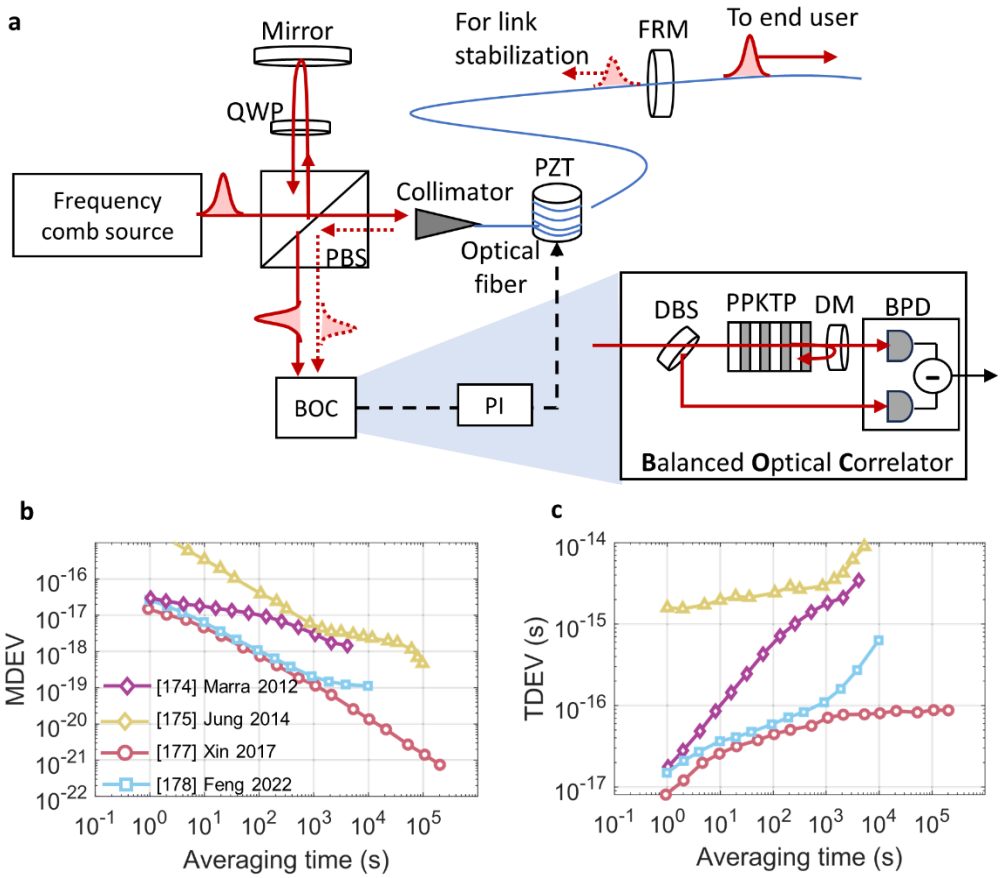

(a) Schematic of time transfer via direct transmission of frequency comb pulses over fiber using the balanced optical cross correlation detection technique. In this technique a pulsed frequency comb source is split into transmitted and local arms. The transmitted light is sent over fiber to the end user at the remote site where a Faraday rotation mirror reflects some of the light back to the transmitting site. The reflected pulses are combined with the local pulses in a balanced optical correlator that measures the time offset between the two pulses. The output of the correlator is used to drive the fiber stabilization control loop via a fiber stretcher or motorized delay stage actuator. At the remote site a similar optical correlator can be used to synchronize other pulsed sources to the incoming timing reference pulses, except the output of the correlator in this case would be used to adjust the timing of the locked laser pulses. QWP, quarter wave plate; PBS, polarizing beam splitter; BOC, balanced optical correlator; PI, proportional integral controller; PZT, piezoelectric fiber stretcher; FRM, Faraday rotation mirror; DBS, dichroic beam splitter; PPKTP, periodically poled $KTiOPO_4$; DM, dichroic mirror; BPD, balanced photo detector. (b) Comparison of time transfer over fiber using frequency comb sources based on the heterodyne optical phase detection in Ref. [173], a fiber-loop optical-microwave phase detection scheme in Ref. [174], the balanced optical cross correlation method in Ref. [176], and the hollow-core fiber method in Ref. [177]. Data presented in MDEV form, consistent with the referenced papers. (c) Conversion of data from (b) to timing deviation for comparison with other time transfer techniques.

station and their arrival time is directly photo-detected at the remote (satellite) location and measured relative to the on-board clock. To meet the requirement of at least partial reciprocity discussed in Section 4, pulses of laser light must also be transmitted from

Figure 11

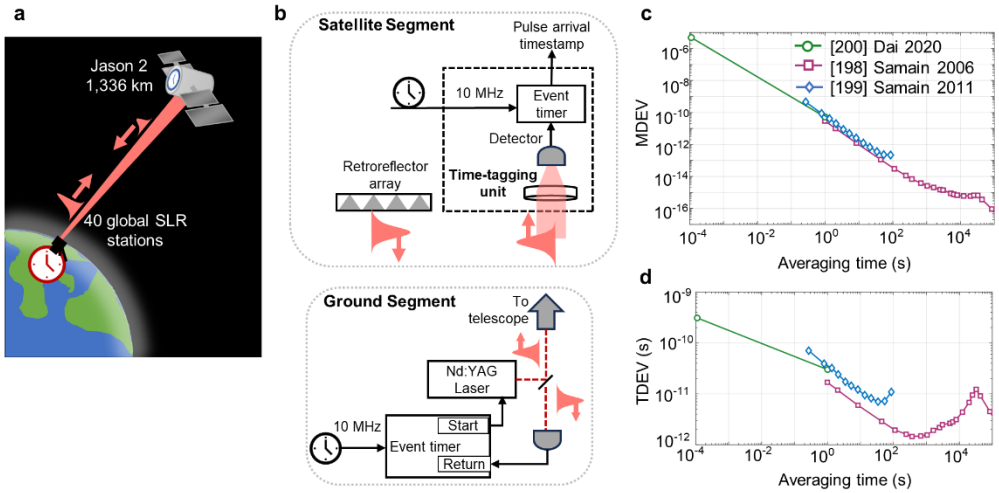

(a) Time Transfer by Laser Link (T2L2) leveraged a global network of SLR stations to send pulses to the Jason 2 satellite for T2L2 experiments. (b) Simplified schematics of satellite and ground segments of T2L2 time transfer demonstrations (c) MDEVs from SLR experiments. Data from the Micius satellite are indicated with green circles [199]. Data from the T2L2 experiment are shown for both the ground-based system tests (purple squares) [197] and a ground-to-space comparison between a hydrogen maser at the Observatoire de la Côte d'Azur and the satellite's on-board DORIS ultrastable oscillator (USO) (blue diamonds) [198]. The ground-to-space comparison is limited by the DORIS USO. (d) TDEVs from Refs. [197–199].

the satellite to the ground. Much like the fiberoptic CW-laser-based frequency transfer discussed in Section 6.1, this can be accomplished through either use of a retroflector on-board the satellite or through use of an active transmitter (pulsed laser) on-board the satellite. The uplinked one-way measurement is either combined with the round-trip time of flight (retroreflector) or the downlinked one-way measurement (active transmitter) along with the appropriate corrections and calibrations to generate a measure of the time offset between the two sites. The corrections and calibrations must take into account not only instrumental calibrations but also atmospheric effects and those due to the motion of the satellite relative to the ground station [194,195].

The T2L2 project [178,193–198] took the approach of using a retroreflector to send a portion of the light back to the ground for direct detection as sketched in Fig. 11(b). This choice allowed for greater simplicity of the satellite segment but made detection at the ground challenging as the link budget must support the round-trip loss. For the ground segments, a typical laser station had a 532-nm neodymium ytrrium iron garnet (Nd:YAG) laser generating pulses at rates between 10 Hz and 2 kHz with pulse widths spanning 50–200 ps [195,197]. Typical pulse energies were on order 50 mJ [195]. Avalanche photodiodes were used both at the ground segments for the direct detection of the returned pulses and on-board the satellite for the direct detection of the uplinked pulses. The event timers used to record the pulse arrival times were designed to have root mean square repeatability errors of 2.5 ps and a linearity better than 1 ps so that errors due to the time tagging of the pulses would be negligible [193].

The Micius quantum satellite also has performed pulse-based time transfer with some additional advantages arising from its larger quantum communications purpose [199]. In contrast to the retroreflector of T2L2, the Micius satellite launches a train of pulses with timing information encoded on single-photon pulses on the downlink and receives classical pulses on the uplink. At the ground station, pulses are emitted from

a 1064-nm laser with typical pulse widths of 0.8 ns and pulse energies of 15 μJ at a 10 kHz repetition rate. These pulses are directly detected on-board the satellite with avalanche photodiodes with the pulse arrival times tagged by a time-to-digital converter. The single-photons downlinked are generated by 850-nm lasers and encoded in Bennett–Braunstein protocol (BB84) polarization states for detection on the ground via single-photon detectors after passing through a BB84 decoder. In addition, the use of a quantum communications satellite allowed the computation of the quantum bit error rate associated with the downlinked quantum key distribution to provide a layer of quantum security to this time transfer demonstration.

The T2L2 and Micius demonstrations are the only ground-to-satellite precision optical time transfer to date with systematic effects limiting the instability to ~1 ps [193,197–199]. Figure 11(c) presents some of the fractional frequency instability data from these two demonstrations with Fig. 11(d) presenting the time instabilities that can be computed from these data. The deployment of the Laboratory Module II of the Chinese Space Station in 2022 includes the infrastructure for a pulsed laser link so an additional set of ground-to-space pulsed laser time transfer experiments are anticipated in the near future [200]. The comparison of the T2L2 project simultaneously with a GPS measurement and a direct measurement between two co-located SLR telescopes also has allowed for the determination that the accuracy of the pulsed-source transfer approach is better than 200 ps [201].

7.2. CW-Laser-Based Frequency Transfer

Free-space frequency transfer using CW lasers transfers an optical frequency reference from one site to another by canceling the atmospheric phase noise introduced by the link via heterodyne detection of the phase fluctuations and subsequent servo control of an AOM [100,180–185]. This is the same phase noise-cancellation technique used in fiber-based frequency transfer (Section 6.1 and Fig. 7) except here the phase fluctuations are induced by optical turbulence in the air rather than the acoustic and thermal fluctuations seen in optical fiber links.

In this free-space frequency transfer technique, the CW frequency reference is transmitted from the local site to the remote site over the air using single-mode free-space optical terminals. The primary challenge with this technique is signal fading due to atmospheric turbulence, which limits the length of averaging windows and therefore long-term stability of the technique. To reduce fades and maximize coupling from the turbulent free-space beam into the single mode fiber at the terminal, tip-tilt correction is often applied. To do this, a portion of the incoming light is detected on an IR camera or quadrant photodetector to inform servo control of tip-tilt mirrors [183,185,202]. Applying tip-tilt correction reduces the frequency and duration of signal losses across the link but does not compensate for loss. As a result, EDFAs are sometimes placed in the receiver to amplify the optical signal. Since current demonstrations have all used light at 1550 nm, the EDFA is well-suited for amplification here, though it can also be a source of noise. Indeed, noise from the EDFA was shown to limit performance at short averaging times (<10 s) across a 1.2-km link in Ref. [181]. Alternatively, increasing the optical power sent over the link can also help to extend the working distance. In Ref. [180], amplifying the optical launch powers to 1 W allowed frequency transfer across 18 km of air. As evidenced by the high launch powers in this work, this technique is most effective over lengths up to a few kilometers.

In order to cancel the turbulence-induced phase noise, part of the transmitted light must be reflected back from the remote site to the local site to measure phase fluctuations by heterodyne detection with a local oscillator copy of the reference light [75]. The

Figure 12

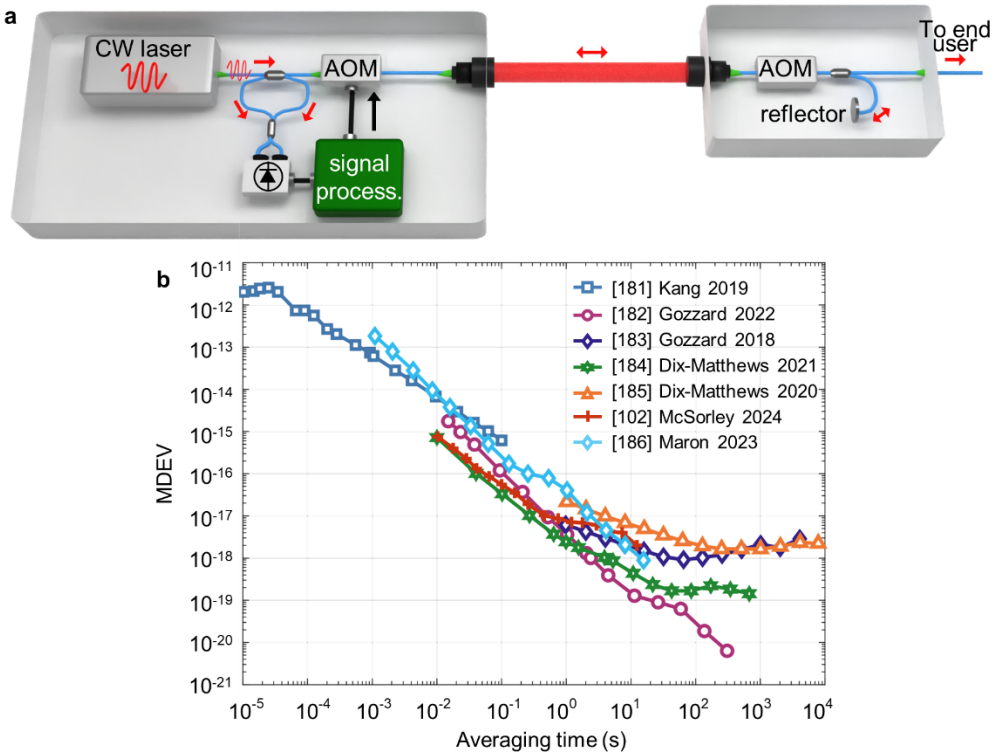

Free-space frequency transfer using a CW laser. (a) Schematic of setup. The CW laser is transmitted over free-space from the local site to the remote site. After coupling into fiber, most of the light is directed to the end user whereas part of the light is reflected back with a Faraday mirror for heterodyne detection at the local site. The round-trip phase noise of the link is then measured and corrected at the local site with an AOM as is done in fiber-based frequency transfer (see Section 6.1a). (b) Fractional frequency instability (MDEV) from CW laser-based frequency transfer demonstrations over free-space with link lengths varying from 150 m to 18 km. Data from [101,180–185].

detected phase is used to feedback to an AOM to cancel the phase noise of the link. Since this technique for free-space frequency transfer directly transfers the optical carrier, it exhibits fractional frequency stabilities that rapidly reach levels capable of supporting optical clock comparisons, averaging below 10^{-18} after a few seconds, as shown in Fig. 12 [181–183]. Importantly, this technique has been verified using out-of-loop measurements across both fiber paths [183] and intralaboratory using folded free-space link geometries [100,101,182,185].

Terrestrially, this technique has been demonstrated across several subkilometer, turbulent free-space links [182,183] and with optical signal amplification this distance has been expanded up to 18 km [180,181,184]. Recent work has also taken initial steps toward making this technique compatible with moving platforms, demonstrating 10^{-18}-level frequency transfer to a tethered balloon [185] and a quadcopter moving at speeds near 1 m/s [100], and, more recently, 15 m/s [101].

7.3. Frequency-Comb-Based Time Transfer

The frequency comb-based approach to free-space time–frequency transfer utilizes a two-way propagation technique [52,53,63,79,102,103,124,186–192]. At each site, a frequency comb phase-locked to a microwave or optical reference generates a local time scale as discussed in Section 5. The stability of the reference is transferred to

Figure 13

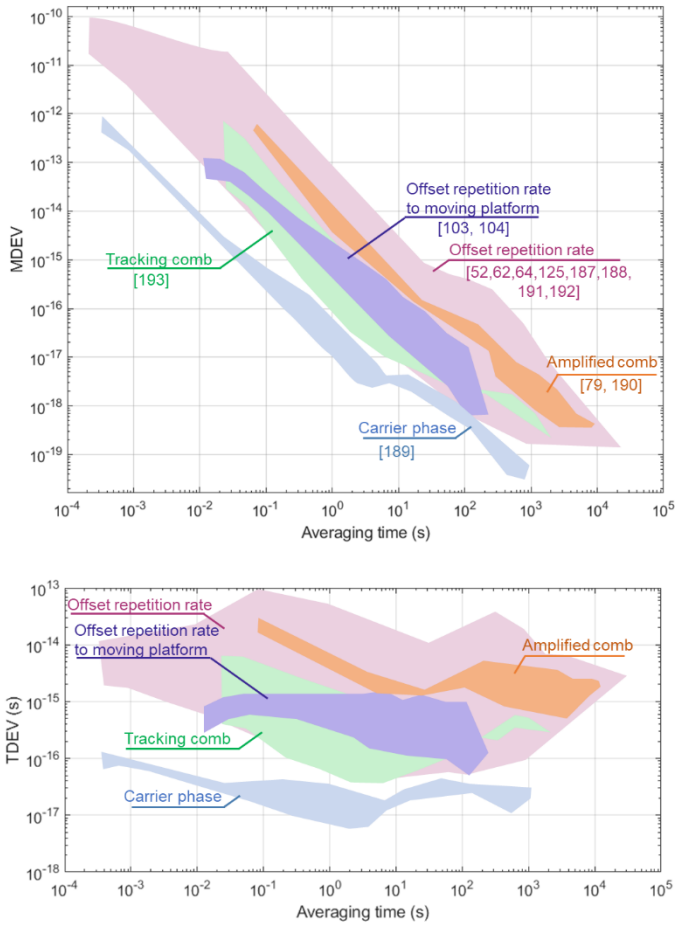

Frequency-comb-based time transfer demonstrations. The colored polygons indicate the range of MDEV and TDEV results achieved by each technique category. The pink polygon covers offset repetition rate linear optical sampling demonstrations, purple covers demonstrations to moving platforms, green covers tracking comb demonstrations, blue covers carrier phase demonstrations, and orange covers amplified comb demonstration. Data from [52,53,63,79,102,103,124,186–192].

the timing of the comb pulses as well as the underlying carrier frequency of the comb output. When those frequency comb pulses are sent bidirectionally through the air, their arrival times can be measured relative to the other site's time scale. To maintain high precision, this measurement occurs through heterodyne detection with a local frequency comb, i.e., a local oscillator comb. The two-way propagation allows for combining the measured timestamps to cancel the atmospheric phase noise common to both sets of timestamps. The result of the two-way measurement is thus a measurement of the time offset between two local time scales, i.e., the clock offset. The derivative of this time offset gives the frequency offset between the clocks.

All of the demonstrations of frequency comb-based time transfer to date have used erbium-fiber-based frequency comb lasers [52,53,63,79,102,103,124,186–192] with all but the earliest demonstration [124] with full $1f - 2f$ carrier-envelope offset frequency, f_{ceo} , stabilization. Locking an optical comb tooth, f_m, to the optical frequency reference laser then stabilizes the repetition rate of the comb, f_r. (See also the discussion in Section 5.) Use of erbium-fiber-based frequency comb lasers enables transmission

of light centered at ~200 THz, well matched to standard telecommunications components. It is worth noting, the while the frequency comb spectral bandwidth can be octave-spanning, the portion of the spectrum launched across the air is much narrower, typically 1–3 THz.

Figure 13 presents both fractional frequency instability and TDEV ranges for several different variations of this approach. Section 7.3a presents a discussion of an approach centered on the detection of the comb pulse arrival times via offsetting of the comb's repetition rates, termed offset repetition rate linear optical sampling [52,53,63,124,186,187,191]. This includes the use of this approach to platforms moving at up to 24 m/s [102,103] as well as demonstration of handoff to the underlying carrier phase [188]. Section 7.3b focuses on the development of amplified optical frequency combs to extend the span achievable via offset repetition rate detection from tens of kilometers to hundreds of kilometers of turbulent air [79,189]. Driven by the results of Ref. [190], Section 7.3c examines possible trade-offs in precision and detection threshold seeking to look beyond existing demonstrations to a wider range of choices in repetition rate and difference in repetition rates. Since microcombs are a rapidly maturing frequency comb technology, Section 7.3d discusses the future use of microcombs for frequency-comb-based time transfer. Section 7.3e then presents an alternative to the offsetting of repetition rates for frequency-comb-based time transfer: use of a tracking comb to achieve optical time transfer at the quantum limit [192]. Finally, Section 7.3f provides a brief comment on other detection methods.

7.3a. Offset Repetition Rate Detection

For the offset repetition rate linear optical sampling approach, measurement of the incoming pulse arrival times through optical heterodyne detection with a local frequency comb in turn preserves the high timing precision of the pulses in detection. This stands in contrast to the pulsed-source time transfer described in Section 7.1, where the direct detection of the pulses limited the timing precision to the picosecond level.

In this approach, the incoming signal comb and local oscillator comb are locked to different f_r values where $f_{r,A} - f_{r,B} = \Delta f_r$ with the A and B subscripts referring to a site A and a site B at opposite ends of a link. When the two combs with offset repetition rates are mixed on a photodetector, the output heterodyne voltage will be proportional to the product of the two electric fields. The two pulse trains will walk over each other in time (analogous to a sampling oscilloscope), generating interferograms that represent downmixed versions of the received optical pulses with an RF carrier set by the difference of optical carrier frequencies between the two frequency combs, as shown in Fig. 14. This sampling method magnifies the timing of the received pulses by a magnification factor of $M = f_r/\Delta f_r$ in the interferogram time series, with typical values consisting of $f_r = 200$ MHz, $\Delta f_r = 2$ kHz, and $M = 10^5$. With this magnification, measuring the arrival of the electronic interferogram signals at the subnanosecond level yields the optical pulse arrival times at the femtosecond level. This precision comes at the cost of an update rate set by Δf_r rather than f_r (see also Section 7.3c). The expected arrival time of an interferogram peak is every $1/\Delta f_r$ seconds, so for $\Delta f_r = 2$ kHz a timing measurements occur every 0.5 ms. The arrival times of the nth interferograms at sites A and B can be written following Ref. [188] as

$$\begin{aligned} t_{n,A} &= \Delta f_r^{-1}(n + f_{r,B}T_{link} - f_{r,B}\Delta\tau), \\ t_{n,B} &= \Delta f_r^{-1}(n - f_{r,A}T_{link} - f_{r,B}\Delta\tau), \end{aligned} \tag{8}$$

where T_{link} is the reciprocal time of flight across the link and $\Delta\tau$ is the desired time offset between the sites' clocks. Removing the expected time advance, $n/\Delta f_r$, and

Figure 14

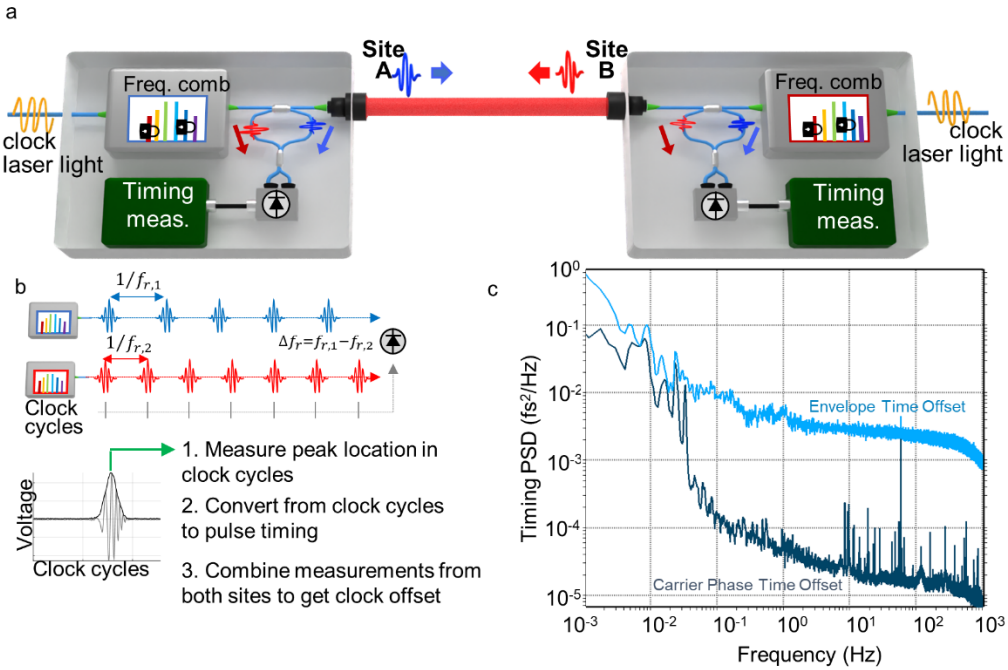

(a) Sketch of concept of frequency-comb-based time transfer based on linear optical sampling. At each site, a frequency comb is tightly phase-locked to a reference oscillator producing a coherent pulse train output whose pulse repetition period, $T_r = 1/f_r$, and pulse phase are determined by the reference oscillator. These pulse trains, with repetition rates slightly offset by Δf_r, are exchanged over a reciprocal single-mode link. At each site, the arrival time of incoming comb pulses is measured by the local frequency comb through a linear optical sampling measurement to produce a series of timestamps at each site. The sum and difference of these timestamps returns the time of flight, modulo the nonambiguity range, and the time offset between the two sites. By using an optical heterodyne approach of one comb sampling another, low noise can be achieved using conventional balanced photodetectors at nanowatt levels of average received power. (b) Concept of offset repetition rate linear optical sampling. The pulse trains from two frequency combs, offset in repetition rate, walk across each other producing a series of interferograms. For each interferogram the offset in the arrival times of the remote pulse train relative to the local pulse train is magnified by a factor of $M = f_r/\Delta f_r$. (c) Timing PSD of offset repetition rate time transfer system from Ref. [188] showing both envelope timing as described in part (b) and carrier phase timing.

combining these as

$$t_n = \frac{t_{n,A} + t_{n,B}}{2} \tag{9}$$

the reciprocal time of flight drops out. (The counterintuitive appearance of a sum of timestamps in Eq. (9) rather than a difference arises from a choice of sign conventions so that the expected time advance, $n/\Delta f_r$, is positive at both sites.) This yields a relationship between the timestamps measured in the laboratory and the underlying time offset of

$$t_n = \frac{f_{r,B}}{\Delta f_r}\Delta\tau. \tag{10}$$

Equation (10) illustrates that the clock offset has been scaled up by the magnification factor, $M = f_{r,B}/\Delta fr$. In other words the precision with which the electronic timestamps,

t_n, must be measured in the laboratory is relaxed by a factor of M from the desired measurement precision of the clock's time offset.

After an initial demonstration of optical time and frequency transfer across 2 km of air [124], Ref. [63] showed synchronization of optical oscillators at or below 1 fs from 0.1 to 6500 s across a 4-km turbulent air path. Reference [186] showed free-space time transfer could be used to generate phase-coherent 10-GHz microwave signals across 4 km. These microwave signals, generated by optical frequency division [118], agreed at the 10^{-14} level at 1 second. Reference [188] showed that the pulse envelope-based timing determination could be combined with optical carrier phase measurements to compare frequencies at the level of 10^{-17} at 1 second, reaching instabilities of 10^{-19} at long time scales.

The demonstrations described above were all terrestrial, point-to-point demonstrations. Note that, in practice, the point-to-point topology is often implemented in a folded-link geometry where sites A and B are colocated at one end of the link and connected through free space via a mirror or retroreflector at the far end of the link. This folded-link geometry enables out-of-loop truth data measurements that can verify system performance with a short optical fiber connecting the sites. Reference [191] extended the link topologies to include three timing nodes at no loss of performance across the network. In an effort to support future ground-to-aircraft or ground-to-space time transfer, Refs. [102,103] showed time transfer off a reflector mounted on a quadcopter moving at modest speeds up to 24 m/s.

Offset repetition rate linear optical sampling has also been used for the comparison of state-of-the-art optical clocks across the city of Boulder, Colorado [53]. As part of the Boulder Atomic Clock Optical Network (BACON) Collaboration, a 1.5-km free-space link connected a strontium optical lattice clock located at JILA on the University of Colorado Boulder campus and a ytterbium optical lattice clock located at the NIST Boulder campus. During this experiment, the atomic ratio was simultaneously measured with a stabilized fiber link and the ratio measurements taken over free space and fiber agreed at the 6×10^{-19} level [52,53].

7.3b. Amplified Combs to Increase Distance

Efforts to increase the working distance of comb-based time transfer using offset repetition rate detection initially led to a 12-km demonstration in Ref. [187] and a 16-km demonstration in Ref. [79]. Amplification of the in-band launched optical comb power allows for this distance to be increased as long as the comb pulses are not distorted and the in-band spectrum remains stable, e.g., no peaking/narrowing of the spectrum due to the erbium gain profile. The choice of location within a frequency comb system to perform the amplification is nontrivial. In Refs. [79,189] amplification after the comb oscillator avoided the need for a bidirectional amplifier, and associated complications, but required control of the subsequent optical paths to avoid the addition of excess noise. Indeed, in the work of Ref. [79], commercial amplifiers increased the launch power from a few milliwatts to 120 mW in a 20-nm band while home-built amplifiers increased the launch power to 250 mW in-band. The latter amplification scheme, however, did result in pulses that were chirped resulting in a 4-ps pulse duration compared with the 180 fs expected for a transform-limited pulse. Following Ref. [79], the work of Ref. [189] generated 1 W of optical power in a 20-nm band, which extended the range to 113 km. The pulses of Ref. [189] were highly chirped to 60–90 ps upon amplification to avoid issues of nonlinearities with careful dispersion management minimizing the differential dispersion and, thus, preserving the timing performance as can be seen in Fig. 13. For comparison, previous efforts [53,63,102,124,186–188,190,191] typically launched less than 5 mW of optical power.

7.3c. Precision Versus SNR Trade Space

All of the demonstrations described in Sections 7.3a and 7.3b used offset repetition rate linear optical sampling with similar magnification factors, M. Most common was the use of 200 MHz repetition rate combs with $\Delta f_r = 2$ kHz to give $M = 1 \times 10^5$. The exceptions include Ref. [124], which used 100 MHz repetition rate combs with a Δf_r of 3 kHz for $M = 3.3 \times 10^4$, and Ref. [189], which used both 200 and 250 MHz repetition rate combs but scaled Δf_r to maintain $M = 9.6 \times 10^4$.

As explored in Ref. [190] for a fixed repetition rate, there is a fundamental trade space in comb-based time transfer when selecting a Δf_r between the received power required to make a single measurement (record an interferogram) and the achievable precision at a given averaging time. Lowering Δf_r (or increasing M) will reduce the required received power to exceed the detection threshold by increasing the SNR per interferogram. However, it also potentially reduces the measurement precision as the more optical pulses that contribute to an interferogram, the greater the potential for the coupling in of additional noise. Indeed, Ref. [190] shows that the power SNR per single measurement (per interferogram) of an offset repetition rate measurement of comb timing scales like $SNR \propto M$, while the timing uncertainty, σ_t, also scales roughly with M due to Gordon–Haus-like jitter. Note that in the absence of Gordon–Haus-like jitter, the choice of M will not affect the measurement precision as it will simply be set by the comb pulse width assuming that the received power is above the detection threshold.

From the definition of M, it is clear that the required received power, i.e., the detection threshold, can be reduced by increasing the repetition rate of the combs. However, the concern about the increased coupling in of noise through use of more optical pulses to generate an interferogram still holds. To maintain a fixed M, both the repetition rate, f_r, and the repetition rate difference between combs, Δf_r must be increased. The allowable maximal value of Δf_r is set by the Nyquist limit of $f_r^2/(4B)$ where B is the optical bandwidth of the comb light so higher repetition rate combs can be offset at higher values of Δf_r.

Increasing the comb repetition rate also reduces the pulse spacing and, thus, the nonambiguity range of a comb, since a 10-GHz repetition rate comb will have a 100-ps pulse spacing whereas a 10-THz repetition will have a 100-fs pulse spacing. This reduced nonambiguity range imposes stricter requirements on any coarse time transfer required to resolve the ambiguity [64]. The nonambiguity range also sets the tolerance for a phase-continuous measurement across atmospheric fades. If the one-way time of flight through the atmosphere surpasses the nonambiguity range during a fade, the time transfer measurement will effectively phase slip. For tracking-comb time transfer, described in Section 7.3e, a smaller nonambiguity range will have the benefit of a shorter signal acquisition period so while most time transfer demonstrations have used 200 MHz combs, there is likely a trade space for repetition rate selection that is application dependent.

7.3d. Microcombs for Time Transfer

Microcombs, or combs generated from a microresonator oscillator, are a source of higher repetition rate combs with f_r in the tens of gigahertz to several terahertz [125]. Because all but one of the demonstrations of fiber-comb-based time transfer have utilized full f_{ceo} stabilization, future microcomb-based time transfer experiments that utilize an octave-spanning comb to enable f_{ceo} stabilization will thus most closely match the architectures that have led to the performance highlighted in Fig. 13. This stabilization has been demonstrated in a microcomb in Ref. [203], but it required

additional amplifiers and nonlinear optical fiber, akin to those used in fiber-based systems, to achieve f_{ceo} generation. We note recent work has also shown the potential to generate octave-spanning spectra directly in Si_3N_4 microresonators [204,205], which is an exciting development. In addition to f_{ceo} stabilization, the microresonator comb must be phase-locked to the optical frequency reference of interest. This has been demonstrated for some optical clock frequencies with Ref. [206] locking the repetition rate of microresonator to a rubidium frequency reference and Ref. [207] locking to a calcium frequency reference. While full f_{ceo} stabilization is the most straightforward path to matching existing demonstrations, it is intriguing to think about one narrow-bandwidth gigahertz-repetition-rate microcomb that could be locked to two teeth of an octave-spanning terahertz-repetition-rate microcomb stabilized to the reference oscillator mirroring the stabilization of the frequency combs to two CW lasers stabilized to the same optical cavity of Ref. [124].

7.3e. Tracking Comb Detection at the Quantum Limit

The offset repetition rate detection approach trades detection threshold for precision leading to an elevated detection threshold far above that predicted by the quantum limit set by the number of received comb photons. To overcome this, the received signal comb and the local oscillator comb can be operated at the same repetition rate rather than offsetting their repetition rates. This method of timing detection, called tracking comb detection or quantum-limited detection for reasons described below, is sketched in Fig. 15(a) and detailed in Refs. [123,192].

Tracking comb detection, like the offset repetition rate detection, relies on an optical heterodyne measurement of one comb against another. However, in contrast to the offset repetition rate detection, it relies on the use of a time programmable frequency comb (TPFC), which is an optical frequency comb with a pulsed output that can be adjusted in time with attosecond-level accuracy [123]. As the local oscillator comb is a TPFC, both signal and local oscillator combs run at the same nominal repetition rate. After a brief acquisition period, feedback to the local oscillator comb ensures that these pulse output times match the incoming signal pulse arrival times, i.e., all local oscillator pulses temporally overlap the incoming signal pulses at a particular reference plane. The variations in the output time of the local oscillator pulses then reflect the remote reference oscillator noise and the atmospheric fluctuations. This is analogous to an RF tracking oscillator.

The error signal driving the feedback to the local oscillator comb is generated through an optical timing discriminator that is an imbalanced Mach–Zehnder interferometer with two optical output channels. For one output channel, the propagation time for the incoming signal pulse is retarded relative to the local oscillator pulses by half a pulse width and the optical heterodyne signal, V_1, is measured. For the other channel, the half-a-pulse-width delay is instead applied to the local oscillator pulses and the optical heterodyne signal, V_2, is measured. If the incoming comb pulses lag behind the local oscillator comb pulses, the amplitude of V_1 decreases but V_2 increases whereas if the incoming comb pulses approach closer to the local oscillator comb pulses, the amplitude of V_1 increases but V_2 decreases leading to an error signal that is approximately linear with a dynamic range of twice the optical pulse width. To differentiate between these differential amplitude fluctuations and the amplitude fluctuations that are common to both channels, as we expect due to turbulent scintillation, the timing error signal is normalized by the sum of the amplitudes $Err = (|V_1| - |V_2|)/(|V_1| + |V_2|)$, shown in Fig. 15(b). (See also Ref. [123] for more details on the optical timing discriminator). This unitless error signal is converted to units of clock cycles through a calibration factor.

Figure 15

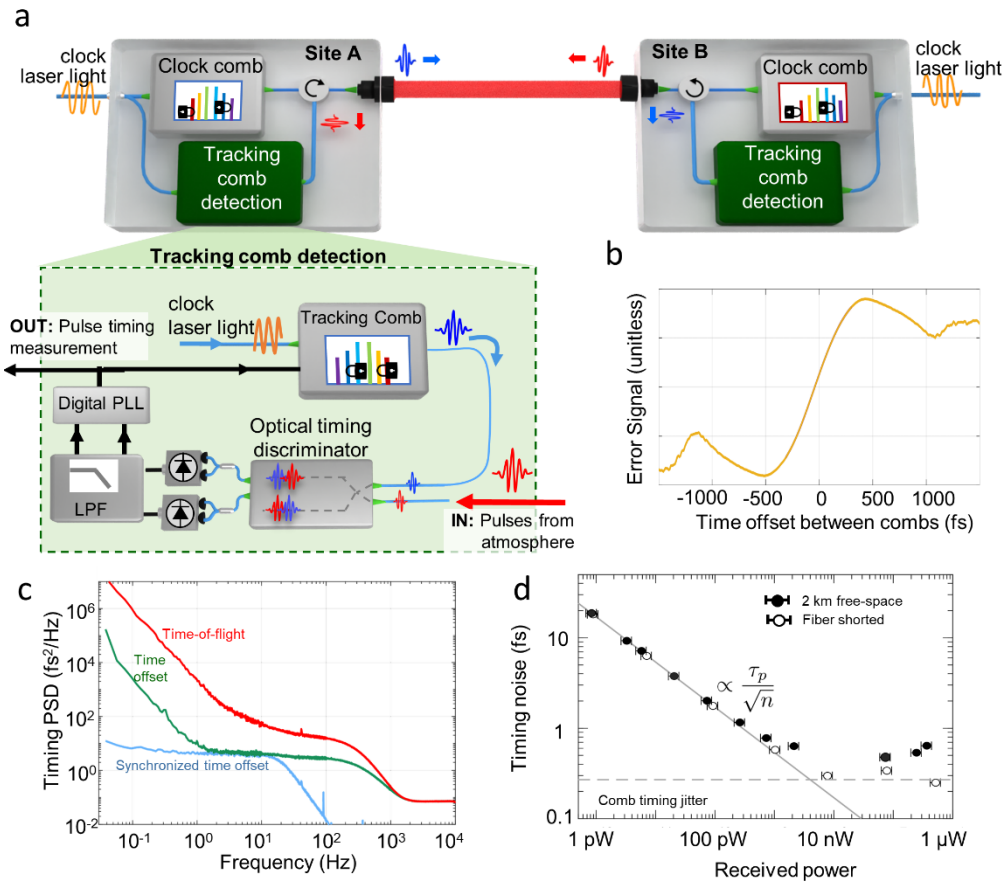

Quantum-limited time transfer based on use of a tracking comb. (a) At each site, pulses from a clock comb tightly phase-locked to the reference oscillator are launched over a reciprocal single-mode link. In this approach, detection of the incoming comb pulses is accomplished through tracking comb detection. A separate time-programmable frequency comb (TPFC) at each site is mixed with the incoming comb pulses in an optical timing discriminator. Filtering of this timing discriminator signal allows for coherent averaging over measurement durations up to 1 ms and, thus, detection of extremely weak incoming comb signals. The control effort applied to the TPFC to keep it phase-locked to the incoming comb pulse train is the desired pulse timing measurement. (b) Example of error signal returned from the optical timing discriminator, which is based on an imbalanced Mach–Zehnder interferometer. As the time offset between the remote clock comb pulses and local oscillator pulses increases the absolute value of error signal increases within the ~1 ps dynamic range of the timing measurement. (c) Representative PSDs of tracking comb time transfer using two cavity stabilized lasers (CSLs) as the reference oscillators and a 300 km free-space link. The average one-way pulse timing jitter (red) can be interpreted as the time-of-flight noise introduced by atmospheric turbulence. The time offset measured between the two clock lasers (green) shows the suppression of the atmospheric timing noise and the frequency drift between the two CSLs at low frequencies. The synchronized time offset (blue) is an out-of-loop measurement of one clock laser synchronized with a 10 Hz bandwidth to the other clock laser. Data from [113]. (d) Demonstration of quantum-limited (shot-noise limited) pulse timing noise for received powers up to 10 nW in the absence of strong turbulence over fiber-shorted and 2-km free-space links. The timing noise scales like $\tau_p/\sqrt{n}$ where τ_p is the pulse width and n is the number of signal photons received per measurement period. Data from [113].

Subsequently, the error signal in units of clock cycles is then used in a control loop to adjust the pulse output time of the local oscillator comb. As the local oscillator comb is a TPFC, the relationship between the control effort, the instantaneous controller output applied to the comb's phase locks, and the change in pulse output time in units of clock cycles is well defined and recorded by the signal processor. The residual timing error, i.e., timing noise at Fourier frequencies above the feedback bandwidth of the control loop, is also recorded by the signal processor, again in units of clock cycles. Further conversion to units of seconds is achieved through knowledge of the optical reference oscillator frequency, comb mode numbers, and rational fractions that set the local clock comb's lock points. (See also Section 5.) A plot of this error signal as a function of signal pulse time is shown in Fig. 15(b).

When continuous tracking of the incoming pulses is engaged, the timestamps, t_A or t_B, composed of the control effort sent to the local oscillator comb plus the residual timing error signal, replicate the timing of the incoming pulse trains. To cancel the reciprocal phase noise of the link and retrieve the desired clock offset the two timestamps are combined as

$$\Delta\tau = \frac{t_A - t_B}{2}. \tag{12}$$

Note that the sign conventions are chosen so that the difference returns the clock offset between sites A and B with the sum returning the reciprocal time of flight. The difference in sign conventions between Eqs. (9) and (12) is due to the former using combs at differing repetition rates, whereas the latter uses combs at the same repetition rate.

By tracking the incoming pulses rather than waiting for the local oscillator to sample them through an offset repetition rate, tracking comb-based detection reduces the dead time seen in offset repetition rate measurements and all incoming pulses contribute to the signal of the timing measurement. This allows tracking comb detection to operate at the photon shot noise limit, also called the quantum limit. The timing uncertainty, σ_t then scales like $1/\sqrt{n_s}$ where n_s is the number of incoming signal comb photons received during the measurement period. (See also the discussion on the quantum limit in Section 8.2.1.) This stands in contrast to the offset repetition rate detection of Sections 7.3.1 and 7.3.2 for which the timing uncertainty scales like the square root of the number of incoming photons in the pulses that overlap in time with the local oscillator pulses during the measurement period. (See also Section 7.3.3 and Ref. [190].) This method of comb-based time transfer reduced the required received power from ~10 nW [63] to ~300 fW [192] using similar frequency comb outputs. This reduced threshold translates to a much higher tolerance for link loss enabling a demonstration of time transfer over 300 km of air with 100 dB of loss [192]. Despite these high losses, Ref. [192] showed frequency transfer at the sub-10^{-18} level and time transfer at the subfemtosecond level.

Modeling shows that the losses seen in this experiment exceed those expected for a ground-to-geosynchronous satellite optical link assuming modest 10 cm apertures. Further modeling of the expected performance of this quantum-limited optical time transfer approach suggests that it could support future intercontinental clock comparisons through a geostationary satellite or support coherence distribution from ground to a geosynchronous satellite [37].

7.3f. Other Detection Methods

Another option exists for timing detection across short distances in well-controlled spaces: that of the balanced optical cross correlation discussed in Section 6.3 [59]. However, the requirement of sufficient received power for the nonlinear response of the

Figure 16

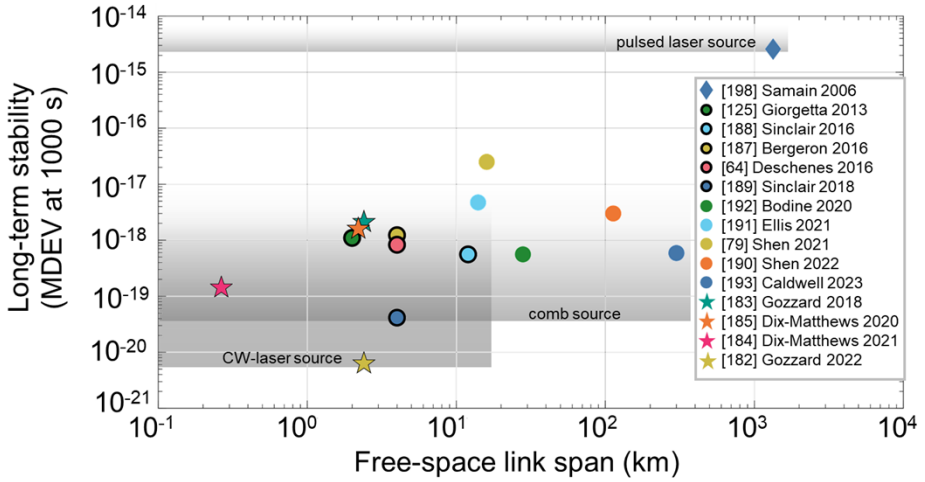

Comparison of free-space time and frequency transfer methods showing long-term stability characterized by the MDEV at 1000 s versus the free-space link span in kilometers. The pulsed-laser demonstration exemplified by T2L2 and described in Section 7.1 is indicated with the diamond. Demonstrations using CW lasers and active link stabilization, described in Section 7.2, are indicated with stars. Comb-based demonstrations, described in Section 7.3, are indicated with circles. The gray boxes indicate roughly the range of demonstrated spans and stabilities. For example, CW-laser-based frequency transfer has been demonstrated out to 18 km, but data were only available for short averaging times [180]. To provide the most complete picture of demonstrations, some points above are taken from slightly shorter averaging times on the MDEV that represented the longest averaging time available. In particular, the point for [188] was taken at 850 s of averaging, the point for [190] was taken at 950 s of averaging, the point for [183] was taken at 670 s of averaging, and the point for [181] was taken from 300 s of averaging.

balanced optical cross correlation makes it unlikely this would support long distance links.

Reference [208] proposes an alternative, two-way method of time transfer that uses two, spectrally separated CW lasers to transfer time. This "two-tone" method of time transfer shows promise for reducing some of the system complexities associated with comb-based time transfer while retaining subfemtosecond network performance. As of this publication, however, it has only been demonstrated over 100-m path lengths.

7.4. Comparison of Free-Space Time–Frequency Transfer Techniques

Figure 16 provides a comparison of the free-space time–frequency transfer techniques discussed in Sections 7.1 –7.3. Of the three free-space techniques discussed in Sections 7.1 –7.3, the pulsed-source time transfer technique represents the most mature technology with ground-to-space demonstrations in the T2L2 and Micius projects [197–199]. At long averaging times, this technique demonstrates frequency transfer at the 10^{-16} level that is comparable to the best microwave-based TWSTFT using the microwave carrier phase [41]. This performance, however, is not sufficient to support state-of-the-art optical clocks, which has driven development of the comb-based and CW-laser based techniques described in Sections 7.2 and 7.3.

Frequency-comb based time transfer reaches 10^{-18} levels at longer averaging times than CW frequency transfer (hundreds of seconds versus 1–10 seconds) but is more robust to link disruptions. For the comb-based time transfer, the nonambiguity range for resuming the measurement is on the order of nanoseconds instead of femtoseconds for a CW optical carrier. This means that if turbulence-induced fades interrupt the measurement, the measurement can be resumed without loss of phase information as long as the time-of-flight through the atmosphere did not change by nanoseconds. An additional benefit of frequency-comb-based time transfer is the ability to perform full time synchronization of a remote site by adjusting the output of the remote frequency comb, a comb which is already part of the time transfer system, to set the time scale of the remote site. With use of a CW optical carrier, the phase must be tracked unambiguously despite the few femtosecond ambiguity range and the steering of the remote time scale will be more complex. These benefits of comb-based time transfer come at the cost of increased experimental complexity as self-referenced frequency combs and the associated electronics for phase-locking and synchronization are more complex than the CW laser, AOM, and servo controller needed for CW frequency transfer.

8. OUTLOOK

8.1. Outstanding Problems in Time and Frequency Transfer Fundamentals

8.1a. Platform Motion

Many future applications of optical timing networks require moving beyond fixed terrestrial links to free-space links between platforms moving at relative velocities of 10^2–10^3 m s^{-1}. When considering ground-to-satellite or satellite-to-satellite links, the choice of orbits will be driven by the scientific goals. For example, tests of relativity may rely on highly elliptical orbits as proposed in Ref. [12], and in order to support as many missions as possible, the time–frequency transfer community should work to maximize link tolerance to high satellite velocity and acceleration. As a consequence, for both CW-laser-based frequency transfer and comb-based time transfer, the ability to support significant platform motion is a critical outstanding problem.

Thus far, only the pulsed-source free-space time transfer, discussed in Section 7.1, has been shown to support motion beyond a few tens of meters per second. Free-space comb-based time transfer used advanced signal processing to show time transfer to a quadcopter and swept delay line moving at 24 m s^{-1} [102,103] while in Ref. [101], an electro-optic modulator (EOM) was added to a CW-laser-based frequency transfer setup to enable frequency transfer to a drone moving at 15 m s^{-1}. Time–frequency transfer to platforms moving at faster speeds using these methods is still an active area of research.

To achieve time–frequency transfer to moving platforms numerous challenges must be overcome including: (1) coupling of the light into the receiver aperture through a tracking single-mode terminal; (2) measuring and tracking of the carrier frequency shifts, which will be in excess of a few gigahertz for ground-to-LEO links; (3) measuring and/or compensating for the now time-varying optical path length; (4) understanding of the fundamental limitations posed by the coupling of atmospheric turbulence and motion; and (5) determining the velocity-dependent calibrations. These challenges are also shaped by the choice of link as the characteristics of a ground-to-aircraft link look very different than those of a GEO-to-LEO link. Time transfer to rapidly moving platforms will also need to take into account relativistic corrections. References [209–211] have made headway in developing a relativistic framework for time–frequency transfer but more work is needed in this area.

For both comb-based time transfer and CW-laser-based frequency transfer, the challenge of coupling light into the receiver aperture is largely the same. Both techniques operate using heterodyne detection so single-mode terminals are necessary. Variations in required received power will drive some design choices such as telescope apertures. The need to determine the Doppler shift on the carrier frequency is common to both techniques as well. For comb-based time transfer there is an additional Doppler shift on the repetition rate.

Link intermittency will be inevitable in time–frequency transfer to moving platforms. Loss of signal will be deterministic, due to, for example, the choice of orbit, or stochastic due to, for example, platform jitter or scintillation. For CW-laser based frequency transfer, these periods of lost signal will reduce the duration over which the frequency offset can be computed and thus reduce the sensitivity of the measurement. At the same time, CW frequency transfer reaches sub-10^{-18} instabilities at shorter averaging times than comb-based time transfer that may be helpful for orbits with short overhead pass time. For comb-based time transfer, the pulse nanosecond-scale nonambiguity range allows phase-continuous measurements across fades and may enable phase-continuous measurements spanning multiple satellite passes with the help of ephemeris data.

The coupling of atmospheric turbulence with satellite motion and finite speed of light will introduce timing noise that is not fully canceled in the two-way combining of comb-based time transfer or the backreflection of a phase-stabilized link [98,99,212,213]. Recent modeling shows that this will likely be the limiting noise source for future ground-to-GEO time transfer [37].

As noted, the pulsed-source time transfer of Section 7.1 takes into account the necessary relativistic corrections and has solved the challenge of physical acquisition of the light with sufficient SNR [178,199]. However, as the summary data of Fig. 11 illustrate, this approach narrowly meets our definition of precision optical time and frequency transfer (sub-10^{-16} instability for frequency transfer and subpicosecond time transfer), which while sufficient for some applications is inadequate for others (see Fig. 3).

8.1b. Loss and Intermittency

For the CW-laser-based approaches whether over fiber (Section 6.1) or free-space (Section 7.2), the nonambiguity range of only a few femtoseconds requires restarting the measurement even for very short signal fades. While a few phase ambiguities over the course of many hours will have almost no effect on the quality of frequency transfer, frequent occurrences will limit the ultimate instability. As a consequence, maintaining high link availability is extremely important to the success of this approach as it transitions from one-off demonstrations to part of an optical metrology backbone. The CW-laser-based frequency transfer over fiber (Section 6.1) has the advantage that it has a more consistent loss profile with the optical fiber compared to free-space channels. As a consequence, the need for high uptimes has translated into on-going efforts in remote monitoring, automated polarization control, and automated relocking [66,67]. For free-space approaches, the inherent received power fluctuations due to atmospheric turbulence have led to efforts on boosting launch powers [180] and using tip/tilt control and adaptive optics within the free-space optical terminals [183] to ensure received powers consistently exceed the detection threshold.

While fixed loss has been overcome for the fiberoptic based approaches of Section 6, ensuring sufficient received optical power is an on-going challenge for the free-space approaches of Section 7. Fiberoptic links can easily interface with a series of bidirectional amplifiers along the link to ensure that the received power is above

the detection threshold. For free-space links to have similar amplifiers or repeater stations requires additional free-space optical terminals to couple light in and out of an amplifier to be inserted along the line-of-sight path: an impossibility in the case of a ground-to-satellite link and an expensive and complex addition in the case of terrestrial links. There are two separate paths being pursued to extend the range for free-space optical time and frequency transfer: (1) amplification of the launched light or (2) lowering of the detection threshold through efficient use of the available photons, as is seen in tracking-comb-style free-space comb time transfer. Amplification has enabled CW-laser-based frequency transfer over 18 km [180] and comb-based optical time transfer over 113 km [189]. Efficient use of the available photons has enabled comb-based optical time transfer at nearly the quantum limit over 300 km [192]. Extrapolation from the two comb-based optical time transfer measurements over horizontal terrestrial air paths suggests that these comb-based optical time transfer approaches would be compatible with losses expected for future ground-to-GEO orbit links [79,189,192]. In both cases, these do not represent the limit of what is achievable; we anticipate that future efforts will continue to push the achievable ranges and detection thresholds, though the latter will require moving beyond the standard quantum limit as described in the following.

Another challenge of intermittency that is common to all precise optical time and frequency transfer approaches is the question of how to handle gapped data when using standard metrics of optical metrology such as a fractional frequency noise PSD or an ADEV. These common metrics all begin with the assumption of uniformly sampled data. With the long duration operation of the French fiber network, the authors of Ref. [68] have begun to try to address this issue. Other recent work has looked at mischaracterizations, which can arise especially for large data gaps and has suggested an algorithm to fill the gaps in order to achieve consistent ADEV estimates [214]. With a move toward applications from technique demonstrations, this will become an increasingly important issue for the field to address in a consistent manner.

8.1c. Advancing Automation and Control

For applications such as general relativity tests and next-generation navigation, robust optical clocks will need to operate for long durations in challenging environments. Recent advances in portable optical clocks enabled multiple optical molecular iodine clocks to operate simultaneously at sea [33]. While these intermediate-performance optical clocks sit just above the boundary of needing precise optical time and frequency transfer, this robust compact operation serves as a clear demonstration of the potential for optical engineering to bring even ultrahigh-performance optical lattice clocks and single-ion clocks out of the metrology laboratory. Multiple groups have developed transportable lattice clocks [10,147] with significant efforts in the field to build upon this. Parallel optical engineering efforts are needed to ensure that optical time and frequency transfer can operate continuously for long durations with automated end nodes while still maintaining a level of performance that ensures future optical timing networks are limited by the clocks themselves rather than the links between them.

Pulsed optical time transfer (Section 7.1) is a globally deployed approach that does not need significant effort on this front but rather could benefit from technology advances that would minimize systematic noise sources. In addition, as discussed in the following, CW-laser-based frequency transfer over fiber (Section 6.1) has moved significantly in this direction. For instance, Ref. [67] describes the operation of the French fiber network over a 2-year span. Similarly, recent work has shown that comb-based time transfer over fiber can form the timing backbone for km-scale accelerator facilities [59].

While CW-laser-based frequency transfer over the air (Section 7.2) can ride on the advances of CW-laser-based frequency transfer over fiber for the frequency transfer itself, the physical coupling from free space to fiber is a separate challenge. With the small nonambiguity range of a few femtoseconds, automated robust control of the coupling of the received light into single-mode fiber is critical to ensuring high uptimes and, thus, high precision [183]. For moving platforms, when rapid tracking is required, robust automated systems are even more essential [101]. In addition, development of tracking, single-mode free-space optical terminals will be critical for time–frequency transfer to moving platforms [202].

Comb-based time transfer over free-space links faces the same coupling problem with the added challenges of chromatic dispersion and more difficult optical amplification due to the broad spectral bandwidth utilized. Low-loss free-space optical terminals have been developed that support this comb-based time transfer [215] but much work remains for the free space to fiber coupling to become turnkey. As both the CW-based and comb-based approaches operate around 1.5 μm and both rely on heterodyne detection, the comb-based time transfer can in principle leverage the recent developments discussed above for the CW-based approach.

The carrier frequency and time acquisition steps of the comb-based time transfer of Ref. [192] were not fully automated. The relative carrier frequency offset between sites was determined via *a priori* information and input by the user. The time acquisition (overlapping of tracking comb pulses with the incoming comb pulses) was initiated after all setpoints were determined by the push of a button. Automated phase-locking of the frequency combs at the right setpoints as well a fully autonomous frequency and timing acquisition will be required if the potential of future ground-to-GEO links is to be achieved such as is outlined in Ref. [37].

8.1d. Exploring a Wider Range of Comb Architectures

The frequency comb-based time and frequency transfer of Sections 6.3 and 7.3 relied primarily upon fiberoptic based comb designs with output spectral bandwidths centered around 1.5 μm. These fiber combs are robust and can be readily integrated with telecommunications-based fiber systems. However, the rapidly evolving field of frequency comb research has led to the development of a number of other platforms that are intriguing for future optical time and frequency transfer [107,108].

Microcombs [107,125,203–207] are appealing for future optical time transfer due to their nominal reproducibility through mass fabrication and their eventual low SWaP footprint. The significant advances in the field of photonic integrated circuits (PICs) in general [216,217] and in integrated microresonator-based combs specifically has led to microcombs for which the entire comb, not just the oscillator itself, has a low SWaP. Further effort is required, though, to generate compact, robust microcombs with more tractable repetition rates in the tens of GHz that can be fully self-referenced.

Frequency combs generated from an EOM, often termed EO combs, are another intriguing option for extending the range of optical time transfer [218]. These combs typically have a very flat optical spectrum and offer agile tuning in some cases [219]. (See the review of Ref. [107] and references therein for further discussion of EO combs.) As with microcombs, advances of the field of PICs hold great promise for low-SWaP robust integrated EO combs. Recent work has shown that the output of a resonator-enhanced EO combs can cover the entirety of the telecommunications L-band (1565–1625 nm) without the need for significant nonlinear broadening downstream [220]. EO combs will also offer an interesting venue for exploring the trade-offs

associated with changing repetition frequencies. In addition, in the case of the offset repetition rate approach (Section 7.3.1), they also offer an avenue to explore the two-dimensional trade-space associated with changing Δf_r and f_r.

Advances in PICs have also led to fiber combs that contain PIC components such as waveguides for the nonlinear broadening required to generate an f_{ceo} signal. This has resulted in lower power consumption in fiber frequency combs allowing for a reduction of the overall SWaP for these as well [221,222]. PICs have also been used in optical transceivers used to combine frequency comb signals for frequency-comb-based time transfer [223]. In the future, further advances in PICs could be leveraged in the amplified comb approach of Section 7.3.2 to reduce SWaP and ameliorate issues with out-of-loop fiber and dispersion.

8.2. Quantum Limit and Beyond

8.2a. Quantum Limit for Optical Time Transfer Based on Heterodyne Detection

As many of the approaches to time and frequency transfer described previously are based on optical heterodyne detection, it is useful to consider the fundamental precision limit that can be achieved with classical light, i.e., the standard quantum limit.

For an optical heterodyne measurement the photodetector current as a function of time, t, is given by $i(t) = i_{LO} + i_S + 2\sqrt{i_{LO} i_S}\cos(2\pi(\nu_S - \nu_{LO})t)$ where i_{LO} is the DC current due to the local oscillator power, i_S is the DC current due to the signal power, ν_{LO} and ν_S are the frequencies of the local oscillator and signal, respectively, and we have assumed the photodetector responsivity is slow enough to be insensitive to oscillations at frequencies of ν_{LO}, ν_S, or higher. The mean square current of the heterodyne signal oscillating at the difference frequency, $\nu_S - \nu_{LO}$ is then given by $\bar{i}^2_{het} = 2 i_{LO} i_S$. In the case that the local oscillator power is much stronger than the signal power, i.e., $i_{LO} >> i_{het} >> i_S$, the noise current due to shot noise is then $i^2_N = 2 e i_{LO} B$, where e is the electron charge and B is the single-sided bandwidth corresponding to an averaging time of $T = (2B)^{-1}$. The power SNR ratio is then given by $SNR_P = i_S/eB = \eta P_S/h\nu_s B$, where h is Planck's constant, η is the quantum efficiency of the detector, $P_S = n_S h\nu_S/T$ is the received signal power, and n_S is the number of signal photons in the measurement duration, T. (See also Ref. [224] for a more extensive discussion of heterodyne detection.)

For the measurement of the deviations of the phase from the expected phase advance, $\delta\theta(t)$, the voltage fluctuations due to shot noise on the detector will result in a statistical uncertainty of $\sigma_\theta \simeq 2\pi/SNR_V$ where $SNR_V = \sqrt{SNR_P}$ is the voltage SNR of the heterodyne measurement. This expression for σ_θ comes from scaling the feature size, in this case the 2π phase cycle, by the SNR_V [225,226]. The limit of $SNR_V \to \infty$ would yield perfect knowledge of the phase ($\sigma_\theta = 0$) and $SNR_V = 1$ gives an uncertainty equal to the feature size. As discussed in Section 2, accumulated time is related to the phase of signal light according to $x(t) = \theta(t)/2\pi\nu_s$ and the deviations from the expected time advance are therefore given by $\delta x(t) = \delta\theta(t)/2\pi\nu_s$. From this, we can write a simple expression for the quantum-limited timing uncertainty

$$\sigma_t \simeq \frac{1}{\nu_S}\frac{1}{SNR_V} = \frac{1}{\nu_S\sqrt{2\eta n_S}}, \tag{13}$$

where ν_S is the frequency of the optical carrier transmitted across the link. For a link with a $\nu_S = 200$ THz carrier frequency, $\eta = 0.9$, $P_S = 1$ pW, and $T = 50$ μs ($B = 10$ kHz), this corresponds to $n_S = 380$ photons and, thus, a quantum-limited uncertainty of $\sigma_t \simeq 0.2$ fs. In the case of a strong received power of 2.0 nW and an averaging time of 1 ms (15 million photons), this uncertainty is reduced to 1 as.

The exceedingly low limit of 0.2 fs even at a received power of 1 pW and an averaging time of only 50 μs demonstrates the power of using the small feature size of the optical carrier. For fiber links with amplification and cascaded repeaters to overcome loss, bandwidth limitations and technical noise always dominate [82,83]. Note that this does not mean that performance is poor: rather the quantum limit is just exceedingly low due to high SNR. As link spans are increased (and, thus, total loss increases), the quantum limit of Eq. (13) may indeed set the limit on achievable performance for CW-based frequency transfer.

References [123,192] follow a similar path to the previous discussion to arrive at a quantum limit for the tracking-comb approach to time transfer over free space. (See Section 7.3.) In this case the feature size is not the optical carrier but the pulse width of the transmitted frequency comb pulse, τ_p, which sets the quantum limit

$$\sigma_t = \gamma \frac{\tau_p}{\sqrt{n_S}}, \tag{14}$$

where the γ prefactor is of order unity and depends on the exact pulse shape as well as the detector quantum efficiency. The timing uncertainty for the same $n_S = 380$ photons as in the CW carrier case, but now with a pulse duration $\tau_P = 350fs$, becomes $\sigma_t =$ 20 fs. This means that tracking-comb time transfer will have a greater quantum-limited timing uncertainty than a CW-laser based approach with all other factors being equal, i.e., same number of received photons per measurement period. However, this is only true if the tracking-comb approach relies solely on the pulse-envelope timing; hand-off to the carrier phase as in Ref. [188] would result in a quantum limit that mirrors that of the CW-laser based approach.

When considering the dependence of the uncertainty on the number of received photons, the power penalty becomes apparent for frequency-comb-based time transfer that uses the offset repetition rate approach (Section 7.3.1). In this case, only the photons of the incoming comb pulses that overlap with the local oscillator pulses contribute to the number of signal photons [190]. As a consequence, the number of signal photons per timing measurement (interferogram) of duration $T = 1/\Delta f_r$, $n_S \simeq M\tau_p P_s/h\nu_s$, is greatly reduced from the maximum possible quantum-limited value, $n_{S,QL} = P_s(\Delta f_r)^{-1}/h\nu_s$, where the magnification factor, $M = f_r/\Delta f_r$, sets the number of comb pulses that contribute to an interferogram, f_r is the comb repetition frequency, and Δf_r is the difference in repetition frequency between the signal comb and the local oscillator comb. An expression for the resulting power penalty can be written as $PP = n_{S,QL}/n_S = 1/(M\Delta f_r\tau_p) = 1/(f_r\tau_p)$. For a 200-MHz repetition rate and a 350-fs pulse width, the power penalty is $\simeq 14,000$ that leads to an increase in the timing uncertainty of $\simeq 120\times$ compared with the quantum limit for the same measurement duration.

8.2b. Entangled Photons for Time Transfer

The use of entangled photon pairs is another approach for optical time transfer and synchronization especially for future quantum networks. An early proof of principle demonstration over 3 km of fiber was able to achieve picosecond resolution [227]. More recent work based on Hong–Ou–Mandel (HOM) interference patterns reached instabilities of a few hundred femtoseconds over 4 km of fiber [228] and over 20 km of fiber [229]. Reference [228] also predicts an achievable TDEV of 10 fs at averaging times greater than 10,000 seconds with improvements to the system. Extension to longer fiber spans may be challenging given the increase in loss expected as entangled photon pairs cannot be amplified in the same manner as classical light (the no cloning theorem [230,231]). Entangled-photon-based time transfer through free space will also face the challenge of fixed loss as well as the variable loss and phase fluctuations

due to atmospheric turbulence. Interestingly, the work of Ref. [232] suggests that in the weak-turbulence limit, HOM interference patterns are sufficiently robust that time transfer over short distance (few kilometers) terrestrial free-space links may be possible.

8.2c. Beyond Conventional Clock Networks

In a conventional optical clock network, each clock is operated independently and then compared. For state-of-the-art optical clocks the fractional frequency instability can be limited by either the quantum projection noise (QPN) or the Dick effect, the aliasing of high-frequency laser noise due to the dead time of the clock operation [233,234]. As the phase noise of the clock laser affects the maximum interrogation (Ramsey free-evolution) time and the magnitude of the Dick effect, moving to more complex clock network architectures can reduce the clock instabilities by making the clock laser noise common mode.

By probing two clocks synchronously and/or probing two clocks with phase-coherent lasers (e.g., one laser distributed across the network) the magnitude of the Dick effect can be reduced below the QPN limit and the QPN limit greatly reduced by extending the interrogation time [235]. Improved performance has now been demonstrated both for the correlated spectroscopy of two single ion clocks separated by 3 m [236] and for a zero-dead-time Yb lattice clock combined with an Al^+ single-ion clock located in different laboratories within the same building [237]. For this to be effective, the relative phase noise between clock (probe) lasers must be $<<1$ rad over the interrogation time. In the demonstration of Ref. [236], an out-of-loop verification showed differential phase fluctuations less than $\pi/20$ out to 12-s probe times. For clock networks that extend beyond the confines of a single building, the challenge will be to employ some of the optical time and frequency transfer approaches outlined here to preserve low differential phase noise over long spans.

Reaching and lowering the QPN limit by extending coherence times is already a significant technical challenge for clock networks with large spans. However, a second lower limit exists for clocks that are fully entangled: the Heisenberg limit. Unlike the QPN limit, sometimes also termed the standard quantum limit, for which the instability (ADEV) scales as $1/\sqrt{N}$, the Heisenberg limit leads to an instability that scales as $1/N$, where N is the atom number, a particularly attractive option for a network composed of multiple single-ion clocks. References [238,239] outline two proposals for entangled clock networks. A recent network of entangled clocks composed of two $^{88}Sr^+$ single-ion clocks separated by 2 m showed the expected $\sqrt{2}$ improvement over the QPN limit [240]. This work used a standard active noise cancellation approach as outlined in Section 6.1 to distribute the same 674-nm probe laser to both clocks [240]. As with the coherent probing of multiple clocks discussed previously, one of the challenges in moving from a few-meter span to the multisatellite vision of Ref. [238] is maintaining relative phase noise well below 1 rad between clock nodes.

8.3. Moving Beyond Developing the Tools to Applications

8.3a. Precision Time and Frequency as a Service

With the advances in time and frequency transfer over fiberoptic links of the last 20 years or so, there are now multiple instances of high-precision time and/or frequency transfer as a service.

Throughout France, the REFIMEVE + project is working to deliver stable 200-THz CW light generated at the SYRTE laboratory to multiple research laboratories within France as well as making international connections to other national metrology institutes (NMIs) [66,67]. With a goal of eventually connecting 10 or more laboratories,

this should enable high-resolution spectroscopy and general remote laser stabilization for a range of projects in locations far from those containing state-of-the-art optical references. Over one of the links, this network showed an impressive uptime of 75% over 2 years of operation [67].

As nascent quantum networks continue to be developed, they will require relative phase stability between nodes and timing synchronization. Since the field of quantum networks itself is rapidly evolving, the exact requirements for this are still uncertain as different quantum network architectures have radically different needs. What is clear is that the classical timing network that supports the quantum network should be robust and turn-key. Recent work has shown that 10-ps optical synchronization of nodes separated by hundreds of kilometers of fiber is more than sufficient to support the optical interference of 100-picosecond-width pulses for quantum key distribution [60,61]. Demonstrating the wide range of potential stability requirements for quantum networking, robust phase transfer over optical fiber was recently shown to support 0.1 rad relative phase noise out to averaging times of 100 ms to achieve quantum bit error rates of less than 1% in support of quantum key distribution [62].

Another place where frequency transfer needs to be robust and turn-key is at phased-array telescopes. Early work on active cancellation of fiber noise at ALMA enables the distribution of CW-laser references to each antenna with the RF reference at the antenna generated by photomixing [152,241]. More recently, active fiber noise cancellation has been pursued to support distribution of a single guide reference to many separate locations necessary for the operation of the SKA currently under construction in Australia and South Africa [153,154,242]. Interestingly, the unique environmental noise constraints, differing spans and differing observational frequency ranges have led to the development of two related but distinct approaches. The SKA site in Australia, SKA-LOW, uses an RF-modulated optical carrier approach to distributing a maser reference across the site [154], whereas the SKA site in South Africa, SKA-MID, uses a photomixing approach capable of supporting the high performance required despite the use of long-haul overhead fibers [153]. As the ngVLA is developed [243], it too will benefit from the development of robust and turnkey frequency transfer [156].

Frequency-comb-based time transfer over fiberoptic links has also moved from a research project of its own to supporting the operation of large-scale scientific facilities such as x ray free-electron lasers [59]. For instance, this approach has now been used for timing at the Linac Coherent Light Source-II (LCLS-II) [244] and at the Swiss X-ray Free Electron Laser (SwissFEL) [245].

8.3b. Intracontinental Sensor Networks

Currently, regional fiber networks that can connect optical clocks exist in parts of the United States [52], Japan [84,157], and Europe where the national metrology institutes of Germany (PTB), France (SYRTE), the United Kingdom (NPL), and Italy (INRIM) are connected via optical fiber [67]. Efforts such as REFIMEVE + in France and the Clock Network Services (CLONETS) Project within the general EU region are seeking to expand these networks. Already, these regional fiber solutions have enabled long-term optical clock comparison over hundreds of kilometers between reaching the level of 5×10^{-17} between SYRTE and PTB [145] and 7×10^{-17} between NPL and PTB [136].

These intracontinental clock networks have already helped perform fundamental physics tests as researchers have searched for dark matter and variations of the fine structure constant using clocks located at NPL, PTB, and SYRTE [18] and performed tests of special relativity with clocks at NPL and SYRTE [32]. Beyond networking

optical clocks, frequency transfer across optical fiber networks can help detect seismic activity and triangulate earthquakes [31,80].

As the techniques used in fiber-based frequency transfer are relatively mature, we anticipate the field will focus on increasing link distance, networking more laboratories, and optimizing uptime. This should lead to increased use of frequency transfer as an enabling tool for a wide range of applications. We anticipate that expansion of stable frequency delivery from optical clock laboratories will lead to more tests of fundamental physics [6], continued support of terrestrial distributed coherent sensing [246], and support the upcoming redefinition of the second [45].

8.3c. Intercontinental Linking of Terrestrial State-of-the-Art Optical Clocks

A mandatory criterion for the redefinition of the second with optical atomic clocks is the validation of optical frequency standard accuracy budgets through frequency ratio measurements between metrology institutes at the level of $<5 \times 10^{-18}$ [45]. While this is supportable through fiberoptic links, some NMIs with optical clocks are not part of a larger fiber network due to geographic isolation and current phase stabilized links are only available at the intracontinental level. Future intercontinental clock comparisons at sufficient precision must rely either on transportable optical clocks or advanced free-space or fiber links.

Transportable clocks have made dramatic progress reaching 10^{-18}-level instabilities in portable packages that can be transported by vehicles [234]. Indeed, frequency ratio measurements of portable optical clocks transported between metrology institutes have been very recently demonstrated as part of the International Clock and Oscillator Networking (ICON) Collaboration [247].

Transoceanic fiber links will necessarily include submarine fiberoptic cables along with the conventional terrestrial bidirectional fiber links discussed in Section 6. Transmission of stable optical frequencies over submarine fiberoptic cables currently allows for the use of existing fiberoptic cables for earthquake detection and for as more general seafloor environmental sensors [31,248]. These submarine fiberoptic cables present an intriguing option as researchers using a conservative noise estimate have found clock comparisons are possible over a 7000-km transoceanic cable at the 1×10^{-16} level using a duplex pair (side-by-side fibers for bidirectional propagation) and at the 1×10^{-19} level using a single bidirectional fiber [249]. This option is particularly appealing as upgrading transoceanic links to be truly bidirectional with bidirectional amplifiers is an extremely challenging proposition in contrast to upgrading terrestrial links with their comparatively easy access.

Finally, advances in free-space time transfer and efforts to push time–frequency metrology to space may eventually enable intercontinental clock comparisons via satellites. Reference [37] proposed a scheme where laboratory-based optical atomic clocks could be connected via an active node in geostationary orbit with frequency combs and a cavity stabilized laser. Such a common-view scenario could hypothetically connect clocks at European NMIs to clocks at NIST in the United States, or similarly clocks at NIST to clocks at NICT in Japan. The modeling in Ref. [37] suggested link performance at a few parts in 10^{-16} at 1 second reaching a few parts in 10^{-19} should be possible.

8.3d. Optical Clocks in Space and Future Space-Based Timing Networks

One of the exciting possibilities that arises from the advances in precision optical time and frequency transfer over free space (Section 7) is that of ground-to-satellite and satellite-to-satellite links. Figure 17 shows a conceptual sketch of one vision for a diverse array of optical time and frequency links. In addition to using a GEO satellite

Figure 17

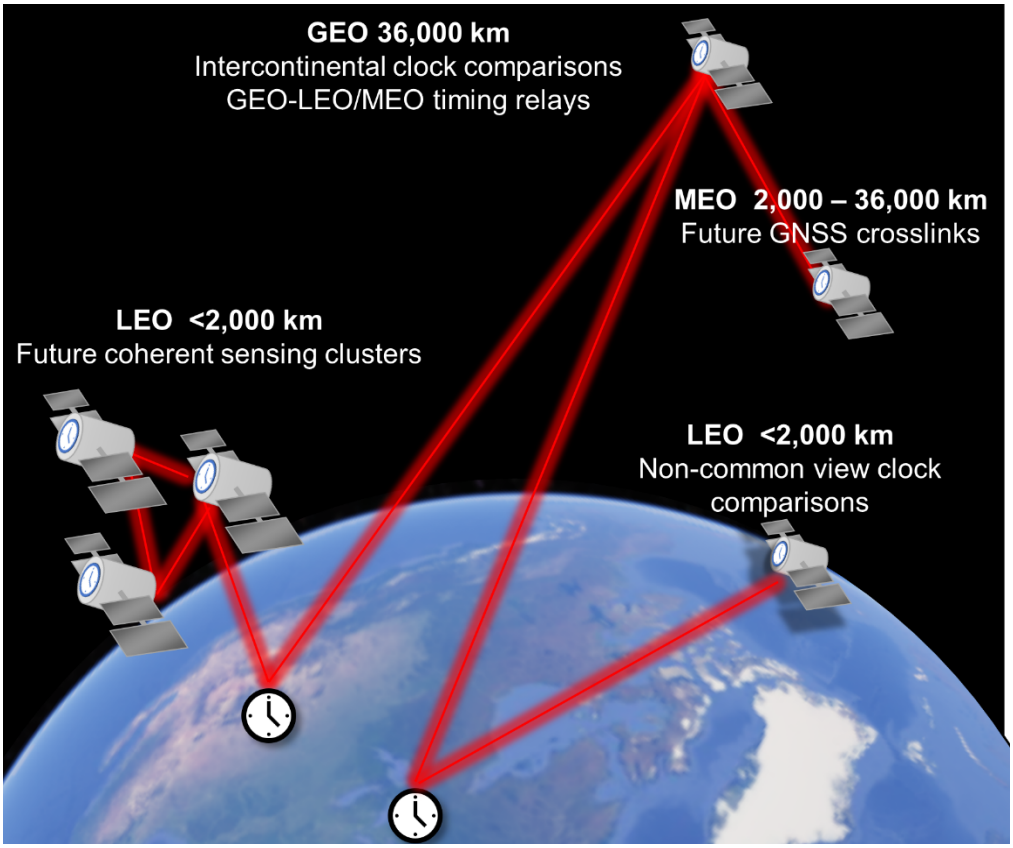

Conceptual schematic of future space-based timing networks. Intersatellite optical links could be used to distribute time and frequency for coherent sensing or future GNSS crosslinks. Ground-to-satellite optical links could enable high-precision comparisons between multiple ground and spaceborne clocks in common-view operation (via GEO) [37] or noncommon-view operation (via LEO) as is proposed for the microwave link for the ACES mission [42]. (Note that this conceptual schematic represents a broad vision for the future rather than an official roadmap of NIST.)

to link terrestrial state-of-the-art clocks across continents as proposed in Ref. [37], placing a state-of-the-art optical clock on a GEO satellite would allow for fundamental physics measurements such as those outlined in Ref. [6] and could also serve as the guide node for multiple follower clocks. By connecting ground stations to the GEO satellite and then linking the GEO satellite to multiple satellites in MEO, for instance, the challenges for the optical links of atmospheric turbulence fluctuations and of significant relative motion would be decoupled. Satellites optically cross-linked with relative timing noise at the femtosecond-level could provide a backbone for future GNSS crosslinks [22]. This could look similar to the proposed Kepler mission [106] linking MEO and LEO satellites but with the precision of state-of-the-art optical clocks and femtosecond-level time transfer. These future links may take advantage of optical links established for quantum physics experiments such as those performed under the Micius satellite program [250] as many of the technical challenges are shared between quantum communications and high-precision optical time and frequency transfer.

Fully space-based distributed coherent sensing would also benefit from precise optical time and frequency transfer. For distributed coherent sensors, the relative timing noise needs to be less than $\sim 1/(10\nu)$ where ν is the observation carrier frequency; observational frequencies of greater than 100 GHz nominally require timing of better

than 1 ps, our definition of precision optical time transfer. These coherent sensors would not face the same atmospheric limitations imposed on terrestrial very-long baseline interferometry (VLBI), for instance, allowing for VLBI at a much wider range of observational frequencies [24]. Small-span satellite clusters in LEO orbits could allow for earth observations beyond that of the 10 GHz observation frequency of the TanDEM-X radar interferometer [251] even observing through the Earth's atmosphere.

For fundamental physics measurements such as tests of relativity or searches for dark matter, clock network configurations may be required beyond those sketched in Fig. 17. For instance, a proposal for placing a state-of-the-art optical clock in space to test relativity would employ a highly elliptical orbit and require measurement of the accumulated time offset on the space clock versus a terrestrial clock [12]. It may be possible to achieve state-of-the-art optical clocks both in elliptical orbits with an optical measurement of the difference in accumulated time via optical time transfer similar to the measurements that used the two Galileo satellites launched into elliptical orbits [8,9].

Future optical clocks may also support deep space navigation. Clocks onboard spacecraft will need to be compared occasionally to terrestrial clocks or clocks located much closer to Earth. As both CW-laser based frequency transfer and comb-based time transfer can reach residual instabilities below 1×10^{-16} rapidly, the duration of these intermittent comparisons can be quite short when comparing intermediate-performance optical clocks or high-performance microwave clocks. When designing these clock networks, the very high losses will need to be considered in order to achieve the desired precision. The recent operation of a trapped-ion clock in space that reached a fractional frequency instability of 3×10^{-15} [252] is an extremely promising step toward realizing future deep space clock networks. It is also intriguing to think about extensions to proposals such as the Lorentz test of Ref. [253] that would see the clock in deep space linked back to state-of-the-art terrestrial clocks.

Clock networks have also been proposed to support gravitational wave sensing in bands not accessible to the laser-interferometer-based detectors. For instance, use of 10-km diameter asteroids as test masses separated by 150 million km has been proposed for future gravitational wave detection in the microhertz band [254]. The proposal of Ref. [254] invokes a variant of pulsed-source time transfer similar to that discussed in Section 7.1. More generally, any variant of optical two-way time transfer, which measures both the range and clock offset, could potentially support such asteroid-based gravitational-wave detectors if the approach can sustain the loss inherent in a 150 million km baseline.

9. CONCLUSION

In conclusion, we have discussed high-precision optical time and frequency transfer with a focus on reviewing the available techniques, discussing applications, and giving perspective on the future of the field. To orient the reader and provide context to later technique comparisons, we began in Section 2 by explaining commonly used metrics in time and frequency metrology and the relationships between phase, frequency, and fractional frequency. Building on this, we highlighted the distinction between frequency transfer and time transfer in Section 3 and offered an overview of which applications require time and which require frequency.

Before discussing specific techniques, in Section 4, we explained several challenges that are common to time and frequency transfer systems based in both fiber and free space, namely phase noise, signal distortions, and link loss and intermittency. To

achieve high precision in either time transfer or frequency transfer it is necessary to mitigate phase noise in the transfer channel. We discussed sources of phase noise for both fiber and free-space channels with a focus on temperature, vibration, and turbulent fluctuations and explained the importance of link reciprocity for many of the techniques described later. Signal distortions arise due to nonlinear and dispersive properties of a channel, so we explained the effect of fiber nonlinearities including Raman scattering, Brillion scattering, and SPM as well as dispersive broadening seen in free space. Link intermittency and channel loss will ultimately drive system uptime and performance at long time scales so we discussed sources of loss and ways to overcome them including terminal design and channel amplification. Finally, we discussed the challenge of platform motion, which is a uniquely free-space challenge, but common to both frequency and time transfer efforts.

In Section 5, we introduced the optical frequency comb, which is a critical piece of technology to optical clockwork and many of the techniques detailed later. This section sought to introduce the reader to the generation and control of the frequency comb and explain the technology's role in the modern metrology lab.

The next sections detailed specific time and frequency transfer techniques, delineating them broadly by medium, fiber or free space, and then by time or frequency. In Section 6, we detailed fiber-based transfer focusing first on frequency transfer using CW lasers. This is a mature technique with many variations so we began by explaining the fundamental technique of fiber-noise cancellation and how noise can be canceled with light reflected back across a fiber link or with repeater lasers. Fiber-based frequency transfer based on these techniques exhibits high link uptimes and reaches sub-10^{-18} level instabilities at tens to hundreds of seconds. We then discussed two-way fiber-based frequency transfer where active sites on either side of a fiber send light to the other site. This technique exhibits some of the lowest instabilities for links up to hundreds of kilometers in length. For fiber-based time transfer we detail CW-based methods that use communication protocols to reach subpicosecond-level time transfer and pulse-based methods that rely on DCF to enable femtosecond-level time transfer.

In Section 7, we detailed free-space methods of time and frequency transfer. First, we explained the pulsed-source time transfer methods used to show picosecond time transfer between ground and satellite. We then moved to CW-laser based frequency transfer over free space, which operates on the same fundamental principles as CW-laser based frequency transfer over fiber. This technique can reach instabilities of 10^{-18} or less at tens of seconds but so far has been limited in link distance over few-kilometer scales. We finished by discussing frequency-comb-based two-way time transfer. This technique can be broken down into several variations including offset repetition rate time transfer, amplified comb time transfer, and tracking comb time transfer. These techniques typically reach sub-10^{-18} at hundreds to thousands of seconds but can operate for extended periods of time and over links up to 300 km in length.

In Section 8, we sought to highlight outstanding problems in the field of time transfer and provide an outlook for future uses and applications. For free space, adapting the available techniques to tolerate the high platform speeds expected for ground-to-space time transfer is one of the leading outstanding challenges. To increase the working distance of any of the techniques described previously, the challenge of additional loss must also be overcome. As time and frequency transfer techniques advance from the development stage to full remote deployment, it will be important to further automate system operation as currently experiments are often run by multiple scientists. Finally, we address efforts to support quantum applications.

We closed our review with a look at future applications of time and frequency transfer. One application is precision time and frequency as a turnkey service: a plug-and-play solution for spectroscopy, quantum networks, and coherent sensing arrays. We also discussed intracontinental sensor network development to connect optical clocks for fundamental physics and fiber networks for earthquake sensing. In the future we also envision intercontinental linking of optical atomic clocks for the redefinition of the second and ground-to-space time transfer for clock comparisons, fundamental physics tests, future GNSS crosslinks, and space-based coherent sensing nodes.

With the development of a broad heterogenous set of techniques for high-precision optical time and frequency transfer, the future for optical timing networks is auspicious. Some of these techniques are already mature enough that their development has turned already to a focus on their use in applications. Other techniques still require more maturation and development to become technologically feasible. We look forward to the continued development of tools for high-precision optical time and frequency transfer and their use in optical timing networks for an ever-developing range of applications.

FUNDING

National Institute of Standards and Technology; National Science Foundation (QLCI Award Number OMA - 2016244); Air Force Office of Scientific Research (MIPR F4FGA02152G001).

ACKNOWLEDGMENTS

We thank Brian Washburn, Ian Coddington, Fabrizio Giorgetta, and Nicholas Nardelli for thoughtful comments on the manuscript. Certain equipment or instruments are identified in this paper in order to specify the experimental procedure adequately. Such identification is not intended to imply recommendation or endorsement of any product by NIST, nor is it intended to imply that the equipment identified are necessarily the best available for the purpose.

DISCLOSURES

The authors declare no conflicts of interest.

DATA AVAILABILITY

No data were generated or analyzed in the presented research.

REFERENCES

1. S. Bize, "The unit of time: present and future directions," C. R. Phys. **20**, 153–168 (2019).
2. F. Riehle, "Optical atomic clocks could redefine unit of time," Physics **5**, 126 (2012).
3. F. Riehle, "Optical clock networks," Nat. Photonics **11**, 25–31 (2017).
4. H. Hachisu, M. Fujieda, S. Nagano, *et al.*, "Direct comparison of optical lattice clocks with an intercontinental baseline of 9000 km," Opt. Lett. **39**, 4072–4075 (2014).
5. B. Hoffmann, "Noon-midnight red shift," Phys. Rev. **121**, 337–342 (1961).
6. M. S. Safronova, D. Budker, D. DeMille, *et al.*, "Search for new physics with atoms and molecules," Rev. Mod. Phys. **90**, 025008 (2018).
7. C.-G. Qin, Y.-J. Tan, and C.-G. Shao, "The tidal clock effects of the lunisolar gravitational field and the Earth's tidal deformation," AJ **160**, 272 (2020).

8. P. Delva, N. Puchades, E. Schönemann, *et al.*, "Gravitational redshift test using eccentric *Galileo* satellites," Phys. Rev. Lett. **121**, 231101 (2018).
9. S. Herrmann, F. Finke, M. Lülf, *et al.*, "Test of the gravitational redshift with *Galileo* satellites in an eccentric orbit," Phys. Rev. Lett. **121**, 231102 (2018).
10. M. Takamoto, I. Ushijima, N. Ohmae, *et al.*, "Test of general relativity by a pair of transportable optical lattice clocks," Nat. Photonics **14**, 411–415 (2020).
11. P. Wolf and L. Blanchet, "Analysis of Sun/Moon gravitational redshift tests with the STE-QUEST space mission," Class. Quantum Grav. **33**, 035012 (2016).
12. A. Derevianko, K. Gibble, L. Hollberg, *et al.*, "Fundamental physics with a state-of-the-art optical clock in space," Quantum Sci. Technol. **7**, 044002 (2022).
13. A. Derevianko and M. Pospelov, "Hunting for topological dark matter with atomic clocks," Nat. Phys. **10**, 933–936 (2014).
14. A. Hees, J. Guéna, M. Abgrall, *et al.*, "Searching for an oscillating massive scalar field as a dark matter candidate using atomic hyperfine frequency comparisons," Phys. Rev. Lett. **117**, 061301 (2016).
15. P. Wcisło, P. Ablewski, K. Beloy, *et al.*, "New bounds on dark matter coupling from a global network of optical atomic clocks," Sci. Adv. **4**, eaau4869 (2018).
16. C. Sanner, N. Huntemann, R. Lange, *et al.*, "Optical clock comparison for Lorentz symmetry testing," Nature **567**, 204–208 (2019).
17. R. Lange, N. Huntemann, J. M. Rahm, *et al.*, "Improved limits for violations of local position invariance from atomic clock comparisons," Phys. Rev. Lett. **126**, 011102 (2021).
18. B. M. Roberts, P. Delva, A. Al-Masoudi, *et al.*, "Search for transient variations of the fine structure constant and dark matter using fiber-linked optical atomic clocks," New J. Phys. **22**, 093010 (2020).
19. B. Altschul, Q. G. Bailey, L. Blanchet, *et al.*, "Quantum tests of the Einstein equivalence principle with the STE-QUEST space mission," Adv. Space Res. **55**, 501–524 (2015).
20. V. Schkolnik, D. Budker, O. Fartmann, *et al.*, "Optical atomic clock aboard an Earth-orbiting space station (OACESS): enhancing searches for physics beyond the standard model in space," Quantum Sci. Technol. **8**, 014003 (2023).
21. T. E. Mehlstäubler, G. Grosche, C. Lisdat, *et al.*, "Atomic clocks for geodesy," Rep. Prog. Phys. **81**, 064401 (2018).
22. Z. Warren and R. Fields, "Optical crosslinks and satellite synchronization for GNSS, communications, and beyond," GPS Solut **26**, 64 (2022).
23. P. Kurczynski, M. D. Johnson, S. S. Doeleman, *et al.*, "The event horizon explorer mission concept," in *Space Telescopes and Instrumentation 2022: Optical, Infrared, and Millimeter Wave*, Vol. 12180 (SPIE, 2022), pp. 215–224.
24. L. I. Gurvits, "Space VLBI: from first ideas to operational missions," Adv. Space Res. **65**, 868–876 (2020).
25. The Event Horizon Telescope Collaboration, "First M87 event horizon telescope results. II. array and instrumentation," The Astrophysical Journal Letters **875**, L2 (2019).
26. A. E. E. Rogers and J. M. Moran, "Coherence limits for very-long-baseline interferometry," IEEE Trans. Instrum. Meas. **IM-30**, 283–286 (1981).
27. K. Haworth, M. D. Johnson, D. W. Pesce, *et al.*, "Studying black holes on horizon scales with space-VLBI," arXiv (2019).
28. V. L. Fish, M. Shea, and K. Akiyama, "Imaging black holes and jets with a VLBI array including multiple space-based telescopes," Adv. Space Res. **65**, 821–830 (2020).
29. F. Roelofs, H. Falcke, C. Brinkerink, *et al.*, "Simulations of imaging the event horizon of Sagittarius A* from space," A&A **625**, A124 (2019).

30. C. Clivati, R. Aiello, R. Aiello, *et al.*, "Common-clock very long baseline interferometry using a coherent optical fiber link," Optica **7**, 1031–1037 (2020).
31. G. Marra, C. Clivati, R. Luckett, *et al.*, "Ultrastable laser interferometry for earthquake detection with terrestrial and submarine cables," Science **361**, 486–490 (2018).
32. P. Delva, J. Lodewyck, S. Bilicki, *et al.*, "Test of special relativity using a fiber network of optical clocks," Phys. Rev. Lett. **118**, 221102 (2017).
33. J. D. Roslund, A. Cingöz, W. D. Lunden, *et al.*, "Optical clocks at sea," Nature **628**, 736–740 (2024).
34. C. Perrella, P. S. Light, J. D. Anstie, *et al.*, "Dichroic two-photon rubidium frequency standard," Phys. Rev. Appl. **12**, 054063 (2019).
35. F. Kuschewski, J. Wüst, M. Oswald, *et al.*, "COMPASSO mission and its iodine clock: outline of the clock design," GPS Solut **28**, 10 (2024).
36. K. W. Martin, G. Phelps, N. D. Lemke, *et al.*, "Compact optical atomic clock based on a two-photon transition in rubidium," Phys. Rev. Appl. **9**, 014019 (2018).
37. E. D. Caldwell, L. C. Sinclair, J.-D. Deschenes, *et al.*, "Application of quantum-limited optical time transfer to space-based optical clock comparisons and coherent networks," APL Photonics **9**, 016112 (2024).
38. A. Bauch, J. Achkar, S. Bize, *et al.*, "Comparison between frequency standards in Europe and the USA at the 10^{-15} uncertainty level," Metrologia **43**, 109–120 (2006).
39. M. A. Lombardi, L. M. Nelson, A. N. Novick, *et al.*, Time and frequency measurements using the global positioning system (GPS)," Cal Lab: The International Journal of Metrology, Vol. 8, pp. 26–33 (2001).
40. G. Petit, A. Kanj, S. Loyer, *et al.*, "1 × 10−16 frequency transfer by GPS PPP with integer ambiguity resolution," Metrologia **52**, 301–309 (2015).
41. M. Fujieda, D. Piester, T. Gotoh, *et al.*, "Carrier-phase two-way satellite frequency transfer over a very long baseline," Metrologia **51**, 253–262 (2014).
42. P. Delva, F. Meynadier, C. Le Poncin-Lafitte, *et al.*, "Time and frequency transfer with a MicroWave Link in the ACES/PHARAO mission," in *European Frequency and Time Forum (EFTF)*, Vol. 2012 (European Frequency and Time Forum, 2012), pp. 28–35.
43. F. Meynadier, P. Delva, C. le Poncin-Lafitte, *et al.*, "Atomic clock ensemble in space (ACES) data analysis," Class. Quantum Grav. **35**, 035018 (2018).
44. STE_Quest Team, "ESA science and technology - STE-QUEST assessment study report (Yellow Book)," https://sci.esa.int/web/ste-quest/-/53445-ste-quest-yellow-book.
45. N. Dimarcq, M. Gertsvolf, G. Mileti, *et al.*, "Roadmap towards the redefinition of the second," Metrologia **61**, 012001 (2024).
46. "IEEE standard definitions of physical quantities for fundamental frequency and time metrology - random instabilities," IEEE Std 1139-1999 (1999), pp. 1–31.
47. E. Rubiola and F. Vernotte, "The companion of Enrico's Chart for phase noise and two-sample variances," IEEE Trans. Microwave Theory Tech. **71**, 2996–3025 (2023).
48. W. Riley and D. A. Howe, *Handbook of Frequency Stability Analysis*, National Institute of Standards and Technology Special Publication 1065 (U. S. Government Printing Office, 2008).
49. S. T. Dawkins, J. J. McFerran, and A. N. Luiten, "Considerations on the measurement of the stability of oscillators with frequency counters," IEEE Trans. Ultrason., Ferroelect., Freq. Contr. **54**, 918–925 (2007).
50. E. Rubiola, M. Lenczner, P.-Y. Bourgeois, *et al.*, "The Ømega counter, a frequency counter based on the linear regression," IEEE Trans. Ultrason., Ferroelect., Freq. Contr. **63**, 961–969 (2016).

51. E. Rubiola, "On the measurement of frequency and of its sample variance with high-resolution counters," Rev. Sci. Instrum. **76**, 054703 (2005).
52. Boulder Atomic Clock Optical Network (BACON) Collaboration, K. Beloy, T. Bothwell, S. M. Brewer, *et al.*, "Frequency ratio measurements at 18-digit accuracy using an optical clock network," Nature **591**, 564–569 (2021).
53. M. I. Bodine, J.-D. Deschênes, I. H. Khader, *et al.*, "Optical atomic clock comparison through turbulent air," Phys. Rev. Res. **2**, 033395 (2020).
54. W. R. Milner, J. M. Robinson, C. J. Kennedy, *et al.*, "Demonstration of a timescale based on a stable optical carrier," Phys. Rev. Lett. **123**, 173201 (2019).
55. V. Formichella, L. Galleani, G. Signorile, *et al.*, "Robustness tests for an optical time scale," Metrologia **59**, 015002 (2022).
56. V. Formichella, G. Signorile, T. T. Thai, *et al.*, "Year-long optical time scale with sub-nanosecond capabilities," Optica **11**, 523–530 (2024).
57. J. Yao, J. A. Sherman, T. Fortier, *et al.*, "Optical-clock-based time scale," Phys. Rev. Appl. **12**, 044069 (2019).
58. F. Eisenhauer, J. D. Monnier, and O. Pfuhl, "Advances in optical/infrared interferometry," Annu. Rev. Astron. Astrophys. **61**, 237–285 (2023).
59. M. Xin, K. Şafak, and F. X. Kärtner, "Ultra-precise timing and synchronization for large-scale scientific instruments," Optica **5**, 1564–1578 (2018).
60. J.-P. Chen, C. Zhang, Y. Liu, *et al.*, "Twin-field quantum key distribution over a 511 km optical fibre linking two distant metropolitan areas," Nat. Photonics **15**, 570–575 (2021).
61. Y. Liu, W.-J. Zhang, C. Jiang, *et al.*, "Experimental twin-field quantum key distribution over 1000 km fiber distance," Phys. Rev. Lett. **130**, 210801 (2023).
62. C. Clivati, A. Meda, S. Donadello, *et al.*, "Coherent phase transfer for real-world twin-field quantum key distribution," Nat. Commun. **13**, 157 (2022).
63. J.-D. Deschênes, L. C. Sinclair, F. R. Giorgetta, *et al.*, "Synchronization of distant optical clocks at the femtosecond level," Phys. Rev. X **6**, 021016 (2016).
64. I. Khader, H. Bergeron, L. C. Sinclair, *et al.*, "Time synchronization over a free-space optical communication channel," Optica **5**, 1542–1548 (2018).
65. N. F. Ramsey, "A molecular beam resonance method with separated oscillating fields," Phys. Rev. **78**, 695–699 (1950).
66. F. Guillou-Camargo, V. Ménoret, E. Cantin, *et al.*, "First industrial-grade coherent fiber link for optical frequency standard dissemination," Appl. Opt. **57**, 7203–7210 (2018).
67. E. Cantin, M. Tønnes, R. L. Targat, *et al.*, "An accurate and robust metrological network for coherent optical frequency dissemination," New J. Phys. **23**, 053027 (2021).
68. M. B. K. Tønnes, F. Schuller, E. Cantin, *et al.*, "Coherent fiber links operated for years: effect of missing data," Metrologia **59**, 065004 (2022).
69. W. H. Glenn, "Noise in interferometric optical systems: an optical Nyquist theorem," IEEE J. Quantum Electron. **25**, 1218–1224 (1989).
70. R. F. Wright, N. Diemler, J. C. Egbu, *et al.*, "Fully distributed optical fiber sensor for humidity monitoring at high temperatures," in *Optical Waveguide and Laser Sensors*, Vol. 11405 (SPIE, 2020), pp. 23–35.
71. P. E. Ciddor, "Refractive index of air: new equations for the visible and near infrared," Appl. Opt. **35**, 1566–1573 (1996).
72. A. Ishimaru, *Wave Propagation and Scattering in Random Media* (Academic Press, 1978).
73. F. Roddier, "The effects of atmospheric turbulence in optical astronomy," in *Progress in Optics*, E. Wolf, ed. (North-Holland Publishing Co., 1981), Vol. 19, pp. 281–376.

74. L. C. Andrews and R. L. Phillips, *Laser Beam Propagation through Random Media*, 2nd ed. (SPIE, 2005).
75. K. Djerroud, O. Acef, A. Clairon, *et al.*, "Coherent optical link through the turbulent atmosphere," Opt. Lett. **35**, 1479–1481 (2010).
76. L. C. Sinclair, F. R. Giorgetta, W. C. Swann, *et al.*, "Optical phase noise from atmospheric fluctuations and its impact on optical time-frequency transfer," Phys. Rev. A **89**, 023805 (2014).
77. C. Robert, J.-M. Conan, and P. Wolf, "Impact of turbulence on high-precision ground-satellite frequency transfer with two-way coherent optical links," Phys. Rev. A **93**, 033860 (2016).
78. B. K. Stuhl, "Atmospheric refraction corrections in ground-to-satellite optical time transfer," Opt. Express **29**, 13706 (2021).
79. Q. Shen, J.-Y. Guan, T. Zeng, *et al.*, "Experimental simulation of time and frequency transfer via an optical satellite–ground link at 10^{-18} instability," Optica **8**, 471–476 (2021).
80. S. Donadello, C. Clivati, A. Govoni, *et al.*, "Seismic monitoring using the telecom fiber network," Commun. Earth Environ. **5**, 178 (2024).
81. B. P. Lipovsky, J.-M. Manos, Y. Ni, *et al.*, "Distributed acoustic sensing in the Puget sound and Puget lowlands, Washington, USA," 2022, S15A-05 (2022).
82. N. R. Newbury, P. A. Williams, and W. C. Swann, "Coherent transfer of an optical carrier over 251 km," Opt. Lett. **32**, 3056–3058 (2007).
83. P. A. Williams, W. C. Swann, and N. R. Newbury, "High-stability transfer of an optical frequency over long fiber-optic links," J. Opt. Soc. Am. B **25**, 1284–1293 (2008).
84. M. Musha, F.-L. Hong, K. Nakagawa, *et al.*, "Coherent optical frequency transfer over 50-km physical distance using a 120-km-long installed telecom fiber network," Opt. Express **16**, 16459–16466 (2008).
85. S. M. F. Raupach, A. Koczwara, and G. Grosche, "Optical frequency transfer via a 660 km underground fiber link using a remote Brillouin amplifier," Opt. Express **22**, 26537 (2014).
86. R. W. Boyd, *Nonlinear Optics* (Academic Press, 2020).
87. G. P. Agrawal, "Nonlinear fiber optics," in *Nonlinear Science at the Dawn of the 21st Century*, P. L. Christiansen, M. P. Sørensen, and A. C. Scott, eds., Lecture Notes in Physics No. 542 (Springer, 2000), pp. 195–211.
88. L. Gruner-Nielsen, M. Wandel, P. Kristensen, *et al.*, "Dispersion-compensating fibers," J. Lightwave Technol. **23**, 3566–3579 (2005).
89. C. Lin, H. Kogelnik, and L. G. Cohen, "Optical-pulse equalization of low-dispersion transmission in single-mode fibers in the 1.3–1.7-μm spectral region," Opt. Lett. **5**, 476–478 (1980).
90. M. Xin, K. Şafak, M. Y. Peng, *et al.*, "One-femtosecond, long-term stable remote laser synchronization over a 3.5-km fiber link," Opt. Express **22**, 14904–14912 (2014).
91. M. Xin, K. Şafak, M. Y. Peng, *et al.*, "Breaking the femtosecond barrier in multi-kilometer timing synchronization systems," IEEE J. Sel. Top. Quantum Electron. **23**, 97–108 (2017).
92. S. Shen and A. M. Weiner, "Complete dispersion compensation for 400-fs pulse transmission over 10-km fiber link using dispersion compensating fiber and spectral phase equalizer," IEEE Photonics Technol. Lett. **11**, 827–829 (1999).
93. O. Terra, G. Grosche, and H. Schnatz, "Brillouin amplification in phase coherent transfer of optical frequencies over 480 km fiber," Opt. Express **18**, 16102 (2010).
94. D. C. Tee, N. Tamchek, and C. H. Raymond Ooi, "Numerical modeling of the fundamental characteristics of ZBLAN photonic crystal fiber for communication in 2–3 μm midinfrared region," IEEE Photonics J. **8**, 1 (2016).

95. N. Chiodo, N. Quintin, F. Stefani, *et al.*, "Cascaded optical fiber link using the internet network for remote clocks comparison," Opt. Express **23**, 33927 (2015).
96. Y. Shoji, M. J. Fice, Y. Takayama, *et al.*, "A pilot-carrier coherent LEO-to-ground downlink system using an optical injection phase lock loop (OIPLL) technique," J. Lightwave Technol. **30**, 2696–2706 (2012).
97. M. Toyoshima, Y. Takayama, H. Kunimori, *et al.*, "In-orbit measurements of spacecraft microvibrations for satellite laser communication links," Opt. Express **49**, 083604 (2010).
98. A. Belmonte, M. T. Taylor, L. Hollberg, *et al.*, "Effect of atmospheric anisoplanatism on Earth-to-satellite time transfer over laser communication links," Opt. Express **25**, 15676–15686 (2017).
99. W. C. Swann, M. I. Bodine, I. Khader, *et al.*, "Measurement of the impact of turbulence anisoplanatism on precision free-space optical time transfer," Phys. Rev. A **99**, 023855 (2019).
100. B. P. Dix-Matthews, D. R. Gozzard, S. M. Walsh, *et al.*, "Towards optical frequency geopotential difference measurements via a flying drone," Opt. Express **31**, 15075–15088 (2023).
101. S. M. P. McSorley, B. P. Dix-Matthews, A. M. Frost, *et al.*, "Free-space optical-frequency comparison over rapidly moving links," Phys. Rev. Appl. **23**, L021003 (2025).
102. H. Bergeron, L. C. Sinclair, W. C. Swann, *et al.*, "Femtosecond time synchronization of optical clocks off of a flying quadcopter," Nat. Commun. **10**, 1819 (2019).
103. L. C. Sinclair, H. Bergeron, W. C. Swann, *et al.*, "Femtosecond optical two-way time-frequency transfer in the presence of motion," Phys. Rev. A **99**, 023844 (2019).
104. S. A. Fuselier, W. S. Lewis, C. Schiff, *et al.*, "Magnetospheric multiscale science mission profile and operations," Space Sci. Rev. **199**, 77–103 (2016).
105. R. Kahle, B. Schlepp, F. Meissner, *et al.*, "The TerraSAR-X/TanDEM-X formation acquisition–from planning to realization," J. Astronaut Sci. **59**, 564–584 (2012).
106. C. Günther, "Kepler – satellite navigation without clocks and ground infrastructure," in *Proceedings of the 31st International Technical Meeting of the Satellite Division of The Institute of Navigation (ION GNSS+ 2018)*, pp. 849–856 (2018).
107. T. Fortier and E. Baumann, "20 years of developments in optical frequency comb technology and applications," Commun. Phys. **2**, 153 (2019).
108. S. A. Diddams, K. Vahala, and T. Udem, "Optical frequency combs: coherently uniting the electromagnetic spectrum," Science **369**, eaay3676 (2020).
109. R. Paschotta, "Timing jitter and phase noise of mode-locked fiber lasers," Opt. Express **18**, 5041–5054 (2010).
110. N. R. Newbury and W. C. Swann, "Low-noise fiber-laser frequency combs (Invited)," J. Opt. Soc. Am. B **24**, 1756–1770 (2007).
111. F. Riehle, P. Gill, F. Arias, *et al.*, "The CIPM list of recommended frequency standard values: guidelines and procedures," Metrologia **55**, 188–200 (2018).
112. D. J. Jones, S. A. Diddams, J. K. Ranka, *et al.*, "Carrier-envelope phase control of femtosecond mode-locked lasers and direct optical frequency synthesis," Science **288**, 635–639 (2000).
113. S. A. Diddams, D. J. Jones, J. Ye, *et al.*, "Direct link between microwave and optical frequencies with a 300 THz femtosecond laser comb," Phys. Rev. Lett. **84**, 5102–5105 (2000).
114. R. Holzwarth, Th. Udem, T. W. Hänsch, *et al.*, "Optical frequency synthesizer for precision spectroscopy," Phys. Rev. Lett. **85**, 2264–2267 (2000).

115. H. Schnatz, B. Lipphardt, J. Helmcke, *et al.*, "First phase-coherent frequency measurement of visible radiation," Phys. Rev. Lett. **76**, 18–21 (1996).
116. J. Stenger, H. Schnatz, C. Tamm, *et al.*, "Ultraprecise measurement of optical frequency ratios," Phys. Rev. Lett. **88**, 073601 (2002).
117. T. Nakamura, J. Davila-Rodriguez, H. Leopardi, *et al.*, "Coherent optical clock down-conversion for microwave frequencies with 10^{-18} instability," Science **368**, 889–892 (2020).
118. T. M. Fortier, M. S. Kirchner, F. Quinlan, *et al.*, "Generation of ultrastable microwaves via optical frequency division," Nat. Photonics **5**, 425–429 (2011).
119. X. Xie, R. Bouchand, D. Nicolodi, *et al.*, "Photonic microwave signals with zeptosecond level absolute timing noise," Nat. Photonics **11**, 44–47 (2017).
120. D. Herman, S. Droste, E. Baumann, *et al.*, "Femtosecond timekeeping: slip-free clockwork for optical timescales," Phys. Rev. Appl. **9**, 044002 (2018).
121. C. Grebing, A. Al-Masoudi, S. Dörscher, *et al.*, "Realization of a timescale with an accurate optical lattice clock," Optica **3**, 563 (2016).
122. W. F. McGrew, X. Zhang, H. Leopardi, *et al.*, "Towards the optical second: verifying optical clocks at the SI limit," Optica **6**, 448–454 (2019).
123. E. D. Caldwell, L. C. Sinclair, N. R. Newbury, *et al.*, "The time-programmable frequency comb and its use in quantum-limited ranging," Nature **610**, 667–673 (2022).
124. F. R. Giorgetta, W. C. Swann, L. C. Sinclair, *et al.*, "Optical two-way time and frequency transfer over free space," Nat. Photonics **7**, 434–438 (2013).
125. A. L. Gaeta, M. Lipson, and T. J. Kippenberg, "Photonic-chip-based frequency combs," Nat. Photonics **13**, 158–169 (2019).
126. L.-S. Ma, P. Jungner, J. Ye, *et al.*, "Delivering the same optical frequency at two places: accurate cancellation of phase noise introduced by an optical fiber or other time-varying path," Opt. Lett. **19**, 1777–1779 (1994).
127. J. Ye, J.-L. Peng, R. J. Jones, *et al.*, "Delivery of high-stability optical and microwave frequency standards over an optical fiber network," J. Opt. Soc. Am. B **20**, 1459–1467 (2003).
128. I. Coddington, W. C. Swann, L. Lorini, *et al.*, "Coherent optical link over hundreds of metres and hundreds of terahertz with subfemtosecond timing jitter," Nat. Photonics **1**, 283–287 (2007).
129. S. M. Foreman, A. D. Ludlow, M. H. G. de Miranda, *et al.*, "Coherent optical phase transfer over a 32-km fiber with 1 s instability at 10^{-17}," Phys. Rev. Lett. **99**, 153601 (2007).
130. H. Jiang, F. Kéfélian, S. Crane, *et al.*, "Long-distance frequency transfer over an urban fiber link using optical phase stabilization," J. Opt. Soc. Am. B **25**, 2029–2035 (2008).
131. M. Kumagai, M. Fujieda, S. Nagano, *et al.*, "Stable radio frequency transfer in 114 km urban optical fiber link," Opt. Lett. **34**, 2949–2951 (2009).
132. G. Grosche, O. Terra, K. Predehl, *et al.*, "Optical frequency transfer via 146 km fiber link with 10^{-19} relative accuracy," Opt. Lett. **34**, 2270–2272 (2009).
133. O. Lopez, A. Amy-Klein, C. Daussy, *et al.*, "86-km optical link with a resolution of 2×10^{-18} for RF frequency transfer," Eur. Phys. J. D **48**, 35–41 (2008).
134. O. Lopez, A. Haboucha, F. Kéfélian, *et al.*, "Cascaded multiplexed optical link on a telecommunication network for frequency dissemination," Opt. Express **18**, 16849 (2010).
135. M. Fujieda, M. Kumagai, S. Nagano, *et al.*, "All-optical link for direct comparison of distant optical clocks," Opt. Express **19**, 16498–16507 (2011).
136. M. Schioppo, J. Kronjäger, A. Silva, *et al.*, "Comparing ultrastable lasers at 7×10^{-17} fractional frequency instability through a 2220 km optical fibre network," Nat. Commun. **13**, 212 (2022).

137. K. Predehl, G. Grosche, S. M. F. Raupach, *et al.*, "A 920-kilometer optical fiber link for frequency metrology at the 19th decimal place," Science **336**, 441–444 (2012).
138. S. Droste, F. Ozimek, T. Udem, *et al.*, "Optical-frequency transfer over a single-span 1840 km fiber link," Phys. Rev. Lett. **111**, 110801 (2013).
139. S. W. Schediwy, D. Gozzard, K. G. H. Baldwin, *et al.*, "High-precision optical-frequency dissemination on branching optical-fiber networks," Opt. Lett. **38**, 2893–2896 (2013).
140. A. Bercy, O. Lopez, P.-E. Pottie, *et al.*, "Ultrastable optical frequency dissemination on a multi-access fibre network," Appl. Phys. B **122**, 189 (2016).
141. D. Calonico, E. K. Bertacco, C. E. Calosso, *et al.*, "High-accuracy coherent optical frequency transfer over a doubled 642-km fiber link," Appl. Phys. B **117**, 979–986 (2014).
142. S. M. F. Raupach, A. Koczwara, and G. Grosche, "Brillouin amplification supports 1×10^{-20} uncertainty in optical frequency transfer over 1400 km of underground fiber," Phys. Rev. A **92**, 021801 (2015).
143. A. Bercy, F. Stefani, O. Lopez, *et al.*, "Two-way optical frequency comparisons at $5{\times}10^{-21}$ relative stability over 100-km telecommunication network fibers," Phys. Rev. A **90**, 061802 (2014).
144. F.-L. Hong, M. Musha, M. Takamoto, *et al.*, "Measuring the frequency of a Sr optical lattice clock using a 120 km coherent optical transfer," Opt. Lett. **34**, 692–694 (2009).
145. C. Lisdat, G. Grosche, N. Quintin, *et al.*, "A clock network for geodesy and fundamental science," Nat. Commun. **7**, 12443 (2016).
146. A. Yamaguchi, M. Fujieda, M. Kumagai, *et al.*, "Direct comparison of distant optical lattice clocks at the 10^{-16} uncertainty," Appl. Phys. Express **4**, 082203 (2011).
147. J. Grotti, S. Koller, S. Vogt, *et al.*, "Geodesy and metrology with a transportable optical clock," Nat. Phys. **14**, 437–441 (2018).
148. T. Takano, M. Takamoto, I. Ushijima, *et al.*, "Geopotential measurements with synchronously linked optical lattice clocks," Nat. Photonics **10**, 662–666 (2016).
149. A. T. Hoang, Z. Shen, and W.-B. Shen, "Unifying the regional height system using optic-fiber clock network: a simulation test for southeast Asia," IEEE Access **11**, 92996–93003 (2023).
150. R. F. C. Vessot, "Clocks and spaceborne tests of relativistic gravitation," Adv. Space Res. **9**, 21–28 (1989).
151. R. F. C. Vessot, M. W. Levine, E. M. Mattison, *et al.*, "Test of relativistic gravitation with a space-borne hydrogen maser," Phys. Rev. Lett. **45**, 2081–2084 (1980).
152. J.-F. Cliche and B. Shillue, "Precision timing control for radioastronomy: maintaining femtosecond synchronization in the Atacama Large Millimeter Array," IEEE Control Syst. **26**, 19–26 (2006).
153. S. W. Schediwy, D. R. Gozzard, C. Gravestock, *et al.*, "The mid-frequency Square Kilometre Array phase synchronisation system," Publ. Astron. Soc. Aust. **36**, e007 (2019).
154. B. Wang, X. Zhu, C. Gao, *et al.*, "Square Kilometre Array telescope—precision reference frequency synchronisation via 1f-2f dissemination," Sci. Rep. **5**, 13851 (2015).
155. Y. He, K. G. H. Baldwin, B. J. Orr, *et al.*, "Long-distance telecom-fiber transfer of a radio-frequency reference for radio astronomy," Optica **5**, 138–146 (2018).
156. H. Kiuchi, M. Fujieda, M. Kumagai, *et al.*, "Possibilities and limitations of the offline scheme frequency transfer method," in *Millimeter, Submillimeter, and*

Far-Infrared Detectors and Instrumentation for Astronomy XII (SPIE, 2024), Vol. 13102, pp. 199–205.
157. T. Akatsuka, T. Goh, H. Imai, *et al.*, "Optical frequency distribution using laser repeater stations with planar lightwave circuits," Opt. Express **28**, 9186–9197 (2020).
158. S. M. Foreman, K. W. Holman, D. D. Hudson, *et al.*, "Remote transfer of ultrastable frequency references via fiber networks," Rev. Sci. Instrum. **78**, 021101 (2007).
159. F. Stefani, O. Lopez, A. Bercy, *et al.*, "Tackling the limits of optical fiber links," J. Opt. Soc. Am. B **32**, 787 (2015).
160. X. Deng, X. Zhang, Q. Zang, *et al.*, "Coherent optical frequency transfer via 972-km fiber link," Chinese Phys. B **33**, 020602 (2024).
161. C. E. Calosso, E. Bertacco, D. Calonico, *et al.*, "Frequency transfer via a two-way optical phase comparison on a multiplexed fiber network," Opt. Lett. **39**, 1177–1180 (2014).
162. S. R. Jefferts, M. A. Weiss, J. Levine, *et al.*, "Two-way time and frequency transfer using optical fibers," IEEE Trans. Instrum. Meas. **46**, 209–211 (1997).
163. P. Krehlik, L. Sliwczynski, L. Buczek, *et al.*, "Fiber-optic joint time and frequency transfer with active stabilization of the propagation delay," IEEE Trans. Instrum. Meas. **61**, 2844–2851 (2012).
164. X. Chen, J. Lu, Y. Cui, *et al.*, "Simultaneously precise frequency transfer and time synchronization using feed-forward compensation technique via 120 km fiber link," Sci. Rep. **5**, 18343 (2016).
165. Ł Śliwczyński, P. Krehlik, A. Czubla, *et al.*, "Dissemination of time and RF frequency via a stabilized fibre optic link over a distance of 420 km," Metrologia **50**, 133–145 (2013).
166. X. Guo, B. Hou, B. Liu, *et al.*, "Time transfer in a 1839-km telecommunication fiber link demonstrating a picosecond-scale stability," Chinese Phys. Lett. **41**, 064202 (2024).
167. J. E. Gilligan, E. M. Konitzer, E. Siman-Tov, *et al.*, "White Rabbit time and frequency transfer over wireless millimeter-wave carriers," IEEE Trans. Ultrason., Ferroelect., Freq. Contr. **67**, 1946–1952 (2020).
168. P. Krehlik, Ł Śliwczyński, Ł Buczek, *et al.*, "Ultrastable long-distance fibre-optic time transfer: active compensation over a wide range of delays," Metrologia **52**, 82–88 (2015).
169. J. Serrano, M. Cattin, E. van der Bij, *et al.*, "The White Rabbit project," in *Proceedings of IBIC2013* (2013), p. THBL2.
170. K. W. Holman, D. D. Hudson, J. Ye, *et al.*, "Remote transfer of a high-stability and ultralow-jitter timing signal," Opt. Lett. **30**, 1225–1227 (2005).
171. G. Marra, H. S. Margolis, S. N. Lea, *et al.*, "High-stability microwave frequency transfer by propagation of an optical frequency comb over 50 km of optical fiber," Opt. Lett. **35**, 1025–1027 (2010).
172. G. Marra, R. Slavík, H. S. Margolis, *et al.*, "High-resolution microwave frequency transfer over an 86-km-long optical fiber network using a mode-locked laser," Opt. Lett. **36**, 511–513 (2011).
173. G. Marra, H. S. Margolis, and D. J. Richardson, "Dissemination of an optical frequency comb over fiber with 3^{-18} fractional accuracy," Opt. Express **20**, 1775–1782 (2012).
174. K. Jung, J. Shin, J. Kang, *et al.*, "Frequency comb-based microwave transfer over fiber with 7×10^{-19} instability using fiber-loop optical-microwave phase detectors," Opt. Lett. **39**, 1577–1580 (2014).
175. J. Kim, J. A. Cox, J. Chen, *et al.*, "Drift-free femtosecond timing synchronization of remote optical and microwave sources," Nat. Photonics **2**, 733–736 (2008).

176. M. Xin, K. Şafak, M. Y. Peng, *et al.*, "Attosecond precision multi-kilometer laser-microwave network," Light: Sci. Appl. **6**, e16187 (2017).
177. Z. Feng, G. Marra, X. Zhang, *et al.*, "Stable optical frequency comb distribution enabled by hollow-core fibers," Laser Photonics Rev. **16**, 2200167 (2022).
178. P. Exertier, E. Samain, C. Courde, *et al.*, "Sub-ns time transfer consistency: a direct comparison between GPS CV and T2L2," Metrologia **53**, 1395–1401 (2016).
179. H. Dai, H. Dai, Q. Shen, *et al.*, "Laser time transfer based on Micius satellite," in *Conference on Lasers and Electro-Optics* (Optical Society of America, 2019), p. STh3 G.5.
180. H. J. Kang, J. Yang, B. J. Chun, *et al.*, "Free-space transfer of comb-rooted optical frequencies over an 18 km open-air link," Nat. Commun. **10**, 4438 (2019).
181. D. R. Gozzard, L. A. Howard, B. P. Dix-Matthews, *et al.*, "Ultrastable free-space laser links for a global network of optical atomic clocks," Phys. Rev. Lett. **128**, 020801 (2022).
182. D. R. Gozzard, S. W. Schediwy, B. Stone, *et al.*, "Stabilized free-space optical frequency transfer," Phys. Rev. Appl. **10**, 024046 (2018).
183. B. P. Dix-Matthews, S. W. Schediwy, D. R. Gozzard, *et al.*, "Point-to-point stabilized optical frequency transfer with active optics," Nat. Commun. **12**, 515 (2021).
184. B. P. Dix-Matthews, S. W. Schediwy, D. R. Gozzard, *et al.*, "Methods for coherent optical Doppler orbitography," J. Geod. **94**, 55 (2020).
185. N. Maron, S. Fernandez, F.-X. Esnault, *et al.*, "Free space optical link to a tethered balloon for frequency transfer and chronometric geodesy," Opt. Express **32**, 4267–4276 (2024).
186. H. Bergeron, L. C. Sinclair, W. C. Swann, *et al.*, "Tight real-time synchronization of a microwave clock to an optical clock across a turbulent air path," Optica **3**, 441 (2016).
187. L. C. Sinclair, W. C. Swann, H. Bergeron, *et al.*, "Synchronization of clocks through 12 km of strongly turbulent air over a city," Appl. Phys. Lett. **109**, 151104 (2016).
188. L. C. Sinclair, H. Bergeron, W. C. Swann, *et al.*, "Comparing optical oscillators across the air to milliradians in phase and 10^{-17} in frequency," Phys. Rev. Lett. **120**, 050801 (2018).
189. Q. Shen, J.-Y. Guan, J.-G. Ren, *et al.*, "Free-space dissemination of time and frequency with 10^{-19} instability over 113 km," Nature **610**, 661–666 (2022).
190. J. L. Ellis, M. I. Bodine, W. C. Swann, *et al.*, "Scaling up frequency-comb-based optical time transfer to long terrestrial distances," Phys. Rev. Appl. **15**, 034002 (2021).
191. M. I. Bodine, J. L. Ellis, W. C. Swann, *et al.*, "Optical time-frequency transfer across a free-space, three-node network," APL Photonics **5**, 076113 (2020).
192. E. D. Caldwell, J.-D. Deschenes, J. Ellis, *et al.*, "Quantum-limited optical time transfer for future geosynchronous links," Nature **618**, 721–726 (2023).
193. E. Samain, P. Vrancken, P. Guillemot, *et al.*, "Time Transfer by Laser Link (T2L2): characterization and calibration of the flight instrument," Metrologia **51**, 503–515 (2014).
194. P. Exertier, E. Samain, N. Martin, *et al.*, "Time Transfer by Laser Link: data analysis and validation to the ps level," Adv. Space Res. **54**, 2371–2385 (2014).
195. E. Samain, P. Exertier, C. Courde, *et al.*, "Time Transfer by Laser Link: a complete analysis of the uncertainty budget," Metrologia **52**, 423–432 (2015).
196. P. Fridelance, E. Samain, and P. Fridelance, "T2L2 - Time Transfer by Laser Link: a new optical time transfer generation," Exp. Astron. **7**, 191–207 (1997).

197. E. Samain, D. Albanese, F. Baumont, *et al.*, "The T2L2 ground experiment time transfer in the picosecond range over a few kilometres," in *Proceedings of the 20th European Frequency and Time Forum* (2006), pp. 538–544.
198. E. Samain, P. Exertier, P. Guillemot, *et al.*, "Time Transfer by Laser Link - T2L2: current status and future experiments," in *Frequency Control and the European Frequency and Time Forum (FCS), 2011 Joint Conference of the IEEE International* (2011), pp. 1–6.
199. H. Dai, Q. Shen, C.-Z. Wang, *et al.*, "Towards satellite-based quantum-secure time transfer," Nat. Phys. **16**, 848–852 (2020).
200. Z. Wu, K. Tang, W. Meng, *et al.*, "Recent advances in pulsed laser time transfer on China space station," in *Proceedings of the 22nd International Workshop on Laser Ranging* (International Laser Ranging Service, n.d.), pp. 1–6.
201. M. Laas-Bourez, C. Courde, E. Samain, *et al.*, "Accuracy validation of T2L2 time transfer in co-location," IEEE Trans. Ultrason., Ferroelect., Freq. Contr. **62**, 255–265 (2015).
202. A. McCann, A. Frost, S. Karpathakis, *et al.*, "Demonstration of a low-SWaP terminal for ground-to-air single-mode fiber coupled laser links," Photonics **11**, 633 (2024).
203. P. Del'Haye, A. Coillet, T. Fortier, *et al.*, "Phase-coherent microwave-to-optical link with a self-referenced microcomb," Nat. Photonics **10**, 516–520 (2016).
204. Q. Li, T. C. Briles, D. A. Westly, *et al.*, "Stably accessing octave-spanning microresonator frequency combs in the soliton regime," Optica **4**, 193–203 (2017).
205. M. H. P. Pfeiffer, C. Herkommer, J. Liu, *et al.*, "Octave-spanning dissipative Kerr soliton frequency combs in Si_3N_4 microresonators," Optica **4**, 684–691 (2017).
206. S. B. Papp, K. Beha, P. Del'Haye, *et al.*, "Microresonator frequency comb optical clock," Optica **1**, 10–14 (2014).
207. D. R. Carlson, D. D. Hickstein, A. Lind, *et al.*, "Photonic-chip supercontinuum with tailored spectra for counting optical frequencies," Phys. Rev. Appl. **8**, 014027 (2017).
208. J. D. Roslund, A. S. Kowligy, J. Fujita, *et al.*, "Optical two-tone time transfer," arXiv (2024).
209. G. Petit and P. Wolf, "Relativistic theory for picosecond time transfer in the vicinity of the Earth," Astron. Astrophys. **286**, 971–977 (1994).
210. G. Petit and P. Wolf, "Relativistic theory for time comparisons: a review," Metrologia **42**, S138–S144 (2005).
211. J. Geršl, "Relativistic theory for time and frequency transfer through flowing media with an application to the atmosphere of Earth," A&A **673**, A144 (2023).
212. M. T. Taylor, A. Belmonte, L. Hollberg, *et al.*, "Effect of atmospheric turbulence on timing instability for partially reciprocal two-way optical time transfer links," Phys. Rev. A **101**, 033843 (2020).
213. L. Wang, W. Jiao, L. Hu, *et al.*, "Residual timing jitter in the free-space optical two-way time and frequency transfer caused by atmospheric turbulence," Opt. Laser Technol. **163**, 109365 (2023).
214. D. A. Howe and N. Schlossberger, "Characterizing frequency stability measurements having multiple data gaps," IEEE Trans. Ultrason., Ferroelect., Freq. Contr. **69**, 468–472 (2022).
215. W. C. Swann, L. C. Sinclair, I. Khader, *et al.*, "Low-loss reciprocal optical terminals for two-way time-frequency transfer," Appl. Opt. **56**, 9406–9413 (2017).
216. D. Zhu, L. Shao, M. Yu, *et al.*, "Integrated photonics on thin-film lithium niobate," Adv. Opt. Photonics **13**, 242–352 (2021).

217. Z. Xiao, W. Liu, S. Xu, *et al.*, "Recent progress in silicon-based photonic integrated circuits and emerging applications," Adv. Opt. Mater. **11**, 2301028 (2023).
218. J. Olson, R. Rockmore, N. D. Lemke, *et al.*, "Electro-optic time transfer with femtosecond stability," arXiv (2024).
219. S. T. Cundiff and A. M. Weiner, "Optical arbitrary waveform generation," Nat. Photonics **4**, 760–766 (2010).
220. M. Zhang, B. Buscaino, C. Wang, *et al.*, "Broadband electro-optic frequency comb generation in a lithium niobate microring resonator," Nature **568**, 373–377 (2019).
221. D. R. Carlson, D. D. Hickstein, A. Lind, *et al.*, "Self-referenced frequency combs using high-efficiency silicon-nitride waveguides," Opt. Lett. **42**, 2314–2317 (2017).
222. P. Manurkar, E. F. Perez, D. D. Hickstein, *et al.*, "Fully self-referenced frequency comb consuming 5 watts of electrical power," OSA Continuum **1**, 274–282 (2018).
223. A. Cingöz, J. Roslund, J. Abo-Shaeer, *et al.*, "Integrated optical transceviers for frequency comb-based time transfer over free space," in *Precise Time and Time Interval Systems and Applications (PTTI)*, Vol. P3A (Institute of Navigation, 2023).
224. R. H. Kingston, *Detection of Optical and Infrared Radiation* (Springer, 1978).
225. P. Fritschel, G. González, B. Lantz, *et al.*, "High power interferometric phase measurement limited by quantum noise and application to detection of gravitational waves," Phys. Rev. Lett. **80**, 3181–3184 (1998).
226. V. Michaud-Belleau, J. Genest, and J.-D. Deschênes, "Optimal detection scheme for shot-noise-limited phase estimation in passive classical-light interferometry," Phys. Rev. Appl. **10**, 024025 (2018).
227. A. Valencia, G. Scarcelli, and Y. Shih, "Distant clock synchronization using entangled photon pairs," Appl. Phys. Lett. **85**, 2655–2657 (2004).
228. R. Quan, Y. Zhai, M. Wang, *et al.*, "Demonstration of quantum synchronization based on second-order quantum coherence of entangled photons," Sci. Rep. **6**, 30453 (2016).
229. Y. Liu, R. Quan, X. Xiang, *et al.*, "Quantum clock synchronization over 20-km multiple segmented fibers with frequency-correlated photon pairs and HOM interference," Appl. Phys. Lett. **119**, 144003 (2021).
230. W. K. Wootters and W. H. Zurek, "A single quantum cannot be cloned," Nature **299**, 802–803 (1982).
231. D. Dieks, "Communication by EPR devices," Phys. Lett. A **92**, 271–272 (1982).
232. S. Prabhakar, C. Mabena, T. Konrad, *et al.*, "Turbulence and the Hong-Ou-Mandel effect," Phys. Rev. A **97**, 013835 (2018).
233. A. D. Ludlow, M. M. Boyd, J. Ye, *et al.*, "Optical atomic clocks," Rev. Mod. Phys. **87**, 637–701 (2015).
234. M. Takamoto, Y. Tanaka, and H. Katori, "A perspective on the future of transportable optical lattice clocks," Appl. Phys. Lett. **120**, 140502 (2022).
235. D. B. Hume and D. R. Leibrandt, "Probing beyond the laser coherence time in optical clock comparisons," Phys. Rev. A **93**, 032138 (2016).
236. E. R. Clements, M. E. Kim, K. Cui, *et al.*, "Lifetime-limited interrogation of two independent $^{27}Al^{+}$ clocks using correlation spectroscopy," Phys. Rev. Lett. **125**, 243602 (2020).
237. M. E. Kim, W. F. McGrew, N. V. Nardelli, *et al.*, "Improved interspecies optical clock comparisons through differential spectroscopy," Nat. Phys. **19**, 25–29 (2023).
238. P. Kómár, E. M. Kessler, M. Bishof, *et al.*, "A quantum network of clocks," Nat. Phys. **10**, 582–587 (2014).

239. E. S. Polzik and J. Ye, "Entanglement and spin squeezing in a network of distant optical lattice clocks," Phys. Rev. A **93**, 021404 (2016).
240. B. C. Nichol, R. Srinivas, D. P. Nadlinger, *et al.*, "An elementary quantum network of entangled optical atomic clocks," Nature **609**, 689–694 (2022).
241. W. Shillue, W. Grammer, C. Jacques, *et al.*, "The ALMA Photonic Local Oscillator system," in *2011 XXXth URSI General Assembly and Scientific Symposium* (2011), pp. 1–4.
242. G. Swart, P. Diamond, L. Ball, *et al.*, "Construction update for the square kilometre array observatory," in *Ground-Based and Airborne Telescopes X*, Vol. 13094 (SPIE, 2024), pp. 325–335.
243. R. J. Selina, E. J. Murphy, M. McKinnon, *et al.*, "The next-generation very large array: a technical overview," in *Ground-Based and Airborne Telescopes VII*, Vol. 10700 (SPIE, 2018), pp. 497–513.
244. K. Şafak, S. Droste, H. P. H. Cheng, *et al.*, "A pulsed-optical timing distribution system for LCLS-II," in *Conference on Lasers and Electro-Optics (2020)* (Optica Publishing Group, 2020), p. SM2N.5.
245. K. Şafak, H. P. H. Cheng, A. Dai, *et al.*, "Single-mode fiber based pulsed-optical timing link with few-femtosecond precision in SwissFEL," in *Conference on Lasers and Electro-Optics (2019)* (Optica Publishing Group, 2019), p. JTh2A.100.
246. C. Clivati, R. Ambrosini, T. Artz, *et al.*, "A VLBI experiment using a remote atomic clock via a coherent fibre link," Sci. Rep. **7**, 40992 (2017).
247. International Clock, Oscillator Networking (ICON) Collaboration, A. Amy-Klein, E. Benkler, P. Blondé, *et al.*, "International comparison of optical frequencies with transportable optical lattice clocks," arXiv (2024).
248. G. Marra, D. M. Fairweather, V. Kamalov, *et al.*, "Optical interferometry–based array of seafloor environmental sensors using a transoceanic submarine cable," Science **376**, 874–879 (2022).
249. C. Clivati, A. Tampellini, A. Mura, *et al.*, "Optical frequency transfer over submarine fiber links," Optica **5**, 893–901 (2018).
250. C.-Y. Lu, Y. Cao, C.-Z. Peng, *et al.*, "Micius quantum experiments in space," Rev. Mod. Phys. **94**, 035001 (2022).
251. G. Krieger, M. Zink, M. Bachmann, *et al.*, "TanDEM-X: a radar interferometer with two formation-flying satellites," Acta Astronaut. **89**, 83–98 (2013).
252. E. A. Burt, J. D. Prestage, R. L. Tjoelker, *et al.*, "Demonstration of a trapped-ion atomic clock in space," Nature **595**, 43–47 (2021).
253. R. Bluhm, V. A. Kostelecký, C. D. Lane, *et al.*, "Clock-comparison tests of Lorentz and CPT symmetry in space," Phys. Rev. Lett. **88**, 090801 (2002).
254. M. A. Fedderke, P. W. Graham, and S. Rajendran, "Asteroids for μHz gravitational-wave detection," Phys. Rev. D **105**, 103018 (2022).

Dr. Emily Caldwell is a staff scientist at the National Institute of Standards and Technology (NIST) in Boulder, Colorado, USA. She holds a B.A. in Engineering Sciences from Dartmouth College and a Ph.D. in Electrical Engineering from University of Colorado at Boulder. Her research focuses on free-space optical time transfer for fundamental physics tests and the redefinition of the SI second. Her recent work has appeared in *Nature* and *APL Photonics* and was covered by *Physics Today*.

Theodora Triano is a Ph.D. student in the Department of Electrical Computer and Energy Engineering at the University of Colorado Boulder. She holds a B.S. in Engineering from the University of California, Davis. Her current research focuses on the use of free-space frequency-comb-based optical time transfer for fundamental physics tests.

Dr. Laura Sinclair is the Optical Time Transfer Project Lead in the Fiber Sources and Applications Group – part of the Communications Technology Laboratory at the National Institute of Standards and Technology (NIST) in Boulder, Colorado. She received a B.S. in Physics from the California Institute of Technology in 2004 and a Ph.D. in Physics from the University of Colorado, Boulder in 2011 and was a postdoc at NIST Boulder, including as a National Research Council (NRC) postdoctoral fellow, before joining the staff. She has been awarded a Presidential Early Career Award for Scientists and Engineers (PECASE) (2019), a Department of Commerce Gold Medal for Scientific/Engineering Achievement as part of the Boulder Atomic Clock Optical Network Collaboration (2019), and a NIST Excellence in Technology Transfer Award (2024) and has been a Senior Member of the IEEE since 2025. Her research focuses on the development of optical frequency combs and their wide-ranging applications, particularly to optical time transfer and ranging.

138 138 107 254 30225 05-19 15:44